TECHNISCHE UNIVERSITÄT MÜNCHEN

Wissenschaftszentrum Weihenstephan für Ernährung, Landnutzung und Umwelt

Lehrstuhl für Aquatische Systembiologie

Mapping and phenologic characterization of lake macrophytes by *in situ* data based reflectance models and satellite imagery

Christine Gloria Fritz

Vollständiger Abdruck der von der Fakultät Wissenschaftszentrum Weihenstephan für Ernährung, Landnutzung und Umwelt der Technischen Universität München zur Erlangung des akademischen Grades eines

Doktors der Naturwissenschaften

genehmigten Dissertation.

Vorsitzender: Prof. Dr. Thomas Knoke

Prüfer der Dissertation:

1. Prof. Dr. Jürgen Geist
2. Prof. Dr. Natascha Oppelt

Die Dissertation wurde am 04.06.2018 bei der Technischen Universität München eingereicht und durch die Fakultät Wissenschaftszentrum Weihenstephan für Ernährung, Landnutzung und Umwelt am 07.08.2018 angenommen.

Contents

List of Tables

List of Figures

Preface

This thesis presents a remote sensing approach to map lake macrophytes and to characterise their phenologic development. The development of an *in situ* data based reflectance model is a necessary basis for macrophyte mapping. The investigation and knowledge of environmental factors that influence the seasonal variations and the phenologic development of lake macrophytes is necessary for a continuous and detailed mapping of lake bottom types and the monitoring of freshwater lakes.

The introduction of this thesis illustrates the ecology of freshwater lakes and presents the established methods of lake macrophyte mapping. Future monitoring approaches and their advantages for a lake type characterization are presented. Following a description of the objectives of this thesis, three distinct research topics dealing with the importance of an improvement of the monitoring method and their required basics are presented. Each topic has been published or submitted as a research paper in a slightly modified form (following the journal requirements).

The thesis ends with a general discussion on the prospective requirements of monitoring methods and the influence of climate change induced environmental variations on the future monitoring. The new findings on the key points of mapping lake macrophytes as well as new types of remote sensing imagery are finally used to develop a systematic monitoring approach for lake macrophytes that may be transferred to many other freshwater lakes.

Abstract

Submersed aquatic vegetation (SAV) is an important structural component of freshwater lake ecosystems. Sensitive to changes in environmental conditions, SAV serves as long-term biological indicator for the trophic state of freshwater lakes. Variations in nutrient concentrations, water temperature, water level and transparency are stressors for the ecological balance. As these effects are related to climate change, they influence the water quality of freshwater lakes as well as the growth and species composition of SAV patches. Alternative to traditional ground-based SAV monitoring, remote sensing is expected to provide fast end effective concepts to map SAV quickly, within large areas and at short intervals.

The main objective of this thesis is the development of species-specific reflectance models for several SAV species. Spectral information on seasonal variations, the species-specific growth and the phenologic development can be derived from SAV's spectral signatures. Combined with satellite imagery, this detailed information enables a ubiquitous SAV monitoring. In field studies, the seasonal variations of littoral bottom coverage and SAV species composition were investigated. The detailed information on spectral variations within the growing season were obtained from reflectance models.

In the first case study, the potential of a semi-empirical method to map littoral bottom coverage by a multi-seasonal approach was analysed. Depth-invariant indices were used to differentiate between SAV and sandy sediments on RapidEye imagery. The increase of SAV patches during the growing season was correctly monitored. The comparison of *in situ* data and Google Earth imagery revealed a kappa coefficient of 0.61 and an overall accuracy of 72.2%. The influence of water constituents and surface phenomena (e.g. sun glint and algal blooms) on the identification success was also demonstrated.

The following study investigated the interrelation between spectral signature, plant physiology and the length of growing season as influenced by the variable water temperature. Systematic collected *in situ* measurements expand and establish spectral libraries as basis to create reflectance models. The combination of spectral information

and phenologic characteristics allows the development of a phenologic fingerprint for each macrophyte species. The developed reflectance models deliver day- and daytime-specific spectral signatures for each SAV species. In the following classification process, a spatial distinction of species-specific SAV growth at different phenologic stages was enabled. The analysis of the phenologic development indicated that the invasive species *Elodea nuttallii* is less affected by water temperature oscillations than the indigenous species *Chara* spp. and *Potamogeton perfoliatus*.

The key aspect of the third study is the analysis and the comparison of the results of a littoral bottom coverage assessment of two different approaches. For the identification of vegetated and non-vegetated patches in shallow water regions, a semi-empirical method using depth-invariant indices and a physically based, bio-optical method using WASI-2D were applied on Sentinel-2A imagery. Under application of the reflectance models, the vegetated areas were differentiated in tall- and meadow-growing SAV species.

In conclusion, the case studies of this thesis revealed that remote sensing methods are suited for a water quality assessment. For an identification on species-level, detailed information on the phenologic development have to be included. The development of species-specific reflectance models is a key element of this process. Based on this findings, a continued development of reflectance models by further SAV species is necessary to improve a water quality assessment by remote sensing methods. As a support for established monitoring methods, remote sensing approaches can be applied ubiquitous and fill gaps in the monitoring net to detect changes at an early stage in the future.

Zusammenfassung

Unterwasservegetation ist ein wichtiger Bestandteil des Ökosystems See. Sie reagiert empfindlich auf veränderte Umweltbedingungen und spielt somit als Langzeit-Bioindikator eine wichtige Rolle bei der Bestimmung des trophischen Zustandes eines Gewässers. Eine Veränderung der Nährstoffstoffbedingungen und des Lichtklimas sowie schwankende Wassertemperaturen und -pegel beeinflussen das ökologische Gleichgewicht eines Sees. Der globale Klimawandel hat ebenfalls einen Einfluss auf diese Variablen und somit auch auf die Wasserqualität sowie das Wachstum und die Artzusammensetzung der Unterwasservegetation. Im Gegensatz zu bisherigen, bodengestützten Methoden zum Makrophytenmonitoring, bietet die Fernerkundung schnelle und effiziente Lösungsansätze, um Unterwasservegetation großflächig und in kurzen zeitlichen Intervallen zu kartieren.

Das übergeordnete Ziel dieser Arbeit ist die Entwicklung von artspezifischen Reflexionsmodellen für mehrere Makrophytenarten. Aus der spektralen Signatur von Unterwasservegetation lassen sich Informationen über jahreszeitliche Schwankungen, das artspezifische Wachstum und die phänologische Entwicklung der jeweiligen Art ableiten. In Kombination mit Satellitenaufnahmen lässt sich so eine großflächige Kartierung von Unterwasservegetation durchführen. Die jahreszeitlichen Schwankungen der littoralen Seebodenbdeckung und der Artzusammensetzung der Makrophyten wurde mittels Feldstudien untersucht. Genaue Informationen über die spektralen Unterschiede, die im Laufe einer Vegetationsperiode auftreten, können aus den Reflexionsmodellen ermittelt werden.

Die erste Fallstudie untersucht das Potential einer halb-empirischen Methode die Seegrundbedeckung mehrmals im Jahr zu kartieren. Tiefenunabhängige Indices wurden dabei eingesetzt, um auf RapidEye-Aufnahmen zwischen Unterwasservegetation und sandigem Sediment unterscheiden zu können. Die Zunahme der bewachsenen Fläche wurde korrekt aufgezeichnet. Der Vergleich von *in situ* Daten und Google Earth Aufnahmen liefern einen Kappa-Koeffizienten von 0,61 und eine Gesamtgenauigkeit von

72,2%. Ebenfalls untersucht wurde der Einfluss von Wasserinhaltsstoffen und Wasseroberflächenerscheinungen (z.B. Sun-glint-Effekte und Algenblüten) auf den Identifikationserfolg.

Die nächste Studie untersucht den Zusammenhang zwischen spektraler Signatur, Pflanzenphysiologie und Länge der Vegetationsperiode, die allesamt von der Variablen Wassertemperatur beeinflusst werden. Systematisch durchgeführte *in situ* Messungen erweitern und etablieren eine Spektralbibliothek, die den artspezifischen Reflexionsmodellen zu Grunde liegt. Die Kombination von spektraler Information und phenologischen Charakteristika ermöglicht die Entwicklung eines phänologischen Fingerabdrucks für jede Makrophytenart. Im nachfolgenden Klassifikationsprozess konnten Makrophyten anhand ihrer artspezifischen, spektralen Merkmale unterschieden werden. Die Untersuchung der phänologischen Entwicklung zeigt, dass die invasive Art *Elodea nuttallii* durch die Temperaturschwankungen weniger beeinflusst wurde als die heimischen Arten *Chara* spp. und *Potamogeton perfoliatus*.

Das Hauptaugenmerk in der letzten Studie lag auf der Analyse und dem Vergleich der Ergebnisse der Bewertung der litoralen Seebodenbedeckung mit zwei unterschiedlichen Ansätzen. Die die Identifikation von bewachsenen und unbewachsenen Bereichen im Flachwasser wurden eine halb-empirische Methode mit tiefenunabhängigen Indices sowie eine physikalisch basierte, bio-optische Methode mit WASI-2D auf Sentinel-2A-Aufnahmen angewandt. Unter Anwendung der Reflexionsmodelle wurden die bewachsenen Bereiche weiterführend in hoch- und niedrigwachsende Makrophytenarten unterteilt.

Zusammenfassend zeigen die Fallstudien dieser Arbeit, dass Methoden der Fernerkundung sich für die Bewertung der Wasserqualität eignen. Für eine Identifikation der Makrophyten auf Artebene müssen genaue Informationen über die phänologische Entwicklung mit einbezogen werden. Die Entwicklung von artspezifischen Reflexionsmodellen ist dabei das Schlüsselelement. Basierend auf diesen Erkenntnissen ist ein kontinuierlicher Ausbau der Reflexionsmodelle um weitere Makrophytenarten notwendig, um die Wasserqualitätsbewertung auf Basis der Fernerkundung voranzutreiben. Fernerkundungsansätze können als Unterstützung zu herkömmlichen

Monitoringmethoden flächendecken angewendet werden. So können so die Lücken im Monitoring-Netz geschlossen werden und Veränderungen in Zukunft frühzeitig erkannt werden.

1 Introduction

1.1 Ecology of freshwater lakes and aquatic macrophytes

Freshwater lakes are important ecosystems and have essential functions in the environment. They serve as habitat for various species and are significant components for hydrological, nutrient and carbon cycles (Moss 2012). Furthermore, freshwater lakes have a prominent function as storage for drinking water, energy production and transport way as well as for fishery and recreation (Stendera et al. 2012, Carvalho et al. 2013). Stressors for the ecological balance in freshwater lakes are eutrophication, inorganic and organic contaminations. These stressors influence the water quality and ecology of freshwater lakes and are superimposed by climate change effects such as increasing water temperatures (Brönmark and Hansson 2002, Dudgeon et al. 2005, Hering et al. 2010, Moss 2012). The aim of international directives, e.g. the European Water Framework Directive (WFD) (European Commission 2000), is to address these problems, to identify the stressors and to achieve and conserve a good qualitative and quantitative trophic status of freshwater lakes. The WFD recommends a regular monitoring that obtains the ecological status of freshwater lakes based on biological components. Currently, the monitoring program is field based and linked to time- and cost-intensive *in situ* sampling and lab analysis (Schaeffer et al. 2013).

One biological indicator for the assessment of the ecological status are aquatic macrophytes (Melzer 1999). They serve as long-term indicators of the trophic state of freshwater lakes. With their occurrence as emergent, floating or submergent plants in the euphotic zone (Silva et al. 2008), they influence the primary production, the oxygen production as well as the food and nutrient cycle and provide a habitat for fishes and aquatic invertebrates (Pieterse et al. 1990, Wilcox and Meeker 1992, Diehl 1993, Weaver et al. 1997, Petr 2000, Marion and Paillisson 2003, Herold et al. 2007, Schultz and Dibble 2012). Submerged aquatic macrophytes are sensitive to changes of the environmental conditions such as nutrient conditions, water temperature, water level and transparency

(Skubinna et al. 1995, Penning et al. 2008, Søndergaard et al. 2010, Poikane et al. 2015). The occurrence and species composition of submerged aquatic macrophytes reflect the environmental conditions and the trophic state of the lake. Therefore, certain lake macrophyte species are used as long-term indicators for freshwater lake ecology (Melzer 1976, Melzer 1999, Melzer and Schneider 2001, Søndergaard et al. 2010). Variations of species appearance and composition indicate a shift of the environmental conditions of the lake. Due to the spatial stability of lake macrophytes, the shoreline can be subdivided in different sections with varying trophic level due to the occurrence and composition of macrophyte species. Based on the distribution of indicator species, an individual trophic status can be assigned to the freshwater lake and its sections.

1.2 Established monitoring methods of lake macrophytes

The WFD requires a regular monitoring of phytoplankton and other aquatic flora in freshwater lakes. While phytoplankton needs to be investigated two times a year, the remaining aquatic flora is presently monitored in a three-year monitoring cycle (European Commission 2000). For lake macrophyte monitoring, a team of divers investigates the aquatic flora along the shoreline (Melzer and Schneider 2001). The mapping of submerged lake macrophytes is carried out separated in four different depth zones of 0 m – 1 m, 1 m – 2 m, 2 m – 4 m and > 4 m. The occurring species are assigned to one of five steps of frequency (Kohler 1978, Melzer 1999). The abundance categories reach from very rare (abundance = 1) and infrequent (abundance = 2) over common (abundance = 3) to frequent (abundance = 4) and abundant (abundance = 5). Therefrom, for each indicator species and for each depth level result a specific frequency, from which the trophic status of the lake is determined.

For transparency and effectively reasons, the shoreline of freshwater lakes is assessed in multiple predefined transects. For each transect, the submerged aquatic vegetation (SAV) is monitored by meandering along a defined transect line in right angle to the shoreline in the different depth zones down to the euphotic depth, the water depth where only 1% of

the radiation of the surface is available (Kirk 2011). Normally, this monitoring is conducted one time every three years during the main growing season of lake macrophytes in July or August, so that the species-specific characteristics are particularly well defined. Constrained to human-, time- and cost resources a closer monitoring net as well as an area-wide mapping is not performed yet. Afterwards, the trophic status of the lake is determined by calculating the macrophyte index MI (Melzer 1999). Based on the value of the indicator group and the abundance categories of the lake macrophytes, the macrophyte index can be calculated for each transect by applying the formula of Melzer (1999) (1).

$$MI = \frac{\Sigma_{a-z}\, I_{a-z} * Q_{a-z}}{\Sigma_{a-z}\, Q_{a-z}} \quad (1)$$

I_{a-z} indicator group of the species a-z

Q_{a-z} quantity of the species a-z

1.3 The importance of frequent mapping of aquatic macrophytes using remote sensing methods

The growing dynamic of lake macrophytes is linked to environmental conditions. In the last years, an increasing dynamic of environmental variables could be observed. The effects of climate change induced variations might be enforced in the coming years. Increasing water temperature, stronger and higher frequent raining events, draughts and the influence of invasive species are potential challenges in the future. These changes may influence the plant ecology and can cause economic problems. For instance, an increased plant growth requires management strategies such as harvesting to avoid propeller damage and a disruption of shipping traffic. A massive macrophyte growth near the shoreline has also a negative impact on tourism. The ecologic changes are shown in macrophyte species composition, growth and distribution.

Due to the rapid ecologic changes in macrophyte growth and distribution, more frequent and consistent monitoring approaches covering a large area are required to achieve the ecological status (Hestir et al. 2015, van Puijenbroek et al. 2015). The conventional monitoring methods to map submerse lake macrophytes seem not to be suitable to solve these problems. Challenges of a successive mapping of submerged macrophytes are the accessibility, the time consuming and cost expensive diving monitoring method and the short phenologic life cycle of the plants (Vis et al. 2003, Kutser et al. 2006). To address the named problems, remote sensing methods gain more and more importance (Palmer et al. 2015). Thus, a monitoring approach with remote sensing methods for mapping benthic bottom coverage and differentiate SAV is a major task in remote sensing applications on coastal and inland waters (Silva et al. 2008). To detect variations in the water body and of the littoral bottom coverage at an early stage, continuous monitoring is required (Palmer et al. 2015). Remote sensing methods have the advantage to allow frequent and regular observations to receive optical information of spots with restricted accessibility. Several observations within one growing season are possible and deliver a detailed monitoring by continuous time series.

Remote sensing methods are time-and cost-effective and deliver data sets at high temporal frequency for spatially explicit analysis. The temporal and spatial coverage by satellite images enable a detection of seasonal and annual changes in water quality and macrophyte coverage (George 1997, Malthus and George 1997, Dekker et al. 2002, Pinnel et al. 2004, Giardino et al. 2007, Yuan and Zhang 2008, Wolf et al. 2013, Roessler et al. 2013a, Palmer et al. 2015, Dörnhöfer et al. 2016a). These investigations can complement the regularly recommended *in situ* mappings of the WFD by divers and may close the gap between single *in situ* measurements. The advantage of remote sensing is the spectral information of a large-area by every single data take. High revisiting times and broad coverage may compensate the reduced information on macrophyte species provided by remote sensing methods. To detect changes in macrophyte distribution and water quality rapidly, detailed information on macrophytes species-specific phenologic development and optical active water constituents in the water column are necessary.

To map SAV by satellites, several challenges and obstacles above and below the water surface have to be overcome (**Figure 1.1**). On the way from top of atmosphere towards the water body, the solar radiation (1) is influenced by absorption and scattering by particles in the atmosphere and the atmosphere itself (2). Arriving at the lake surface level, the incoming solar radiation is reflected by emergent (3) and floating (4) vegetation at the shoreline. Above the water body, the radiation is affected by reflection effects such as sun glint (5) at the transition from air to water. Within the water body, optically active constituents (e.g. Chlorophyll-a (Chl-a), colored dissolved organic matter (cDOM) and suspended particulate matter (SPM)) influence the pathway by absorption, scattering and reflection in the shallow (6) and in the deep (7) water zone. The concentration of optically active water constituents varies within the water body and is temporally variable. In optically deep water, the water surface, the water body and water constituents are main sources of radiation. In shallow water areas, the radiation is additionally influenced by the bottom substrate. The investigations on spectral differences of SAV (8) and bare sediment patches (9) by submersible spectroradiometers deliver detailed information on the type of lake bottom substrate. On the way back towards the satellite, the radiation has to pass the same path as on the way down. The radiation arriving at the sensor (10) enables an analysis of lake bottom substrate types by remote sensing satellite images.

In the focus of this thesis are the reflectance processes at the lake bottom (8 & 9) and the attenuation processes within the water column (6 & 7). It is analysed how these processes change over time and how they affect the analysis of remote sensing images (10) (**Figure 1.1**, highlighted in red). Therefore, spectral information of the different lake bottom substrate types is measured within one day and at different times within the growing season by *in situ* measurements. Those measurements are performed directly above the macrophyte canopy or above the sediment to exclude the water column effects on the spectral information of the littoral bottom types. The influence of water constituents on the spectral signature is investigated by further measurements in the water column. This applied measurement setup provides spectral information for the phenologic development for each investigated macrophyte species. All those information on lake

bottom type, macrophyte species, phenologic development state and sun height is listed in the spectral database and serves as basis for the species-specific reflectance models. These models form a basis for an operational freshwater lake analysis by using remote sensing methods.

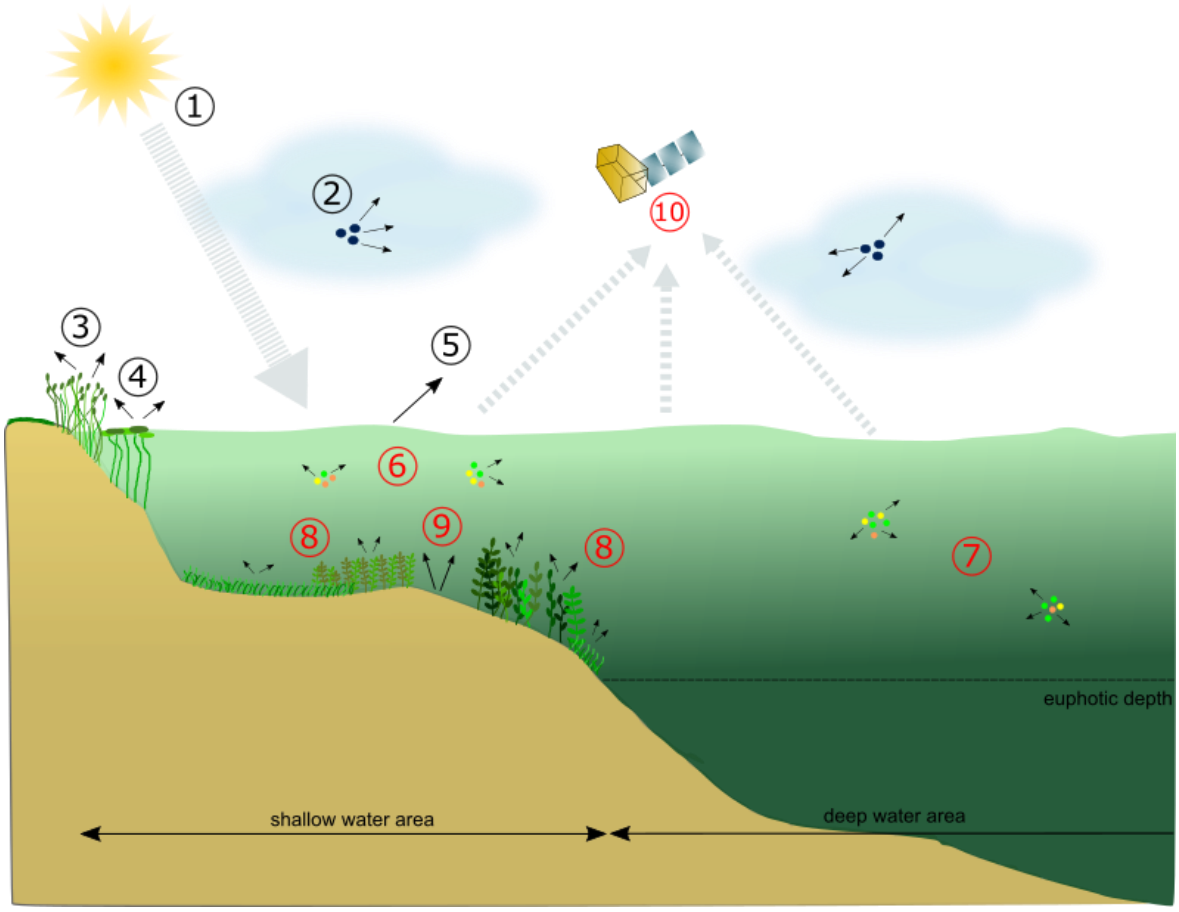

Figure 1.1: The pathway of solar radiation from top of atmosphere towards, in the water body and back to the sensor. Along the path above the water body, the radiation (1) is influenced by particles in the atmosphere (2), by reflection at emergent (3) and floating (4) vegetation and the water surface (5). In the water body, water constituents in shallow (6) and deep (7) water zones and the characteristic reflectance of SAV species (8) and sediment (9) influence the radiation. The radiation arriving at the sensor (10) is the basis for an analysis of lake bottom substrate types by remote sensing satellite images. The focus in this study lies on the subsurface processes highlighted in red.

1.4 Objectives

Submerged macrophyte species show a high spatial, spectral and temporal variability. To gain information on species level, appropriate monitoring methods with a high spatial, spectral and temporal resolution are required. The knowledge of the annual spectral variation of macrophyte species is an important prerequisite. The phenologic development of each species depends on several environmental factors. For example, temperature, light availability and water constituent concentrations affect the lake ecosystem and therefore the spectral fingerprint of SAV species. The global climate change is expected to intensify this effect with high dynamics.

In a stepwise approach, this thesis analyses the applicability of several analysis methods of lake bottom substrate types on data from different remote sensing systems and variable lake types. Daily and seasonal variations of the littoral bottom coverage have been investigated, as well as daily and seasonal spectral variations within individual macrophyte species. *In situ* based spectral measurements are assumed to be the most appropriated method to record the spectral variations of SAV species.

In detail, the main objectives of this thesis were:

- Mapping of seasonal variations of littoral bottom coverage in shallow water areas with a semi-empirical method of depth-invariant indices in a eutrophic lake by using a RapidEye time series
- Spectral investigation on seasonal variations and species-specific growth and phenologic development of native and invasive submerged macrophytes
- Development of species-specific reflectance models for several macrophyte species, covering the complete growing season
- Investigation on annual effects of water temperature oscillations on species-specific growth and phenologic development at the same macrophyte species and test sites

- Mapping of seasonal variations of littoral bottom coverage, even on species level, in shallow water areas in an oligotrophic lake using Sentinel-2 time series. The additional information of the species-specific phenologic development status is delivered by the reflectance models

2 Mapping submerged aquatic vegetation using RapidEye satellite data: the example of Lake Kummerow (Germany)

A similar version of this chapter was published: Fritz C., Dörnhöfer K., Schneider T., Geist J., Oppelt N. Mapping submerged aquatic vegetation using RapidEye satellite data: the example of Lake Kummerow (Germany). Water 2017, 9, 510. Published online DOI: 10.3390/w9070510

2.1 Abstract

Submersed aquatic vegetation (SAV) is sensitive to changes in environmental conditions and plays an important role as a long-term indictor for the trophic state of freshwater lakes. Variations in water level height, nutrient condition, light availability and water temperature affect the growth and species composition of SAV. Detailed information about seasonal variations in littoral bottom coverage are still unknown, although these effects are expected to mask climate change-related long-term changes, as derived by snapshots of standard monitoring methods included in the European Water Framework Directive. Remote sensing offers concepts to map SAV quickly, within large areas, and at short intervals. This study analyses the potential of a semi-empirical method to map littoral bottom coverage by a multi-seasonal approach. Depth-invariant indices were calculated for four Atmospheric & Topographic Correction (ATCOR2) atmospheric corrected RapidEye data sets acquired at Lake Kummerow, Germany, between June and August 2015. RapidEye data evaluation was supported by *in situ* measurements of the diffuse attenuation coefficient of the water column and bottom reflectance. The processing chain was able to differentiate between SAV and sandy sediment. The successive increase of SAV coverage from June to August was correctly monitored. Comparisons with *in situ* and Google Earth imagery revealed medium accuracies (kappa coefficient = 0.61, overall accuracy = 72.2%). The analysed time series further revealed how water constituents and

temporary surface phenomena such as sun glint or algal blooms influence the identification success of lake bottom substrates. An abundant algal bloom biased the interpretability of shallow water substrate such that a differentiation of sediments and SAV patches failed completely. Despite the documented limitations, mapping of SAV using RapidEye seems possible, even in eutrophic lakes.

2.2 Introduction

Monitoring submersed aquatic vegetation (SAV) is important, since occurrence and species composition are long-term indicators for the trophic state of freshwater ecosystems (Melzer 1999). SAV is sensitive to nutrient conditions, water temperature, water level and transparency (Skubinna et al. 1995, Penning et al. 2008, Søndergaard et al. 2010, Poikane et al. 2015). Changing water temperatures can induce changes in plant species composition, expansion, and date of vegetation emergence and senescence (Short and Neckles 1999, Rooney and Kalff 2000, Silva et al. 2008). SAV is one of the biological quality elements (BQE) used in monitoring the ecological status of surface waters within the process recommended by the European Water Framework Directive (WFD). The present regulation requires mapping on a species level every third year, preferably by divers (European Commission 2000). Global change affects ecological balance in freshwater lakes. To detect changes at an early stage, Palmer et al. (2015) recommended more frequent observations of freshwater lakes. Remote sensing provides time- and cost-effective methods to observe seasonal and annual changes in water quality and macrophyte coverage (George 1997, Malthus and George 1997, Dekker et al. 2002, Pinnel et al. 2004, Giardino et al. 2007, Yuan and Zhang 2008, Wolf et al. 2013, Roessler et al. 2013a, Dörnhöfer and Oppelt 2016b). Palmer et al. (2015) concluded that changes in SAV covered areas can be detected by recently available remote sensing systems that are well suited to complement regular *in situ* sampling, as required by the WFD. The approach is expected to bridge observation gaps between snapshots of *in situ* mappings (Malthus and Karpouzli 2003, Palmer et al. 2015). High revisiting time and broad coverage of shallow

lakeshore areas of remote sensing data may compensate for the reduced information on species compared to mappings.

The information provided by remote sensing relies on the interpretability of spectral signatures delivered by the employed systems. The vegetation/sediment ratio controls the spectral response from the lake bottom. At the beginning of the growing season, sediment dominates the spectral response. During this period, the organic overlay on the sediment such as detritus or epiphytes modifies the spectral response of the pure sediment (Armstrong 1993, Fyfe 2003, Williams et al. 2003, Silva et al. 2008, Wolf et al. 2013). SAV displays a highly dynamic appearance within the short vegetation period, which lasts approximately from mid-June to mid-September. Along with SAV growth, the spectral signature of the SAV changes. Varying leaf size, leaf orientation, pigment content and ratio within the vegetation period influence signal intensity and shape (Fyfe 2003, Silva et al. 2008, Wolf et al. 2013). After bottom coverage and biomass are at a maximum, the senescence phase begins. Pigment degradation and canopy structural changes characterize this stage (Wolf et al. 2013), especially the degradation of chlorophyll a (Chl *a*) content in ageing leaves affects the spectral signature (Gausman 1984, Gitelson et al. 2002). The results from Pinnel et al. (2004) and Wolf et al. (2013) indicated that the different developmental patterns of competing macrophyte species along the vegetation period may be the key for differentiation on a species level.

Hyperspectral imaging at close intervals along the vegetation period is best suited to provide necessary spectral information (Heege et al. 2003, Pinnel et al. 2004, Dekker et al. 2011, Roessler et al. 2013a, Giardino et al. 2015). Nevertheless, operational monitoring as required by the WFD, needs high revisiting frequencies and large area coverage. Costs associated with hyperspectral imaging hinder such an approach. Palmer et al. (2015), Roessler et al. (2013a) and Dekker et al. (2011) suggested using multi-seasonal imaging by high spatial resolution multispectral satellite data in order to compensate for the reduced spectral information.

Multi-seasonal imaging is inevitably connected to the need to provide comparable data sets over time. This means that external factors influencing the spectral signal have to be corrected, i.e., changes in the atmosphere, water column and lake surface.

A freely available, sensor-generic atmospheric correction algorithm for freshwater body correction is presently not available. For freshwater, atmospheric algorithms of land applications therefore are a trade-off between availability and accuracy of results. A widely used software is Atmospheric & Topographic Correction (ATCOR2) (Richter and Schläpfer), which proved to be helpful in the case of airborne hyperspectral data evaluations for water depth estimation (Gege 2014a), for water constituents and littoral bottom mapping (Giardino et al. 2015), but also for mapping SAV (Villa et al. 2015) with RapidEye data (Roessler et al. 2013a).

Water constituents differ among water bodies and may change rapidly in concentration and composition within a water body. In combination with varying water depths, they strongly affect the signal. Different strategies exist to consider the attenuation by the water column, particularly bio-optical and semi-empirical modelling (Lyzenga 1978, Lyzenga 1981, Heege et al. 2003, Giardino et al. 2012, Gege 2014b). While bio-optical model inversion on the front end of water content and bottom type determination rely on sample spectra, semi-empirical modelling may be operated without such 'a-priori' information. Previous studies revealed that depth-invariant indices provide a possibility for the detection and distinguishing of bottom coverage of lakes and shorelines. Armstrong (1993) mapped seagrass and estimated its biomass at the shallow water areas in the Bahamas using Landsat Thematic Mapper in combination with field surveys and plant collection. Manessa et al. (2014) analysed WorldView2 imagery to study the distribution of seagrass and corals of shallow water coral reefs in Indonesia. Ciraolo et al. (2006) used the airborne Multispectral Infrared Visible Imaging Sensor (MIVIS) to detect the distribution of seagrass (*Posidonia oceanica*) in a coastal lagoon in Italy. To assess the littoral bottom coverage of inland waters, Brooks et al. (2015) and Shuchman et al. (2013) investigated SAV (notably *Cladophora* spec.) at the Laurentian Great Lakes. They used a depth-invariant SAV mapping algorithm (Shuchman et al. 2013) using Landsat Thematic

Mapper and Multispectral Scanner Imagery time series from the mid-1970s to 2012. Roessler et al. (2013a) applied depth-invariant indices to detect and distinguish SAV (*Elodea nuttallii* and *Najas marina*) at Lake Starnberg (Germany) using a time series of multispectral RapidEye data.

Varying expansion behaviour in successive years due to shifts in vegetation periods, different water clarity, nutrient loading and lake substrate remobilization processes (Dekker et al. 2011) may influence detectability of SAV, all of which are unpredictable factors exacerbated by global warming. RapidEye data time series seem well appropriated for seasonal SAV mapping. The five-identical-system-constellation promises frequent observation opportunities, a prerequisite for phenologic change observations within the vegetation period.

The present study had the core objective of testing the applicability of RapidEye satellite systems with their high spatial and low spectral resolution, to map SAV in shallow areas of freshwater lakes in a multi-seasonal approach. While in previous studies, oligotrophic lakes were investigated (Heege et al. 2003, Pinnel et al. 2004, Roessler et al. 2013a) in this case study, Lake Kummerow, a eutrophic lake in Mecklenburg-Western Pomerania (MV), North-East Germany, was chosen. A semi-empirical method by Lyzenga (1978, 1981) was used to correct the influence of the water column in the RapidEye time series during the vegetation period from June to August 2015.

2.3 Materials and Methods

2.3.1 Study site

Lake Kummerow (53.808° N, 12.856° E) is a eutrophic lake, which developed as a proglacial lake in Germany's Northern Lowland during the last ice age. Its wind-exposed location and relatively shallow depth (average depth: 8.1 m, maximum depth: 23.3 m) determine its polymictic mixing character (Wöbbecke et al. 2003). Sandy or muddy sediments dominate the substrate. Wöbbecke et al. (2003) described that macrophytes had disappeared in the 1960s. Detailed mappings of lakeshore vegetation and submersed

macrophytes were lacking until the 2000s. With the implementation of WFD, *in situ* mappings along transects were conducted in the years 2003, 2007, 2008, 2009, 2011 and 2013. These inventories revealed the existence of different macrophyte populations in Lake Kummerow. In 2013, the growth limit was, on average, down to a depth of 2.5 ± 0.4 m from the surface at the 15 transects mapped ((LU-MV 2015), **Figure 2.1**). *Potamogeton pectinatus* predominates macrophyte coverage in the northern part of the lake. The southern part shows a wider variety of pondweeds such as *Potamogeton pectinatus, Potamogeton perfoliatus*, *Ceratophyllum demersum, Myriophyllum spicatum*, and singularly occurring species (*Elodea canadensis*, *Myriophyllum alterniflorum*, *Myriophyllum spicatum*, *Potamogeton obtusifolius* und *Potamogeton friesii*). The overall evaluation of Lake Kummerow's ecological status, performed with the software PHYLIB (version 4.1) (Schaumburg et al. 2011) based on the BQE macrophytes, revealed a 'poor ecological status' for the year 2013 (LU-MV 2015).

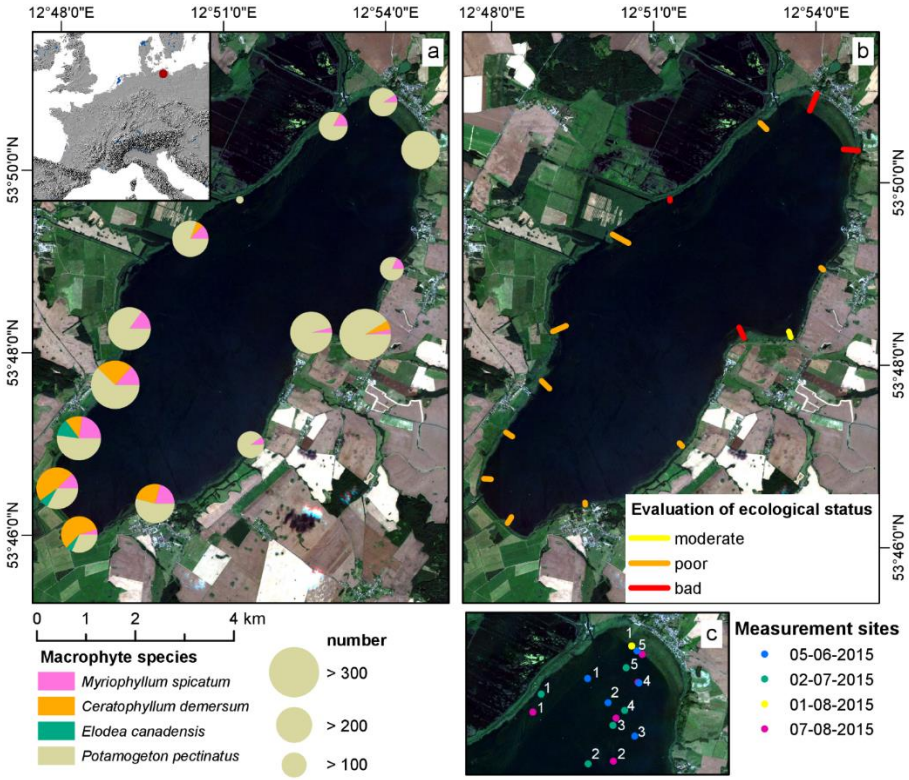

Figure 2.1. The study area Lake Kummerow. (**a**) Share of macrophyte species used in ecological status assessment at each transect. The size of circles indicates the number of macrophytes found within each transect; (**b**) Length and ecological status of transects according to PHYLIB; (**c**) Date and position of the *in situ* measurement sites. Background shows a RapidEye true-colour-composite (1st August 2015). Contains material © (2015) Planet Labs. All rights reserved.

2.3.2 Data collecting and processing

Between June and August, we conducted several measurement campaigns at Lake Kummerow aiming to validate water quality from RapidEye satellite imagery. *In situ* measurements included water sample analyses and radiometric measurements with two submersible RAMSES spectroradiometers (TriOS 2016) at three to five sites in optically deep water, i.e., where the bottom was not visible (**Figure 2.1**). A Trimble Juno SB GPS device (2–5 m positional accuracy (Trimble 2016)) tracked global positioning system (GPS) coordinates of measurement sites during data acquisition. The measurement setup consisted of a floating frame in which both sensors were mounted on a depth adjustable bar so that the detectors were always at the same water depth (z). One sensor (ARC-VIS) measured upwelling radiance, $L_u(\lambda, z)$ [W m^{-2} nm^{-1} sr^{-1}], while the other sensor (ACC-VIS) measured downwelling hemispherical irradiance $E_d(\lambda, z)$ [W m^{-2} nm^{-1}], at two depths below water, i.e., −0.21 m (z_1) and −0.67 m (z_2). At each measurement point, the ACC-VIS sensor was lifted above the water surface for one additional measurement of $E_d^{0+}(\lambda)$. The sensors collected radiometric data between 325 nm and 900 nm in 3.3 nm intervals. Single measurements were linearly interpolated to 1 nm intervals. Remote sensing reflectance $R_{rs}^{0+}(\lambda)$ [sr^{-1}] was calculated according to Equation (2) (Mobley 1999).

$$R_{rs}^{0+}(\lambda) = \frac{L_w(\lambda)}{E_d^{0+}(\lambda)} \tag{2}$$

For determining the water-leaving radiance, $L_w(\lambda)$, $L_u(\lambda, z)$ measurements from the two depths were linearly extrapolated to just beneath the water surface using the attenuation coefficient of upwelling radiance ($K_u(\lambda)$ [m^{-1}] and corrected for air-water interface (Mobley 1999); $\frac{t}{n_w^2}$ = constant = 0.54, n_w= refractive index of water, t = Fresnel reflectance of air-water interface; Equation (3).

$$L_w(\lambda) = -0.54 \cdot [K_u(\lambda)(z_1, z_2) \cdot \ln(L_u(\lambda)(z_1, z_2)) - z_{1,2}] \tag{3}$$

Median, 25% and 75% quartiles of $R_{rs}^{0+}(\lambda)$ were resampled to the RapidEye spectral response curves and used for the validation of ATCOR2 atmospheric correction. The

vertical attenuation coefficient of $E_d(\lambda, z)$, $K_d(\lambda)$ [m^{-1}] was calculated using the equation by Maritorena (1996) [Equation (4)].

$$K_d(\lambda)(z_1, z_2) = -\frac{\ln(\frac{E_d\,(z_1, \lambda)}{E_d\,(z_2, \lambda)})}{z_2 - z_1} \quad (4)$$

$E_d(z_1,\lambda)$ and $E_d(z_2,\lambda)$ in Equation (4) were the median spectra of around 30 measurements. Retrieved $K_d(\lambda)$ spectra were resampled to the RapidEye spectral response curves and averaged from all measurement sites for each measurement day. Additional irradiance reflectance spectra ($R^{0+}(\lambda)$ [-]) of bare sediment and vegetation (*Potamogeton pectinatus*) were collected ex situ with an ASD LabSpec4515 (Analytical Spectral Devices Inc.; range: 350 nm to 2500 nm; interval: 1 nm). Following the method of Giardino et al. (2015) SAV was harvested and its spectral response was then being measured at the beach (ex situ). Mean and standard deviations of single measurements were computed and resampled to RapidEye spectral response curves.

2.3.3 RapidEye Data and Processing

RapidEye Science Archive (RESA) provided multispectral L3A RapidEye data (included bands: blue 440–510 nm, green 520–590 nm, red 630–690 nm, red-edge 690–730 nm and near-infrared 760–880 nm) acquired at Lake Kummerow on 12th June, 1st July, 1st August and 7th August 2015. L3A products included a standard geometric correction resampled to a 5×5 m² pixel size (coordinate system: WGS 1984, UTM Zone 33 N); units were at-sensor radiances [W m^{-2} nm^{-1}]. Atmospheric correction (including atmospheric absorption and scattering, sensor and solar geometry) from at-sensor radiances to bottom of atmosphere irradiance reflectance [-] was conducted using ATCOR2 (Richter 1997, Richter and Schläpfer 2016) for each date. ATCOR2 irradiance reflectance was converted to field measurement-comparable $R_{rs}^{0+}(\lambda)$, followed a division by pi (Mobley et al. 2015). ATCOR2 automatically adapted visibility and corrected for adjacency effects with an adjacency range of 1 km. This effect was particularly strong at boundaries of surfaces with contrasting irradiance reflectance intensities, such as land and water above 700 nm wavelength. The aerosol model chosen was maritime mid-latitude summer, since north-

easterly or north-western wind directions predominated during image acquisition. Thus, maritime aerosols from the Baltic Sea strongly influenced the study area. ATCOR2 estimated aerosol optical thickness at 550 nm (AOT 550 nm) on a per pixel basis applying the dense dark vegetation approach (Kaufman et al. 1997). Moderate-resolution Imaging Spectroradiometer (MODIS) products served as a basis for evaluating the ATCOR2 results. Specifically, calculated AOT values were compared with MODIS AOT (Levy et al. 2015a, Levy et al. 2015b) acquired close to RapidEye image acquisition time. Specific settings of atmospheric correction and weather conditions close to image acquisition were summarized (**Table 2.1**).

Table 2.1. Settings of atmospheric correction, solar and sensor geometry and weather conditions close to image acquisition (± 1 hour).

Acquisition date	Acquisition time (UTC)	Satellite	Wind direction [°]	Wind speed [m s^{-1}]	Solar zenith [°]	Viewing angle [°]	Aerosol model	Calculated visibility [km]	*In situ* data
12 June 2015	10:53	RE-3	50-80	2-3	30.6	12.9	Maritime mid-latitude summer	45.6	- 7 days
01 July 2015	10:52	RE-3	40-70	2-3	30.7	14.8	Maritime mid-latitude summer	111.7	+ 1 day
01 August 2015	11:03	RE-5	60	2-5	35.7	2.9	Maritime mid-latitude summer	88.9	+ 3 hours
07 August 2015	11:11	RE-1	290-350	1-6	37.2	6.7	Maritime mid-latitude summer	25.1	± 2 hours

To evaluate the performance of atmospheric correction, atmospherically corrected RapidEye data were also compared with *in situ* measured $R_{rs}^{0+}(\lambda)$ spectra. Arithmetic means and standard deviations were calculated from atmospherically corrected RapidEye

data ($R_{rs}^{0+}(\lambda)$) based on a 5×5 pixel window surrounding the pixel which corresponded to the GPS coordinate of the respective measurement site. Accuracy indicators were calculated for bands 1 to 4, including root-mean-squared error (RMSE), Pearson's correlation coefficient (r), and percentage bias (pbias) using the R package hydroGOF (Zambrano-Bigiarini 2014). RMSE gives an indication of the absolute difference between *in situ* and atmospherically corrected spectra, r assesses accordance in shape, and pbias provides a relative statement.

Distinguishing water and land area was conducted by thresholding RapidEye near the infrared band (RapidEye band 5; central wavelength 805 nm). Pixels with $R_{rs}^{0+}(\lambda)$ values higher than 0.16 sr^{-1} were classified as land, masked and not further analysed. Water pixels were further processed by applying the deep water corrected Red Index (RI) (Spitzer and Dirks 1987) [Equation (5)]. The RI value separates shallow water areas from optically deep water.

$$RI = \frac{R_{rs}^{0+}(657) - R_{rs}^{0+}(657,\infty)}{R_{rs}^{0+}(657)} \quad (5)$$

with $R_{rs}^{0+}(657)$ representing remote sensing the reflectance value of each pixel in the red, and

$R_{rs}^{0+}(657,\infty)$ representing red remote sensing reflectance over optically deep water.

RI depends on the water constituents and was empirically defined for Lake Kummerow with a threshold at 0.43. For this, water pixels with a RI higher than 0.43 were defined as shallow water and included in the further analysis.

Varying water constituent concentrations and water depths influence the signal received by sensors. To retrieve information about littoral bottom types, the influence of the water column at different water depths had to be considered. Absorption by water and its constituents reduce the availability of radiation with increasing depth, and the fraction of scattered radiation superimposes the radiation reflected by the lake bottom surface type. Depth-invariant indices ($Y_{i,j}$) calculated from two spectral bands i and j are an option to

reduce the influence of water constituents, and to investigate different littoral bottom types. To reduce the influence of the water column in satellite data, we applied the method of Lyzenga (1981) considering that the attenuation coefficients $K_d(\lambda_i)$ and $K_d(\lambda_j)$ accounted for the present water constituent conditions in the water column and the absorption of the water column itself. Thus, the spectral features of the littoral bottom became visible. $R_{rs}^{0+}(\lambda)$ was linearized for each band using the natural logarithm of each spectral band [Equation (6)]. The logarithm was calculated for shallow water remote sensing reflectance $[R_{rs}^{0+}(\lambda_i); R_{rs}^{0+}(\lambda_j)]$ from which deep water remote sensing reflectance $[R_{rs}^{0+}(\lambda_{i,\infty}); R_{rs}^{0+}(\lambda_{j,\infty})]$ was subtracted. Lyzenga's equation [Equation (6)] was applied to each RapidEye scene and to ex situ measurements of sediment and aquatic vegetation.

$$Y_{i,j} = \frac{K_d(\lambda_j) * \ln\left(R_{rs}^{0+}(\lambda_i) - R_{rs}^{0+}(\lambda_{i,\infty})\right) - K_d(\lambda_i) * \ln\left(R_{rs}^{0+}(\lambda_j) - R_{rs}^{0+}(\lambda_{j,\infty})\right)}{\sqrt{K_d(\lambda_i)^2 + K_d(\lambda_j)^2}} \quad (6)$$

i: RapidEye band i,

j: RapidEye band j, where $i < j$,

$K_d(\lambda_i); K_d(\lambda_j)$: Diffuse attenuation coefficients of $E_d(\lambda)$ at band i and j,

$R_{rs}^{0+}(\lambda_i); R_{rs}^{0+}(\lambda_j)$: Remote sensing reflectance at band i and j of each pixel,

$R_{rs}^{0+}(\lambda_{i,\infty}); R_{rs}^{0+}(\lambda_{j,\infty})$: Deep-water remote sensing reflectance at band i and j.

2.3.4 Evaluation of SAV mapping

To obtain *in situ* data on macrophyte distribution at the northern end of the lake, we conducted lake substrate mappings in shallow water (< 0.8 m water depth) close to the shoreline during the summer of 2015. These mappings served to evaluate the calculated index values, the size, position, and type of the lake bottom substrate. We mapped 21 easily accessible patches close to the shoreline with homogenous substrate or SAV coverage using a Trimble Juno SB GPS device (Trimble 2016). Mapping homogeneous patches *in situ* at least three times larger than the pixel size as suggested by Dekker et al. (2011) was limited to a small extent, particularly for SAV covered areas. Google Earth

imagery (acquisition date: 9th August 2015) therefore served as a further evaluation basis. By visually comparing the mapped areas with patterns in Google Earth imagery, we could digitise larger patches (dense SAV coverage, mixed coverage SAV dominated, mixed coverage sediment dominated, pure sediment) better suited for a comparison with RapidEye results. We randomly chose five clearly identifiable patches per coverage class. The patches of dense SAV/pure sediment were chosen to be smaller (patch size ~500 m²) than patches of mixed classes (patch size ~800 m²) to avoid mixing. We calculated an error matrix as cross-tabulations between validation data and categorised depth-invariant index pixels. Cohen's kappa and overall accuracy were calculated to assess the accuracy of the entire map as well as class specific accuracy measures (producer's and user's accuracy) (Congalton 1991, Foody 2002).

2.4 Results

The spectral signatures of SAV and sediment revealed clear differences of irradiance reflectance for each wavelength region. For each acquisition date, several combinations of depth-invariant indices indicated a distinct discrimination between the two considered littoral bottom substrates. The results further demonstrated that Rapid Eye was able to map seasonal changes in SAV coverage.

2.4.1 Differentiation of littoral bottom coverage

Mean $K_d(\lambda)$ for each measurement date, resampled to RapidEye, corresponded well in shape and intensity (**Figure 2.2**). Water constituents derived from *in situ* taken samples [suspended particulate material (SPM), Chl *a*, absorption by coloured dissolved organic matter (cDOM)] and Secchi depths varied for acquisition dates. Between 1st July and 7th August, Chl *a* concentration increased, while Secchi depth and SPM concentration decreased (**Table 2.2**).

Table 2.2. Average water constituent concentrations and number of measurement points at *in situ* campaigns close or concurrently to RapidEye data acquisition.

RapidEye Acquisition Date	*In situ* Data Collection	RAMSES Measurement Points	Secchi Depth [m]	SPM [g·m^{-3}]	Chl-a [mg·m^{-3}]	$a_{cDOM}(440)$ [m^{-1}]
12 June 2015	5 June 2015	3	3.8 ± 0.3	0.7 ± 0.6	1.4 ± 0.3	1.38 ± 0.05
1 July 2015	2 July 2015	5	2.3 ± 0.7	1.3 ± 1.2	11.6 ± 4.1	1.28 ± 0.06
1 August 2015	1 August 2015	1	No measurement	0.7 ± 0.3	1.7 ± 1.8	1.28 ± 0.00
7 August 2015	7 August 2015	4	1.8 ± 0.5	3.6 ± 0.5	16.7 ± 2.9	1.27 ± 0.11

Mean ex situ irradiance reflectance spectra of bare sediment and dense SAV were resampled to RapidEye bands (**Figure 2.3**a). The spectra clearly differed in intensity and shape. Calculating depth-invariant indices revealed a good discrimination between dense SAV and bare sediment for several combinations ($Y_{1,2}$, $Y_{1,3}$, $Y_{2,4}$, $Y_{3,4}$) (**Figure 2.3**b). For each acquisition date, distinct thresholds for bare sediment and dense SAV were calculated. Depth-invariant indices $Y_{1,2}$ and $Y_{1,3}$ revealed a clear differentiation, but these band combinations were omitted due to the influence of cDOM. Even though the difference between dense SAV and the bare sediment of index $Y_{2,4}$ was higher, index $Y_{3,4}$ between RapidEye band 3 (657 nm) and band 4 (710 nm) was chosen for mapping SAV coverage. The influence of the atmosphere in the adjacent red (band 3) and red edge (band 4) region of the spectra was less than between green (band 2) and red edge bands. In particular, $Y_{3,4}$ covered a characteristic vegetation feature, the red edge, i.e., the passage where reflectance strongly increases between visible red and near infrared wavelengths. Due to strong attenuation of water in near-infrared wavelengths (**Figure 2.2**) this feature is normally superimposed by water absorption (Armstrong 1993). To minimize the influence of water absorption $K_d(\lambda)$ was included in the index calculation. Thus, the influence of the exponential decline of radiation with increasing water depth can be omitted (Kirk 1994). Depth-invariant index $Y_{3,4}$ revealed clearly different index values for the two substrate types. Based on ex-situ measured spectra, $Y_{3,4}$ values around 0 indicated

dense coverage with SAV and values above 0.8 indicated bare sediment (**Figure 2.3**b). Values in between these thresholds referred to pixels with a mixed coverage of SAV and sediment.

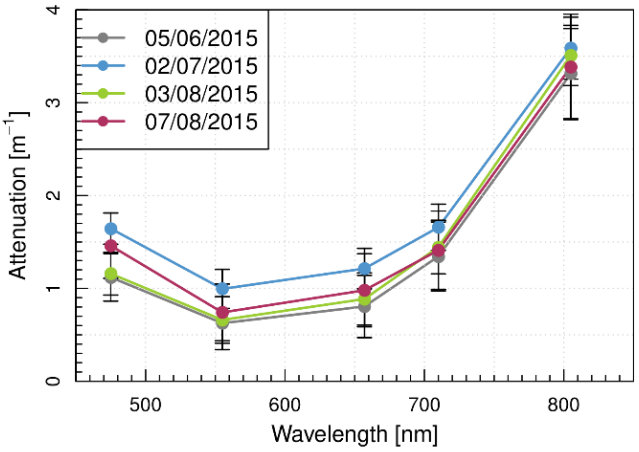

Figure 2.2. Mean $K_d(\lambda)$, retrieved from $E_d(\lambda, z)$ *in situ* measurements of Lake Kummerow for four RapidEye scenes. Error bars indicate standard deviation.

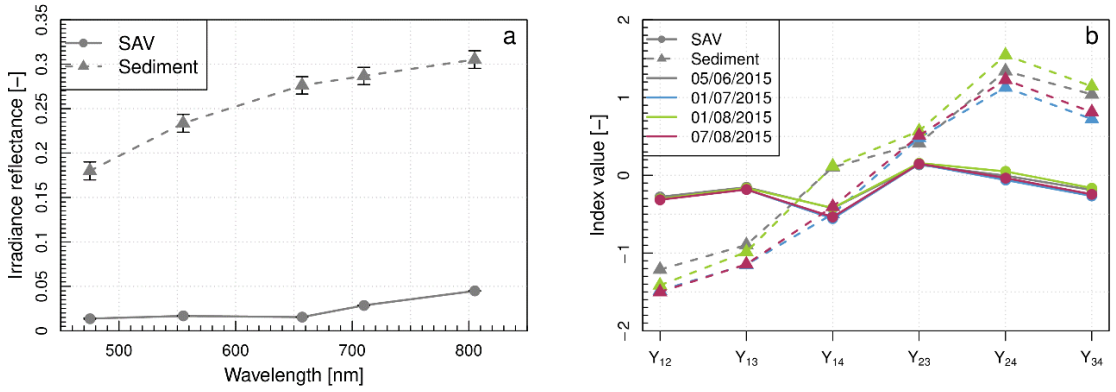

Figure 2.3. (a) Irradiance reflectance of submerse aquatic vegetation (SAV) and bare sediment, measured ex situ and resampled to RapidEye. Error bars indicate standard deviation; (b) Depth-invariant indices for sediment and SAV for the different days, calculated according to the equation of Lyzenga (1981) (Equation (6)).

2.4.2 Seasonal changes of littoral bottom coverage

Due to its extensive shallow water area, the northern part (**Figure 2.4**b) of Lake Kummerow seemed most suitable for analysing bottom substrate (**Figure 2.4**a). Different bottom colours (bright and dark) and structures (e.g., bright triangle, **Figure 2.4**b, white box) were visible in the true-colour composite and indicated varying bottom coverage. The depth-invariant index $Y_{3,4}$ (**Figure 2.4**c - f) illustrated changes in SAV coverage at the northern littoral. The SAV coverage was scaled between 0% (equivalent to bare sediment, red) and 100% (equivalent to complete macrophyte cover, green). Invalid pixels (black) were those upon which the depth-invariant index could not be executed.

In the RapidEye data set from 5th June (**Figure 2.4**c), most parts of the shallow area were classified as sediment. A few areas displayed mixed pixels with values between the thresholds of bare sediment and dense SAV. First, distinct SAV patches appeared in the data set from 1st July (**Figure 2.4**d) close to the shoreline (**Figure 2.4**, box A). A small strip of bare sediment was present at the transition to the deep water region (**Figure 2.4**d, box B). On 1st August, SAV patches spread and formed large SAV-covered areas (**Figure 2.4**e, box A and B); most of the former bare sediment areas changed their index value indicating mixed pixels now. Patches predominated by sediment, such as the linear structure near deep water (**Figure 2.4**d, box C), expanded as well. In the northern part, a triangular sediment structure (**Figure 2.4**d, box D) became apparent. On 7th August (**Figure 2.4**f), a separation between deep and shallow water failed. The index classified most deep water pixels as sediment. The actual shallow water appeared as a heterogeneously mixed area except for the sediment triangle in the north and dense SAV patches near the shoreline.

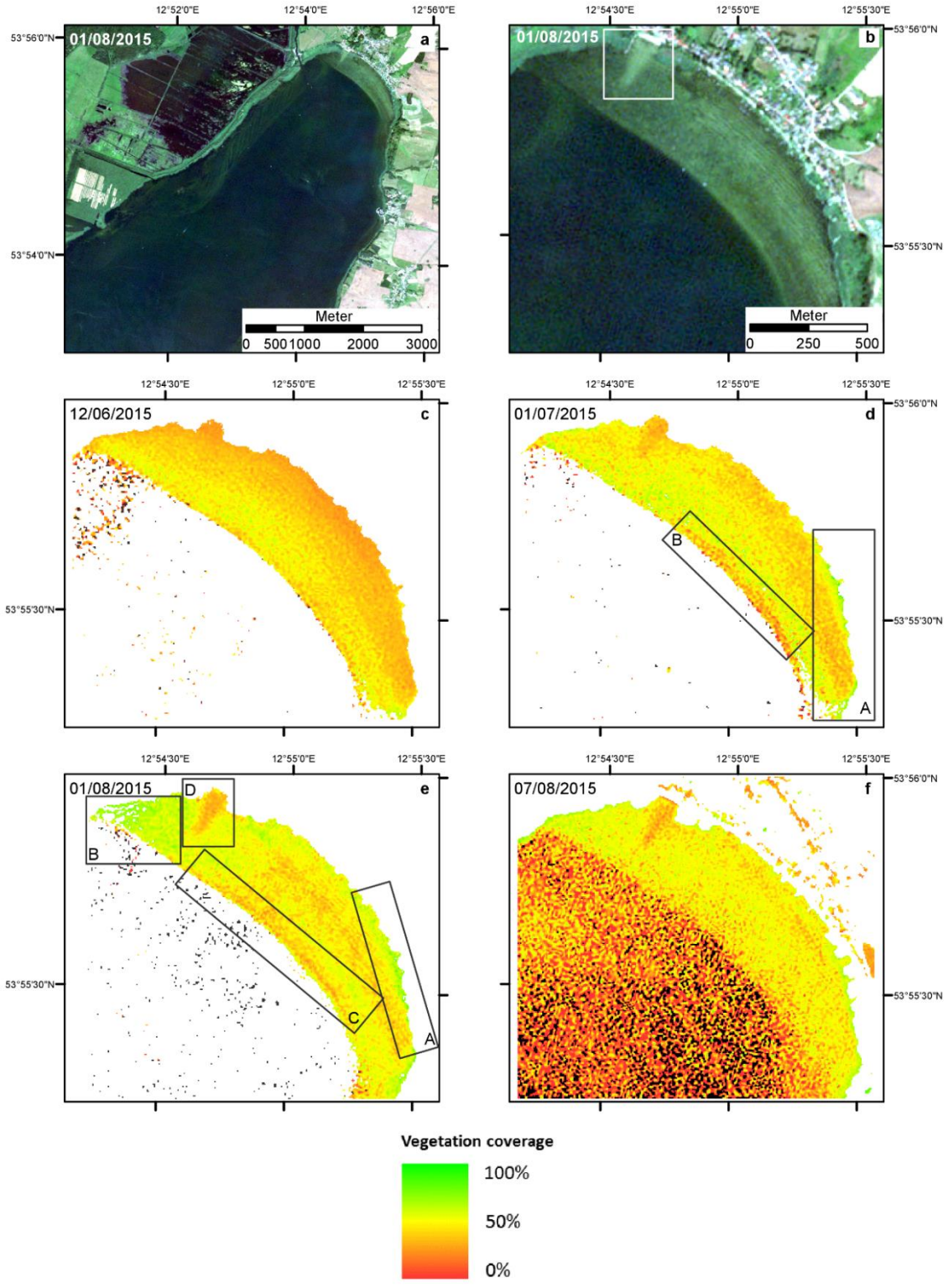

Figure 2.4. Seasonal changes in littoral bottom coverage of Lake Kummerow (**a**) northern littoral; (**b**) illustrated by the depth-invariant index $Y_{3,4}$; (**c**) 12th June 2015; (**d**) 1st July 2015; (**e**) 1st August 2015; (**f**) 7th August 2015. Bare sediment covered areas are displayed in red, dense SAV in green, mixed areas in yellow. Land and deep water areas are masked (except for 7th August 2015 where only land areas have been masked successfully), invalid pixels are displayed black. Contains material © (2015) Planet Labs. All rights reserved.

2.4.3 Evaluation of SAV mapping

To evaluate the depth-invariant index classification, local scale *in situ* mappings covering diverse structures of littoral bottom and Google Earth imagery (acquisition date: 9th August) served as a basis (**Figure 2.5**a). Mapping during summer months revealed that SAV started to grow sparsely at the beginning of June. In accordance with the official WFD monitoring (conducted in 2013, **Figure 2.1**a), *Potamogeton pectinatus* was the predominating patch-forming species. Patches mapped as pure sediment corresponded to bright areas visible in the Google Earth image. Patches mapped as pure SAV coverage (*Potamogeton pectinatus*) mainly matched with dark areas. In particular, at small patches, problems associated with GPS positional accuracy became apparent. Mixed coverages with dominating sediment showed patterns similar to ripple marks, i.e., an approximately 10 m wide sediment strip followed an approximately 5 m wide SAV strip (**Figure 2.5**a). The validation areas were digitised referring to the following categories: dense SAV, mixed coverage dominated by SAV, mixed coverage dominated by sediment and pure sediment (**Figure 2.5**b). **Figure 2.5**c displays the categorized depth-invariant index $Y_{3,4}$ of 1st August. We determined thresholds between classes based on ex situ measured spectra and *in situ* mapped patches similar to Brooks et al. (2015). **Table 2.3** lists the tabulated error matrix and accuracy measures. SAV mapping in the northern part of the lake revealed an overall accuracy of 72.2% and a kappa coefficient of 0.61.

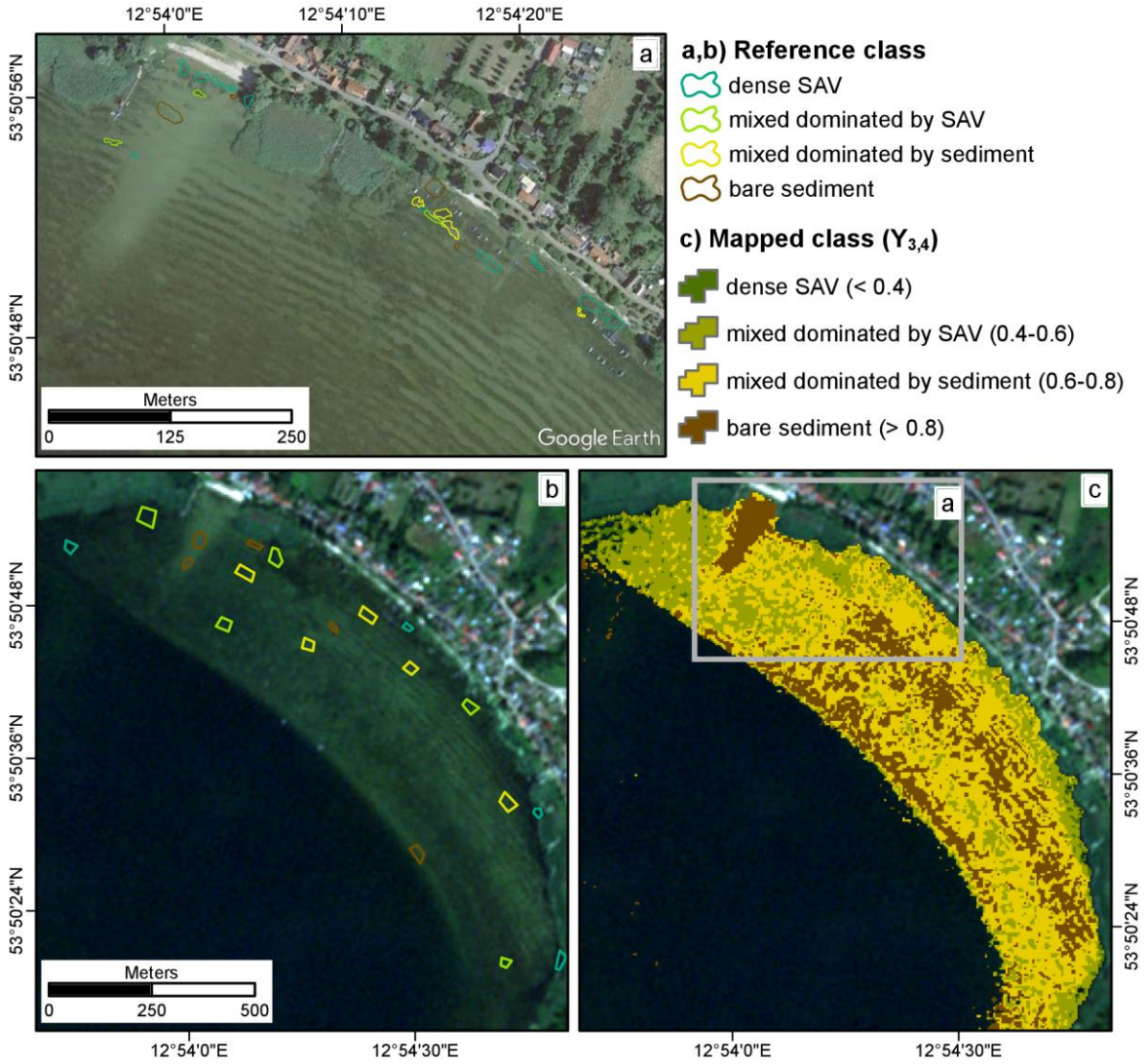

Figure 2.5. Evaluation of SAV mapping with (**a**) *In situ* observed littoral bottom coverage highlighted in Google Earth imagery (acquisition date: 9th August, Image © 2017 TerraMetrics); (**b**) Reference areas based on Google Earth imagery and transferred to RapidEye (acquisition date: 1st August); (**c**) Categorised depth-invariant index $Y_{3,4}$ of RapidEye data. Contains material © (2015) Planet Labs. All rights reserved.

Table 2.3. Error matrix and class accuracy measures of categorized $Y_{3,4}$(1st August) based on Google Earth imagery (9th August) reference data. The number of reference pixels is about 2.5% of the investigated area

Class		Reference Data (number of pixels)					User's Accuracy [%]
		Dense SAV	Mixed SAV Dominated	Mixed Sediment Dominated	Pure Sediment	Sum	
Depth-invariant index data [number of pixels]	dense SAV	26	9	0	0	35	74.3
	mixed SAV dominated	19	106	19	1	145	73.1
	mixed Sediment dominated	3	48	113	8	172	65.7
	pure sediment	0	1	25	101	127	79.5
	Sum	48	164	157	110	479	
Producer's accuracy [%]		54.2	64.6	72.0	91.8		
masked		43	4	0	0	47	

2.4.4 Atmospheric correction

Between the three evaluation dates, comparing *in situ* and RapidEye $R_{rs}^{0+}(\lambda)$ spectra revealed differences in both shape and intensity (**Figure 2.6**). Largest discrepancies occurred in band 5, which consistently showed higher RapidEye than *in situ* $R_{rs}^{0+}(\lambda)$ values. For most measurement sites, *in situ* and RapidEye $R_{rs}^{0+}(\lambda)$ spectra correlated reasonably in shape between band 1 and 4 (r > 0.6). ATCOR2 overestimated absolute $R_{rs}^{0+}(\lambda)$ values except for 1st August and 2nd July (measurement site 1). On 2nd July, calculated RMSE and percentage bias were low for sites 3–5 on this date, indicating a good correspondence in intensities between atmospherically corrected and *in situ* measured data (**Table 2.4**). On 1st August, *in situ* measurements were available from one site only, over bare sediment in optically shallow water (around 1.5 m water depth). On

this day, atmospherically corrected RapidEye $R_{rs}^{0+}(\lambda)$ spectra showed lower values compared to the *in situ* data, but corresponded well in shape (**Figure 2.6**b). On 7th August, ATCOR2 corrected RapidEye $R_{rs}^{0+}(\lambda)$ spectra were significantly higher than *in situ* data and showed the highest pbias and RMSE (**Table 2.4**). Evaluation of this date indicated an erroneous atmospheric correction; only measurement site 5, located close to shallow water, showed acceptable correspondence in $R_{rs}^{0+}(\lambda)$ shape and intensity (**Figure 2.6**c). The second indicator of atmospheric performance was ATCOR2-calculated AOT (550 nm) in comparison to the MODIS AOT product. During the investigation period, AOT (550 nm) was highest on 7th August; lowest values occurred on 1st August. AOT (550 nm) values from MODIS products showed the same tendency between acquisition dates (**Table 2.5**). Retrieved values slightly differed between MODIS product and ATCOR2-RapidEye.

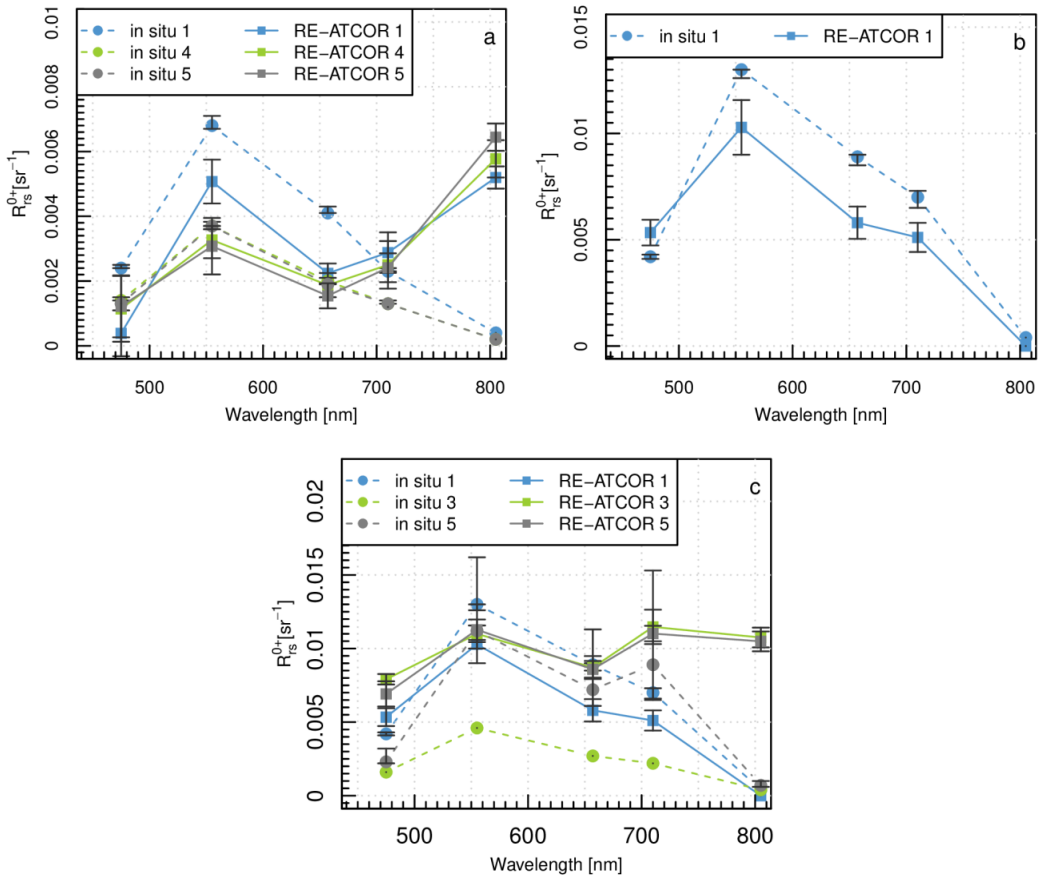

Figure 2.6. Comparison between resampled *in situ* measured median $R_{rs}^{0+}(\lambda)$ spectra and RapidEye 5 × 5 pixel environment mean $R_{rs}^{0+}(\lambda)$ spectra. Error bars indicate standard deviation (RapidEye) and 25% resp. 75% percentile (*in situ*). (**a**) *In situ* data acquisition on 2nd July and RapidEye acquisition on 1st July; (**b**) 1st August; (**c**) 7th August.

Table 2.4. Accuracy measures of each measurement site calculated between corresponding RapidEye 5 × 5 pixel environment mean and resampled *in situ* measured $R_{rs}^{0+}(\lambda)$ median spectra (bands 1- 4).

RapidEye Acquisition Date	***In situ* Data Acquisition Date**	**Measurement Site**	**RMSE [sr^{-1}]**	**r [-]**	**Percentage Bias [%]**
1 July 2015	2 July 2015	1	0.0017	0.82	−32.2
1 July 2015	2 July 2015	2	0.0013	0.64	59.4
1 July 2015	2 July 2015	3	0.0006	0.81	3.8
1 July 2015	2 July 2015	4	0.0007	0.74	4.6
1 July 2015	2 July 2015	5	0.0007	0.74	0.6
1 August 2015	1 August 2015	1	0.0023	0.88	−19.8
7 August 2015	7 August 2015	1	0.0067	0.68	281.1
7 August 2015	7 August 2015	2	0.0050	0.58	87.7
7 August 2015	7 August 2015	3	0.0071	0.52	252.2
7 August 2015	7 August 2015	4	0.0058	0.71	187.3
7 August 2015	7 August 2015	5	0.0026	0.95	27.7

Table 2.5. Mean and standard deviation of AOT at 550 nm values retrieved from RapidEye data during ATCOR2 atmospheric correction in comparison to MODIS product AOT at 550 nm values (Levy et al. 2015a, Levy et al. 2015b) in a 3 × 3 (30 × 30 km²) pixel environment covering the study area.

Date	MODIS Acquisition Time (UTC)	AOT MODIS	RapidEye Acquisition Time (UTC)	AOT ATCOR2	RMSE [-]	Percentage Bias [%]	r [-]
12 June 2015	TE 10:25	0.119 ± 0.037	10:53	0.181 ± 0.005			
12 June 2015	AQ 12:10	0.174 ± 0.043	10:53	0.181 ± 0.005			
1 July 2015	TE 9:15	0.127 ± 0.019	10:52	0.116 ± 0.009			
					0.072	−13.5	0.94
1 August 2015	AQ 12:00	0.119 ± 0.048	11:03	0.102 ± 0.002			
7 August 2015	TE 11:15	0.390 ± 0.017	11:11	0.301 ± 0.003			
7 August 2015	AQ 13:00	0.437 ± 0.045	11:11	0.301 ± 0.003			

2.5 Discussion

The present study tests the applicability of RapidEye satellite data with its high spatial resolution and its high revisiting frequency to map SAV in shallow areas of eutrophic freshwater lakes. The identification of SAV patches and the monitoring of the phenologic development of SAV was successful, even though the atmospheric correction of RapidEye satellite data was conducted using ATCOR2.

2.5.1 Differentiation and seasonal changes of littoral bottom coverage

The results indicated that multi-seasonal RapidEye data are suitable for monitoring changes in littoral bottom coverage as previously proposed by several authors (Shuchman et al. 2013, Wolf et al. 2013, Roessler et al. 2013a, Brooks et al. 2015, Giardino et al. 2015). Our approach follows several studies which successfully applied depth-invariant indices

to discriminate between SAV and sediment (Shuchman et al. 2013, Roessler et al. 2013a, Brooks et al. 2015). In our study, the depth-invariant index $Y_{3,4}$, combining RapidEye band 3 and 4, performed well in mapping the general trend of SAV expansion within the observation period (**Figure 2.4**c-f). In the shallow water zone, SAV favour calm regions near the shoreline resulting in dense patches while sediment dominates in areas with high disturbance due to wind (Koch 2001), waves and human activities.

High wind and wave activities influenced the expansion of macrophytes at the beginning of the vegetation period. On 12th June, sediment covered most of the lake bottom. Vegetation was sparsely distributed; field observation confirmed the growth of SAV at the beginning of June. Moreover, detritus, plant residuals, epiphytes, or sparsely growing SAV influenced the spectral signal, resulting in an index value of mixed coverage (Armstrong 1993, Fyfe 2003, Williams et al. 2003, Silva et al. 2008, Wolf et al. 2013).

From 1st July to 1st August, the SAV covered area increased, especially at calm regions near the shoreline (**Figure 2.4**d, box A; **Figure 2.4**e, box A and B), where the spectral signature showed a vegetation dominated signal. Sediment dominated highly disturbed areas such as the beach (**Figure 2.4**e, box D). The linear sediment zone near the deep water border (**Figure 2.4**d, box B; **Figure 2.4**e, box C) may be attributed to wave pounding.

Limitations of the index method appeared to be related mainly to the concentration of optically active water constituents and the $K_d(\lambda)$ measurement. Within one week (1st August–7th August), SPM and Chl-a concentrations in the water column increased strongly; the water transparency decreased accordingly (**Table 2.2**). Low Secchi depths indicated high light attenuation in the water column. An algal bloom, as imaged on 7th August 2015 (**Figure 2.4**f and Dörnhöfer et al. (2018)) hampered a successful discrimination between deep and shallow water; RI failed to separate shallow and deep water. Therefore, the depth-invariant index was calculated for the entire water body. During the algal bloom, surface-floating algae increased RapidEye $R_{rs}^{0+}(657{,}710)$ values over the entire lake. *In situ* $K_d(\lambda)$ measurements (**Figure 2.2**), however, remained at a similar intensity. Water samples and measurement setup may have caused this discrepancy: water samples were collected close to the water surface. Floating algae

therefore may have influenced the water samples and satellite signals. For $K_d(\lambda)$ measurements the sensors were installed on a floating device which may have partially removed the algae carpet. The resulting $K_d(\lambda)$ values would therefore have failed to represent actual water conditions. Non-representative $K_d(\lambda)$ values resulted in high RapidEye $Y_{3,4}$ values, which in turn indicated high sediment coverage (**Figure 2.4**f). Consequently, extreme events such as algal blooms have to be considered, and data collected during such events have to be carefully checked for such a bias.

2.5.2 Evaluation of SAV mapping

Validating SAV distribution and coverage is a challenging task. The littoral bottom coverage is often difficult to access. *In situ* observations therefore are conducted on selective transects by divers or from boat and therefore cover only small areas hardly transferable to the satellite level. GPS inaccuracies and a system that is in motion introduce positional errors to the observation. Several studies therefore evaluate mappings qualitatively (Giardino et al. 2007, Heblinski et al. 2011, Roessler et al. 2013a, Giardino et al. 2015). Studies which determined discrete classes (e.g., less dense SAV, bare substrate, submerged, floating vegetation) collected field data by boat or ancillary maps to tabulate error matrices and associated accuracy measures (Dogan et al. 2009, Hunter et al. 2010, Shuchman et al. 2013, Bolpagni et al. 2014, Brooks et al. 2015). Dekker et al. (2011) recommend a minimum patch size of at least three times the pixel size covering homogenous coverage. The limited overview during *in situ* mapping, however, hampers identifying homogenous patches of at least 75 m². We therefore followed an approach which recently proved valuable in remote sensing studies on land use/cover (Bey et al. 2016, Manakos et al. 2017, Wang et al. 2017), i.e., a comparison with Google Earth imagery. We verified the visual interpretation of Google Earth imagery with *in situ* mapped patches. The spatial resolution of Google Earth images is higher than RapidEye, the information (e.g., species, bottom type) is less detailed than *in situ* mappings, but grants a spatial overview. Upscaling the extent of *in situ* data by means of very high spatial resolution aerial or Google Earth imagery may help to overcome the limitation associated with comparing limited *in situ* and satellite data.

Other studies conducting accuracy assessments (Dogan et al. 2009, Hunter et al. 2010, Shuchman et al. 2013, Bolpagni et al. 2014, Brooks et al. 2015, Villa et al. 2015) show kappa coefficients ranging between 0.57 and 0.92. The result of our study is at the lower end of the scale (kappa=0.61). Producer's and user's accuracies highlight varying performance of the different classes. Bare sediment is easy to detect and performs best (**Table 2.3**). Reference patches of dense SAV often include land-masked pixels; dense SAV that grew up to the water surface developing surface floating leaves may have led to erroneous land masking. Mixed coverage dominated by SAV partially mixes up with mixed coverage dominated by sediment. A clear differentiation between both classes is difficult for both Google Earth digitisation and $Y_{3,4}$. The spatial resolution of RapidEye misses the structures similar to ripple waves, which are clearly apparent in the Google Earth imagery (**Figure 2.5**).

Bridging the gap between *in situ* and satellite mapping via Google Earth is only possible when near-term imagery is available as for the RapidEye data set from 1st August 2015. The evaluation of at least one data set offers a first impression of the applied method's accuracy. To evaluate growth patterns, mapping of pilot sites is necessary close to satellite acquisitions. Assessing the plausibility of growth patterns or recurring uniform patches (e.g., triangular structure of sediment) may be a further option for a qualitative evaluation.

2.5.3 Atmospheric correction

To adjust and evaluate the atmospheric correction process of the RapidEye data with ATCOR2, two different approaches were employed, i.e., the comparison with *in situ* submersible spectroradiometer data and the MODIS products as delivered by the NASA standard processing chain. Both methods are prone to errors and contain uncertainties; nevertheless, they allowed for a complementary evaluation of results.

Simultaneously taken *in situ* and remote sensing data sets are considered the most reliable proof for a successful atmospheric correction. The empirical line approach (Smith and Milton 1999), for instance, is based on this assumption. The policy of the RapidEye

company (later BlackBridge, now Planet Labs) gave priority to commercial orders and, prohibited a precise acquisition planning and field data collection. For this reason, evaluation of atmospheric correction was only possible based on a relatively small *in situ* data set. Simultaneous *in situ* and satellite measurements were available solely on 1st and 7th August; on 1st July a time gap of one day existed.

In situ data included measurements of upwelling radiance below water surface, which are then extrapolated to above water surface reflectance ($R_{rs}^{0+}(\lambda)$). Water surface effects, such as sun and sky glint, therefore remained unaddressed in the resulting *in situ* $R_{rs}^{0+}(\lambda)$ spectra. Contrarily, two overlaying phenomena probably contaminated the ATCOR2 atmospherically corrected $R_{rs}^{0+}(\lambda)$ spectra: sky/sun glint and insufficiently addressable adjacency effects. The latter, in particular, affects bands in wavelength regions above 700 nm (Santer and Schmechtig 2000, Kay et al. 2009, Sterckx et al. 2011). The spectral signature of water is influenced by additional radiation from neighbouring, vegetated land surfaces with much higher reflectance in these wavelengths. This effect may contribute to water pixels up to 5 km away from the shoreline ((Santer and Schmechtig 2000, Sterckx et al. 2011), **Figure 2.6**a and c, i.e. bands 3-5). On 1st August, only one *in situ* data set existed; in this case, however, an almost perfect match in shape indicated a good performance of atmospheric correction at least at this site in optically shallow water.

During the algal bloom (7th August), below-water surface *in situ* radiometric measurements may not have captured the actual conditions at the water surface; surface cum algae, however, seem to dominate the RapidEye signal leading to be observed differences between *in situ* and RapidEye $R_{rs}^{0+}(\lambda)$ spectra.

Due to the limited match with *in situ* measurements, MODIS AOT products served as a second indicator for evaluating the atmospheric correction. Overall, ATCOR2 AOT of RapidEye data was slightly lower compared to MODIS (pbias = − 13.5%) but are highly comparable (r = 0.94). Low AOT (550 nm) values (**Table 2.4**) indicated clear atmospheric conditions. On these days, RapidEye data matched fairly well with *in situ* $R_{rs}^{0+}(\lambda)$ spectra. On 7th August (**Figure 2.6**c), AOT values at 550 nm were relatively high, i.e., 0.301 for corrected ATCOR2-RapidEye data and 0.390 for the MODIS product; both values

indicated a hazy, dense atmosphere and a consequently difficult correction of atmospheric effects (e.g., absorption and scattering).

The differences between *in situ* and atmospherically corrected spectra reflected the challenges for this correction procedure, which were further aggravated by an algae bloom. The successful differentiation of optically deep and shallow water and subsequent delineation of macrophytes/sediment coverage, however, depended on the performance of atmospheric correction. Further improvements of strategies and sensor-generic software packages for freshwater lake atmospheric correction, therefore, are necessary when envisaging a systematic SAV monitoring. Until such algorithms are available comparisons with *in situ* measurements help to consider issues related to atmospheric correction when interpreting SAV mapping.

2.6 Conclusions

This study used four ATCOR2 corrected RapidEye data sets (June to August 2015) to map SAV in the shallow water areas of the eutrophic Lake Kummerow (North-Eastern Germany). Radiometric field measurements supported parameterising a depth-invariant index, which reduced the influence of the overlaying water on the bottom signal. The index enabled mapping the growth and spatial distribution of SAV. Growth patterns showed the expected spatio-temporal development of SAV. The index, however, failed during a surface scum forming algal bloom. Gathering reference data for quantitative evaluations is a challenge; comparisons with field mappings and Google Earth imagery revealed realistic and sufficient accuracies (kappa coefficient = 0.61, overall accuracy = 72.2%) in comparison to other studies. The spectral resolution of RapidEye may be insufficient to gain information on species level especially for mono-temporal data investigations. Implementing ecologic and physiological characteristics, such as phenologic or structural changes of SAV and information on species-specific canopy height, may help to identify species. In view of global warming, multi-year time-series may obtain information about trends in SAV coverage. Recent data may help to detect areas, which undergo changes; targeted diver mappings may reveal specific details. Thus,

satellite systems with high spatial resolution and revisiting frequency offer the potential to support *in situ* macrophyte surveys as conducted within the WFD.

3 Seasonal variation in spectral response of submerged aquatic macrophytes: A case study at Lake Starnberg (Germany)

A similar version of this chapter was published: Fritz C., Schneider T., Geist J. Seasonal variation in spectral response of submerged aquatic macrophytes: A case study at Lake Starnberg (Germany). Water 2017, 9, 527. Published online DOI: 10.3390/w9070527

3.1 Abstract

Submerged macrophytes are important structural components of freshwater ecosystems that are widely used as long-term bioindicators for the trophic state of freshwater lakes. Climate change and related rising water temperatures are suspected to affect macrophyte growth and species composition as well as the length of the growing season. Alternative to the traditional ground-based monitoring methods, remote sensing is expected to provide fast and effective tools to map submerged macrophytes at short intervals and over large areas. This study analyses interrelations between spectral signature, plant phenology and the length of growing season as influenced by the variable water temperature. During the growing seasons of 2011 and 2015, remote sensing reflectance spectra of macrophytes and sediment were collected systematically *in situ* with hyperspectral underwater spectroradiometer at Lake Starnberg, Germany. The established spectral libraries were used to develop reflectance models. The combination of spectral information and phenologic characteristics allows the development of a phenologic fingerprint for each macrophyte species. By inversion, the reflectance models deliver day and daytime specific spectral signatures of the macrophyte populations. The subsequent classification processing chain allowed distinguishing species-specific macrophyte growth at different phenologic stages. The analysis of spectral signatures within the phenologic development indicates that the invasive species *Elodea nuttallii* is

less affected by water temperature oscillations than the native species *Chara* spp. and *Potamogeton perfoliatus*.

3.2 Introduction

Macrophytes are important structural components and sensitive bioindicators of the long-term trophic state of freshwater lakes (Melzer 1999). Occurrence and species composition depend on the nutrient conditions, water level, water temperature and transparency (Skubinna et al. 1995, Melzer 1999, Penning et al. 2008, Søndergaard et al. 2010, Poikane et al. 2015). Changing environmental conditions affect variations in macrophyte species composition, distribution, vegetation begin and senescence (Short and Neckles 1999, Rooney and Kalff 2000, Silva et al. 2008). A regular update of the macrophyte index (Melzer 1999) in freshwater lake ecosystems is recommended by the European Water Framework Directive (WFD). The present regulation requires a mapping of macrophytes on species level every third year, preferably by divers (European Commission 2000). Global change affects the environmental conditions rapidly. Therefore, Palmer et al. (2015) recommend more frequent observations of freshwater lakes to detect changes in water quality at an early stage. Remote sensing offers a time- and cost-effective method to support monitoring approaches including those recommended by the WFD. Due to its capability to deliver information at high spatiotemporal resolution, remote sensing methods offer the potential to observe detailed seasonal changes in macrophyte distribution and water quality (George 1997, Malthus and George 1997, Dekker et al. 2002, Pinnel et al. 2004, Giardino et al. 2007, Yuan and Zhang 2008, Wolf et al. 2013, Roessler et al. 2013a, Dörnhöfer and Oppelt 2016b). It can complement hitherto *in situ* data collection along transects by divers and is suggested for closing the gap between the snapshots of *in situ* mappings of the WFD (Malthus and Karpouzli 2003, Palmer et al. 2015). It is expected that a high revisiting frequency may compensate the information loss compared to *in situ* mapping by divers.

Annual variations of different environmental parameters such as water clarity, temperature, sediment quality and nutrient loading are well known factors controlling the

distribution and phenologic development of submersed macrophyte populations (Barko and Smart 1986, Barko et al. 1991, Madsen and Brix 1997, Squires and Lesack 2003, Zhu et al. 2008, Shuchman et al. 2013, Hoffmann et al. 2014, Singh and Singh 2015). For several years, these natural variations have been superimposed by continuously increasing mean annual water temperatures, higher frequencies of heavy rain events, and prolongations as well as other temporal shifts of growing seasons. These effects are attributed to climate change and can be accompanied by the sprawl of some endemic macrophyte species such as *Najas marina* (Hoffmann et al. 2013, Hoffmann and Raeder 2016) and invasions of non-native species, both of which can potentially change ecosystem functioning.

For a successful macrophyte monitoring by satellite remote sensing, several challenges above and below the water surface have to be overcome to obtain reliable spectral information of the littoral bottom coverage (Mertes et al. 1993, Bostater et al. 2004, Morel and Belanger 2006). Below the water surface, the received signal is influenced by the overlaying water column and refraction. The radiative transfer is affected by suspended and dissolved materials in the water column and the water itself (Mumby et al. 1998, Mobley 1999, Silva et al. 2008). Littoral bottom coverage with sediment and macrophytes differs from lake to lake. In addition, annual as well as seasonal changes strongly affect the signal. Malthus and George (1997) used airborne remote sensing systems to differentiate between floating-leafed and emergent macrophyte species. Additional *in situ* spectrometer data by Pinnel et al. (2004) suggested a potential differentiation of bottom substrates as well as a possible discrimination among high growing macrophytes on species level using HyMap data at Lake Constance, Germany. Giardino et al. (2007) investigated macrophyte colonization patches and distribution within one growing season at Lake Garda, Italy, by combining Multispectral Infrared and Visible Imaging Spectrometer (MIVIS) and ex-situ spectral information. Heblinski et al. (2011) documented spatial vegetation dynamics of Lake Sevan, Armenia, with algorithms that can differentiate bottom coverage types as well as several macrophyte species and sediment types. To exclude the influence of the water column and water depth, Roessler et al. (2013a) and Fritz et al. (2017a) used a method of depth-invariant indices to differentiate between bottom substrates. *In situ* reflectance spectra of littoral bottom coverage (e.g.,

macrophytes or sediments) are very helpful to control atmospheric and water column corrections of remote sensing data and to distinguish macrophyte signal from water column attenuations (Pinnel 2007, Silva et al. 2008, Heblinski et al. 2011).

The information extraction in water related to remote sensing is primarily based on the evaluation of spectral signatures. The vegetation/sediment ratio and the different phenologic stages within the growing season control the spectral response. At the beginning of the growing season, the spectral response, even of sparsely vegetated areas, is sediment-dominated. Organic material on the lake bottom such as epiphytes and detritus may alter the spectral response of bare sediment (Armstrong 1993, Fyfe 2003, Williams et al. 2003, Silva et al. 2008, Wolf et al. 2013). During the growing season, changes in macrophyte/sediment coverage ratio, leaf size and orientation, leaf pigment concentrations and cellular structure specifically influence intensity and shape of spectral signatures (Fyfe 2003, Silva et al. 2008, Wolf et al. 2013). The maximum in macrophyte bottom coverage and biomass content heralds the senescence phase. During this period, the spectral signature is affected by degrading Chlorophyll a (Chl-a) content in ageing leaves (Gausman 1984, Gitelson et al. 2002) and the change of canopy structure by collapsed macrophytes (Silva et al. 2008, Wolf et al. 2013). Knowledge about the development pattern of the investigated macrophyte species during the growing season is required for the envisaged differentiation on species level by means of remote sensing (Pinnel et al. 2004, Wolf et al. 2013). Therefore, detailed information of the species composition and canopy structure of the macrophytes at the sampling dates are required (Hestir et al. 2008). Pinnel (2007) and Wolf et al. (2013) analysed *in situ* spectral signatures of various submersed macrophyte species (*Chara* spp., *Elodea nuttallii*, *Najas marina*, and *Potamogeton perfoliatus*) in different lakes in the Alpine foreland to detect spectral variations during the growing season. From these studies (Pinnel 2007, Wolf et al. 2013), we learn that the phenologic development within the year and the related spectral signatures are species-specific and deliver a phenologic fingerprint, an approach successful applied in forestry for forest tree species identification, if recorded continuously (Elatawneh et al. 2014, Stoffels et al. 2015).

In the long-term concept for a submersed macrophyte monitoring system for freshwater lakes, the spectral and temporal information is provided by *in situ* measurements. This information needs to be transferred to high resolution satellite systems such as Sentinel-2 type systems. For this task two main processing steps are required: first, the calculation of the expected spectra for the date and imaging time of the remote sensing system (database output of the species specific phenologic model); and, second, the inversion of bio-optical models adapted from of the extracted database spectra, delivering water contents and littoral bottom substrate distribution, showing macrophyte patches down to the species level. When completed, the system allows a trophic status determination of freshwater lakes.

The environmental conditions of the respective growing season cannot be reconstructed precisely. As an important variable influencing the growth pattern of submersed macrophytes (Madsen and Brix 1997, Zhu et al. 2008, Shuchman et al. 2013, Hoffmann et al. 2014, Singh and Singh 2015), water temperature was chosen in this study. The effect of sediment quality on macrophyte growth (Barko and Smart 1986, Barko et al. 1991, Squires and Lesack 2003) was beyond the scope of this study, mainly because the same patches were analysed for both years. A previous study by Wolf et al. (2013) already demonstrated the phenologic pattern changes within the growing season. However, that study did not link spectral patterns with temperature effects and it did not apply a modelling approach for phenologic and seasonal comparisons.

The primary objectives of this study therefore were to investigate: (1) whether temporal patterns of phenologic development phases facilitate species differentiation on base of spectral signatures, applying the identical sample design and instrumentation as Wolf et al. (2013); (2) whether annual water temperature oscillations affect species-specific growth of submersed macrophytes; and (3) if native and invasive species have different tolerance to an increase in water temperature.

3.3 Materials and Methods

3.3.1 Study site

The study site is located in the northern part of Lake Starnberg near the town Starnberg (47.9° N, 11.3° E), situated 25 km south of Munich in Southern Germany (**Figure 3.1**). The current state of the lake is oligotrophic Arle et al. (2013). With a surface area of 56.4 km² and a maximum depth of about 127 m, Lake Starnberg is Germany's fifth largest lake (Wöbbecke et al. 2003). At this test site, populations of three coexisting macrophyte species were measured within the growing seasons of 2011 and 2015. The invasive species *Elodea nuttallii* as well as the two indigenous species *Chara* spp. and *Potamogeton perfoliatus* were investigated. The test site *Chara* is covered by *Chara aspera* (80%), *Chara delicatula* (10%) and *Chara intermedia* (10%). The 3 test sites are pure stands, one for each species. During both growing seasons, all measurements were taken at exactly the same positions. The water temperature of Lake Starnberg is continuously monitored by Bavarian Environmental Agency (Bavarian Environmental Agency 2016) every hour at the study site in the northern part of the lake.

Monthly water temperatures of Lake Starnberg are displayed for 2011 and 2015 (**Figure 3.2**). In 2015, mean monthly water temperatures were higher in January (+0.7 °C), February (+0.9 °C), March (+0.9 °C), July (+2.4 °C) and August (+1.5 °C) compared to 2011. The remaining 7 months (April (−1.2 °C), May (−1.1 °C), June (−0.9 °C), September (−1.8 °C), October (−1.3 °C), November (−0.3 °C) and December (−0.1 °C)) had lower values than in 2011. In summary, the beginning of 2015 was warmer (January to March), while the spring temperatures were lower (April to June). During the main growing season in July and August, the temperatures in 2015 were higher. In contrast, 2011 had warmer autumn temperatures (September and October). Overall, the mean water temperature in 2015 was +0.05 °C higher.

Figure 3.1. Study site at Lake Starnberg. Measurement points of macrophyte test sites (red: *Chara*, blue: *E. nuttallii*, green: *P. perfoliatus*) and water temperature (yellow) (Google Earth Imagery, Image 2017 Landsat/ Copernicus). Landsat 8 true-color composite (acquisition date: 7 April 2014; data source: USGS).

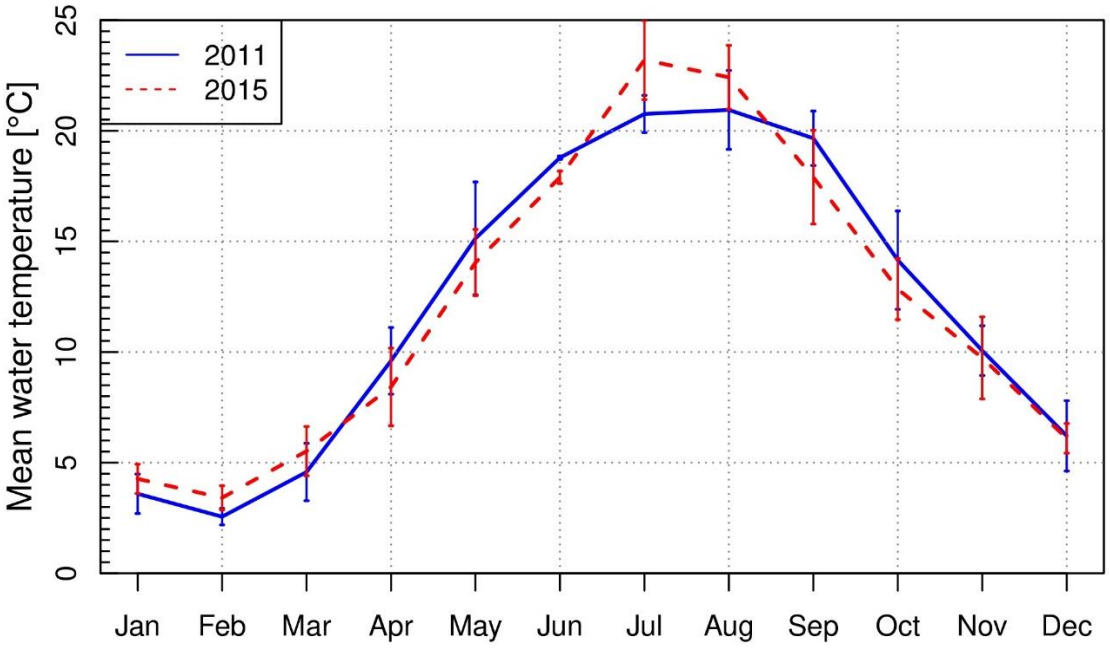

Figure 3.2. Monthly mean water temperature and standard deviation at Lake Starnberg in 2011 and 2015.

3.3.2 *In situ* measurements

During the growing seasons of 2011 and 2015, remote sensing reflectance spectra of pure stands of three macrophyte species were recorded systematically at the same study site and with the same measurement setup to cover different phenologic stages. The setup was performed on a jetty (**Figure 3.3**). With the aid of an extension arm a distance of 3 m between sensors and jetty was maintained. This stationary setup avoided drifting as well as shading and neighbourhood effects due to an optimal sun-object-sensor geometry. The measurement setup consisted of three submersible RAMSES spectroradiometers (ACC-VIS and ARC-VIS; spectral range: 320 nm to 950 nm; TriOS Mess- und Datentechnik GmbH, Rastede, Germany) (TriOS 2016) and an underwater camera system (Canon PowerShot G10, Canon, Tokyo, Japan). The camera was used to monitor the sensor position and to document the bottom coverage of the measurement spot by live stream. The downwelling and upwelling hemispherical irradiance (E_d and E_u) as well as the upwelling radiance L_u (with a field of view of 7°) were collected simultaneously within a range of 320 nm to 950 nm in 3.3 nm intervals. The data collection took place above sediment surface (depth b) before appearance of vegetation as well as just beneath the

water surface (depth 0). During the plant growing period, the measurements at depth b were done above the macrophyte canopy. The distance between sensors and plant canopy respectively sediment was always 45 cm. The sensor depth in relation to the water surface was documented with a measuring tape fixed to the extension arm.

In both years, field campaigns were planned approximately every 3 weeks under cloud free conditions. The measurements at each single day were designed to start in the morning hours and to last until late afternoon. During the main growing season from mid-June to mid-September, sun position 1.5 h before and after noon in mid-September (Central European Time) was defined as the reference sun-zenith angle which should be captured by all daily measurement series. Under optimum conditions, up to 7 datasets per day and macrophyte patch were registered. The repetitions were conducted at the same places for each species. Each dataset consisted of 20 replicates within 3 min at the same fixed place and depths. For stable conditions, measurements in depth b and depth 0 were passed in quick succession.

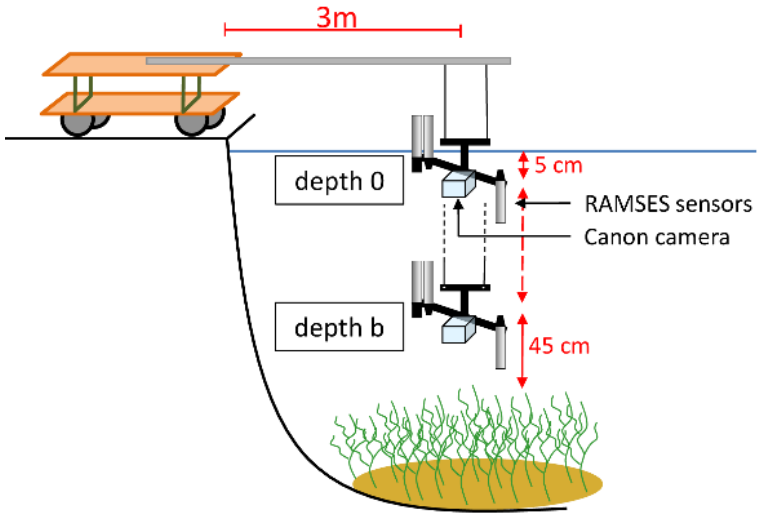

Figure 3.3. Measurement setup of *in situ* data collection (modified from Wolf et al. (2013)).

3.3.3 Data processing

The data processing chain was developed with Python (version 2.7.8, Python Software Foundation, Delaware, USA). For each dataset, the remote sensing reflectance spectra R_{rs}(b) and R_{rs}(0) of the two depths (depth b and 0) were calculated for 20 measurements

of E_d and L_u (Mumby et al. 1998). Afterwards, the spectra were smoothed by Savitzky–Golay filter of length 5 (Savitzky and Golay 1964). For each of the 20 measurements of the dataset, the median was calculated. In line with Pinnel (2007) and Wolf et al. (2013) the spectra were cropped to a range of 400 to 700 nm to exclude strong sensor noise. R_{rs}(b) spectra above the canopy or sediment surface had to be corrected to eliminate the influence of the remaining water column of 45 cm between sensors and object. The water column correction was according to absorption models for phytoplankton (Bricaud et al. 1995) and colored dissolved organic matter (Gitelson et al. 2002), to backscattering models for phytoplankton (Brando and Dekker 2003) and non-algal particles (Giardino et al. 2012), as well as absorption and backscattering coefficients of water and to the radiative transfer model of Albert and Mobley (2003). For calculating the required water constituent concentrations (Chl-a), colored dissolved organic matter (cDOM) and suspended particulate matter (SPM) were derived by an inversion of the diffuse vertical attenuation coefficient for downwelling irradiance K_d as implemented in the water colour simulator WASI (Gege 2004, Gege 2014b). The attenuation coefficient K_d was calculated with the method of Maritorena (1996) by using E_d measurements in two different depths (b and 0) at the same spot.

3.3.4 Reflectance model

The corrected *in situ* R_{rs}(b) spectra were used to create a model of remote sensing reflectance intensities. The reflectance model was a database model calculated in R (version 3.0.3, R Core Team, Vienna, Austria.) (R Core Team 2014). To cover the complete vegetation season as well as the differing sun heights, the collected remote sensing reflectance data had to be interpolated. A method for linear interpolation of irregular gridded data was applied (R package akima (Akima et al. 2013), R package stats (R Core Team 2014)). The interpolation was carried out in two consecutive steps. First, a linear interpolation of the reflectance along the sun zenith angles for each measurement day was performed in steps of 1°. In the second step, reflectance intensities of the measurement days along the year were interpolated for each sun zenith angle separately. The model is limited to wavelengths from 400 nm to 700 nm and to sun zenith angles from 25° to 65°.

Due to strong absorption of water in the near-infrared wavelengths the characteristic spectral features normally are superimposed by water absorption (Armstrong 1993). Hence, several surface models of reflectance intensities could be processed for each sun zenith angle. For each of the species sampled in the database, a spectrum can be produced together with confidence intervals.

3.3.5 Species-specific R_{rs} spectra

Out of the species-specific reflectance models, time series with an interval of 2 weeks and the same sun zenith angles were extracted for each species. The spectral responses on the appropriate dates of the investigated years were compared within the complete wavelength range. For the comparison of phenologic development of the different species, the 1st derivation of the R_{rs} spectra were calculated within the wavelengths 550 nm and 650 nm. The species were analysed for August because for this month the vegetation maximum and the greatest temperature effects were expected.

3.3.6 Classification process

The classification was based on the spectral libraries and was conducted with simulated spectra as derived from the reflectance model and followed a stepwise classification process chain (Wolf 2014) (**Figure 3.4**). For each classification level, a linear discriminant analysis was conducted and the spectrum was assigned to the best matching class. This procedure was conducted and repeated consecutively for each classification step. In the process, input spectra were adjusted to R_{rs} spectra in the spectral database with systematic measurements of 2010, 2011 and 2015 at Lake Starnberg. To facilitate the classification process, a pre-selection was conducted based on the date of the input spectra. The classification process was divided in four steps. Classification Step 1 was a separation in one of the categories: plant, sediment, plant/sediment, plant/water and water. Water and sediment were already final classes. Step 2 was assigning plant spectra of Step 1 to one of the macrophyte classes (*Chara* spp., *E. nuttallii* and *P. perfoliatus*). In Step 3 the species spectra were assigned to a phenologic stage. Step 4 was independent of Steps 2 and 3. In this step, input spectra classified as plant/sediment in Step 1 were

attributed to defined species and phenologic stage. If the input spectrum was classified as plant/water in Step 1, this was assigned to tall growing species *P. perfoliatus*. Spectra with ambiguous phenologic stages were assigned to "no stage classifiable". The validation of this classification method was performed with data from 2010 and 2011; the overall accuracies were calculated for each single classification step separately.

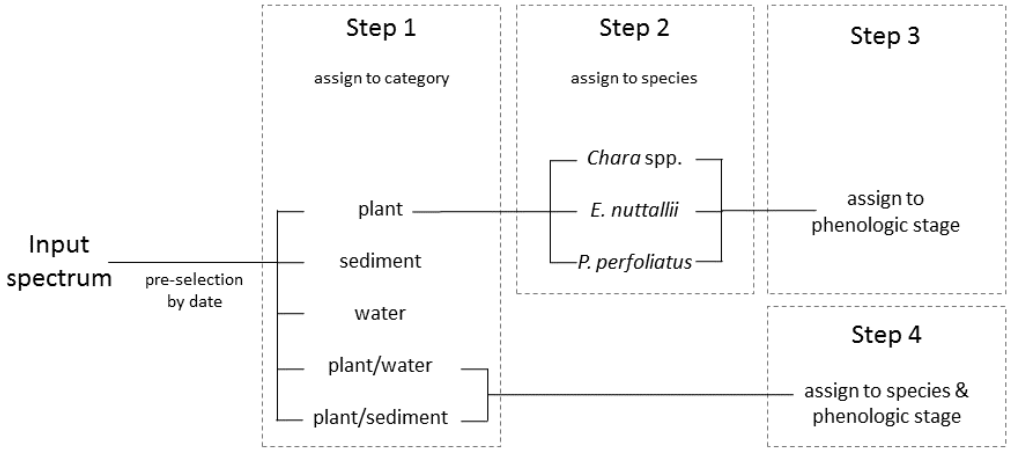

Figure 3.4. Schematic diagram of the stepwise classification after Wolf (2014).

With this classification process chain, four main phenologic stages were distinguished. Stage 0 declares pure sediment, and Stage 1 sparsely vegetated sediment. Stage 2 describes a fully grown and upright standing vegetation. If the vegetation is already degrading and collapsing, it is classified as Stage 3. Differing subdivisions within one classification stage are attributed to varying bottom coverage and height of the macrophyte canopy.

3.4 Results

3.4.1 Reflectance model

The reflectance models and the species-specific spectral response revealed clear differences between seasonal dates and phenologic stages. Spectral properties could be linked with diverse phenologic stages. A classification on species level and phenologic information revealed differences in accuracy for the different species. The highest

accuracy was obtained for the test sites *Chara* (no misclassification on species level) and *P. perfoliatus* (two misclassifications on species level).

Reflectance models for 2011 and 2015 were simulated with linear interpolation method for the three macrophyte species *Chara* spp., *E. nuttallii* and *P. perfoliatus* separately (**Figure 3.5**). Depending on the first and last measurement day of the season, the models covered different time periods. For each species, the sun zenith angles were the same in both years. Variations of R_{rs} within a year could be observed. Overall, R_{rs} showed higher intensities at the beginning of the year. The intensities in the blue wavelength region (400 nm to 490 nm) were lower, the ones in green (490 nm to 560 nm) higher. A local reflectance minimum at around 680 nm could be observed for all sites and species. A difference in shape and intensity between both years and between the different species was obvious. However, a general trend could be observed for all species. The reflectance intensities decreased from May to August, followed by an increase towards the end of the growing season in September.

3.4.2 Species-specific R_{rs} spectra

R_{rs} spectra of different dates within the growing season of three macrophyte species were displayed side by side with top of view photographs of the test sites (**Figure 3.6** - **Figure 3.8**). The spectra were simulated with the linear interpolation model. For 2011 and 2015, R_{rs} was plotted for same dates with in an interval of 10 days for the same sun zenith angle of each species. R_{rs} spectra covered wavelengths from 400 nm to 700 nm. The photos for documentation were recorded at the sampling days and do not show the situation at the day and daytime for which the spectra were simulated.

3.4.2.1 Test site *Chara*

The simulated R_{rs} spectra of *Chara* spp. revealed the situation at a sun zenith angle of 35° in the afternoon from May (**Figure 3.6**a) to September (**Figure 3.6**e). In May (**Figure 3.6**a), the spectra of both years revealed a similar shape for the simulated days, differing in R_{rs} intensity. The R_{rs} intensity increased from 400 nm to 550 nm, followed by a plateau until 650 nm. Afterwards, R_{rs} intensity deceased, resulting in a local minimum at 680 nm.

Within the year, the shape formed a maximum at about 570 nm, the minimum at 680 nm was more distinct (**Figure 3.6**b - **Figure 3.6**d). Throughout August (**Figure 3.6**d), a difference in the phenologic development could be observed. Both shape and bottom coverage varied in the investigated years. The shape of 2015 clearly flattened in yellow and orange wavelength regions between 560 nm and 650 nm. This trend could be observed in September (**Figure 3.6**e) for both years.

3.4.2.2 Test site *P. perfoliatus*

The simulated R_{rs} spectra of *P. perfoliatus* were modelled with linear interpolation method and represented the situation from May (**Figure 3.7**a) to September (**Figure 3.7**e) at a sun zenith angle of 27° in the afternoon. In May (**Figure 3.7**a), the shapes of both years increased from 400 nm to 600 nm and a distinct local minimum at 680 nm was evident. In June (**Figure 3.7**b) and July (**Figure 3.7**c), a maximum at 570 nm was observed. In August (**Figure 3.7**d) and September (**Figure 3.7**e) differences in the species-specific development could be detected. In the investigated years, shape, bottom coverage and canopy structure varied. In August (**Figure 3.7**d), the maximum was evident in 2015. The shape of 2011 was flattened without a clear maximum. Flattened and compressed spectra in yellow and orange wavelengths (560 to 650 nm) were shown in 2015 in September (**Figure 3.7**e). The spectra of 2011 still revealed a distinct maximum in the green region.

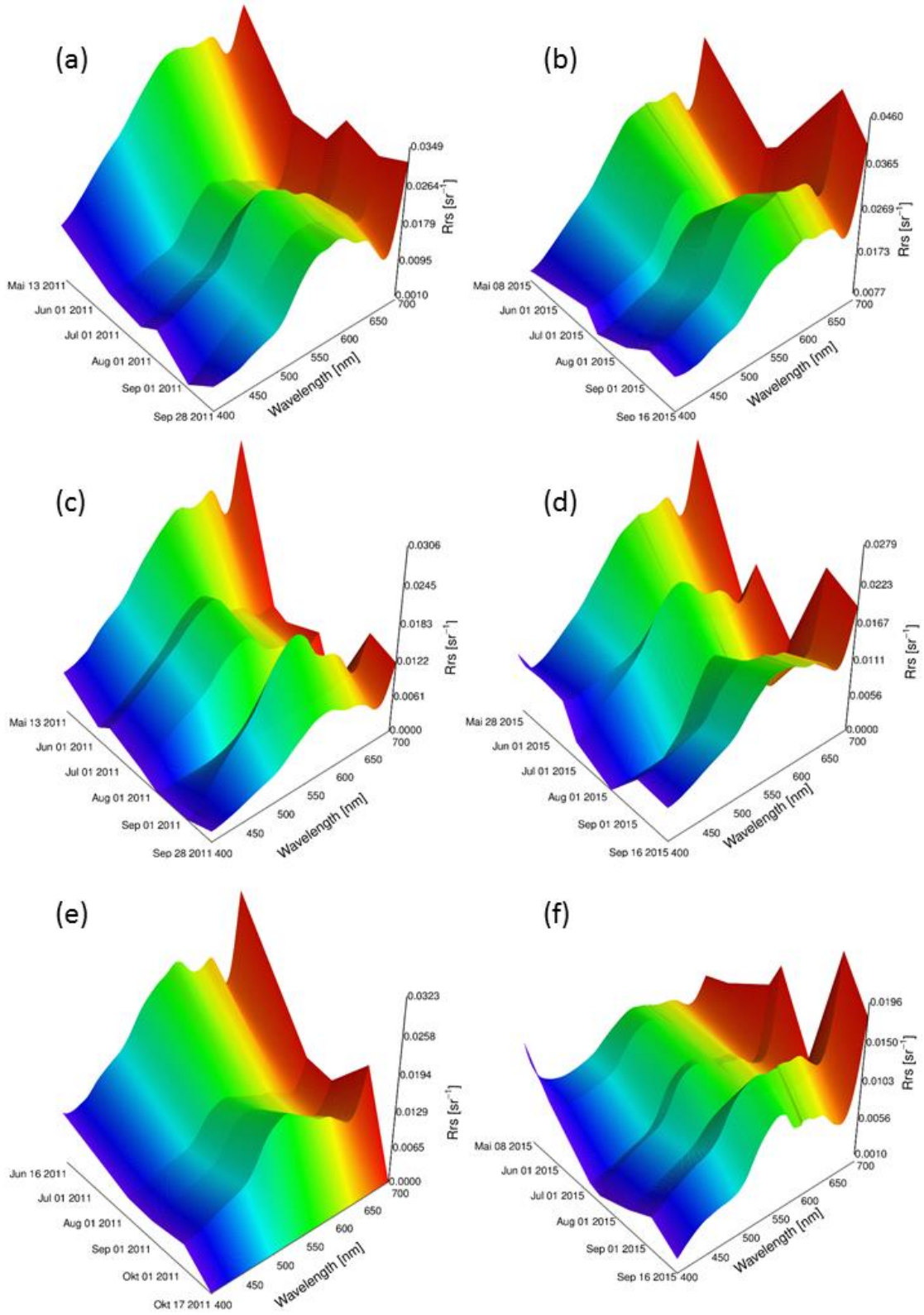

Figure 3.5. Reflectance models of three macrophyte species for 2011 and 2015. *Chara* spp. for sun zenith angle 35° in: (**a**) 2011; and (**b**) 2015; *P. perfoliatus* for sun zenith angle 27° in: (**c**) 2011; and (**d**) 2015; and *E. nuttallii* for sun zenith angle 31° in: (**e**) 2011; and (**f**) 2015.

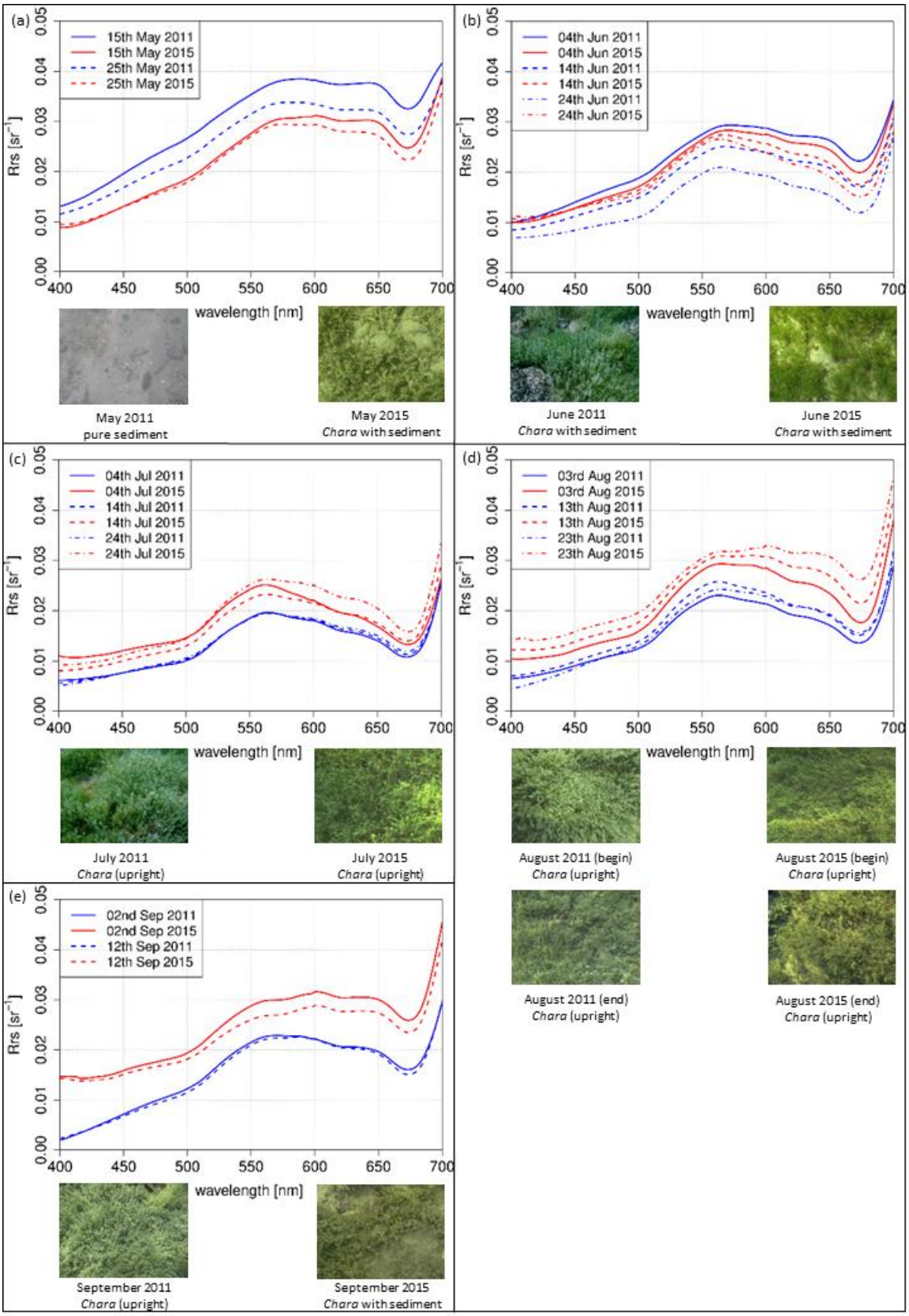

Figure 3.6. Simulated R_{rs} intensities of *Chara* spp. modeled with a linear interpolation method of 2011 (blue) and 2015 (red). Top view photos of the investigated test sites of the sampling days: (**a**) May; (**b**) June; (**c**) July; (**d**) August; and (**e**) September.

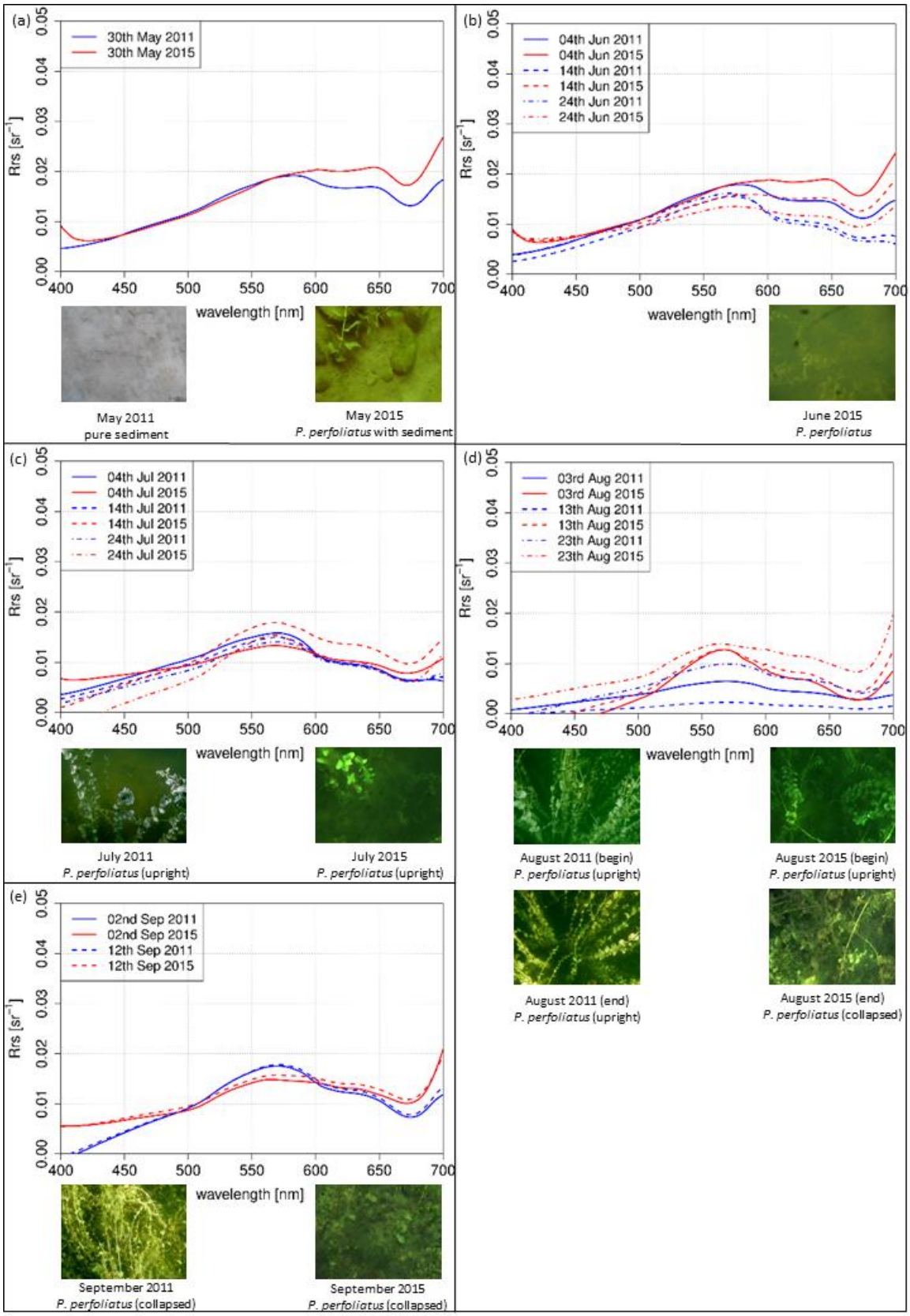

Figure 3.7. Simulated R_{rs} intensities of *P. perfoliatus* modelled with a linear interpolation method of the years 2011 (blue) and 2015 (red). Top view photos of the investigated test sites of the sampling days. (a) May, (b) June, (c) July, (d) August, (e) September.

3.4.2.3 Test site *E. nuttallii*

The simulated R_{rs} spectra of *E. nuttallii* from May (**Figure 3.8**a) to September (**Figure 3.8**e) were calculated with linear interpolation method for a sun zenith angle of 31° in the afternoon. In May (**Figure 3.8**a) completely different shapes were evident for both years. The shape of the spectral curve in 2011 increased continuously. In June (**Figure 3.8**b) the spectra of 2011 displayed a continuous increase up to 560 nm followed by a plateau. Local minima were at 620 nm and 680 nm. In contrast, the simulated R_{rs} intensity of 2015 had a distinct maximum in the green region. In July (**Figure 3.8**c) the shapes in July were similar in both years, with a distinct maximum in the green wavelengths. Similar results were observed for August (**Figure 3.8**d), with a trend to flatten in the yellow and orange wavelength regions. In September (**Figure 3.8**e) the shapes were quite similar in both years with a distinct maximum in the green and lower intensity values in the blue and red regions, representing a vital and upright standing vegetation as confirmed by the photos.

3.4.2.4 Water temperature effect on species-specific growth

The first derivation of *in situ* R_{rs} spectra reflected the variations of the gradient between the investigated species within August (**Figure 3.9**). The species-specific variations differed in the different years. *E. nuttallii* showed slight variations of the gradient within months and between both years in this wavelength range. Clear differences between both years were observed for the indigenous species *Chara* spp. and *P. perfoliatus*. Overall, the gradient in 2011 was lower. The monthly variations of the gradient were higher in 2015, especially in the wavelength range between 570 nm and 610 nm. In this year, the mean water temperatures were higher during main growing season in July and August (**Figure 3.2**).

3.4.3 Spectral classification on species level

The classification results revealed a continuous succession of phenologic stages for the test site *Chara* (**Table 1**). The overall accuracy of Step 1 was 70%, and of Step 2 82%. The

accuracy of the assignment to a phenologic stage was between 79% (*E. nuttallii*) and 91% (*Chara* spp.).

The growing season is starting with sediment (2011) and plant/sediment (2015) spectra in May, followed by plant/sediment (2011) and plant (2015) spectra in June and July. In 2011, an interruption of the phenologic succession could be observed on 14 July, 24 July and 3 August. For the test site *P. perfoliatus*, a continuous succession of phenologic stages could be observed for both years. In 2011, the succession was interrupted on 3 and 13 August. The test site *E. nuttallii* showed several irregularities in both years. In 2011, one misclassification took place on 4 June. The other spectra were classified as plant/sediment or sediment consistently. Due to the small spectral differences, no classification on species level was possible at the test site *E. nuttallii.* In 2015, irregularities in the phenologic succession could be located on 4 June, 14 June and 24 July.

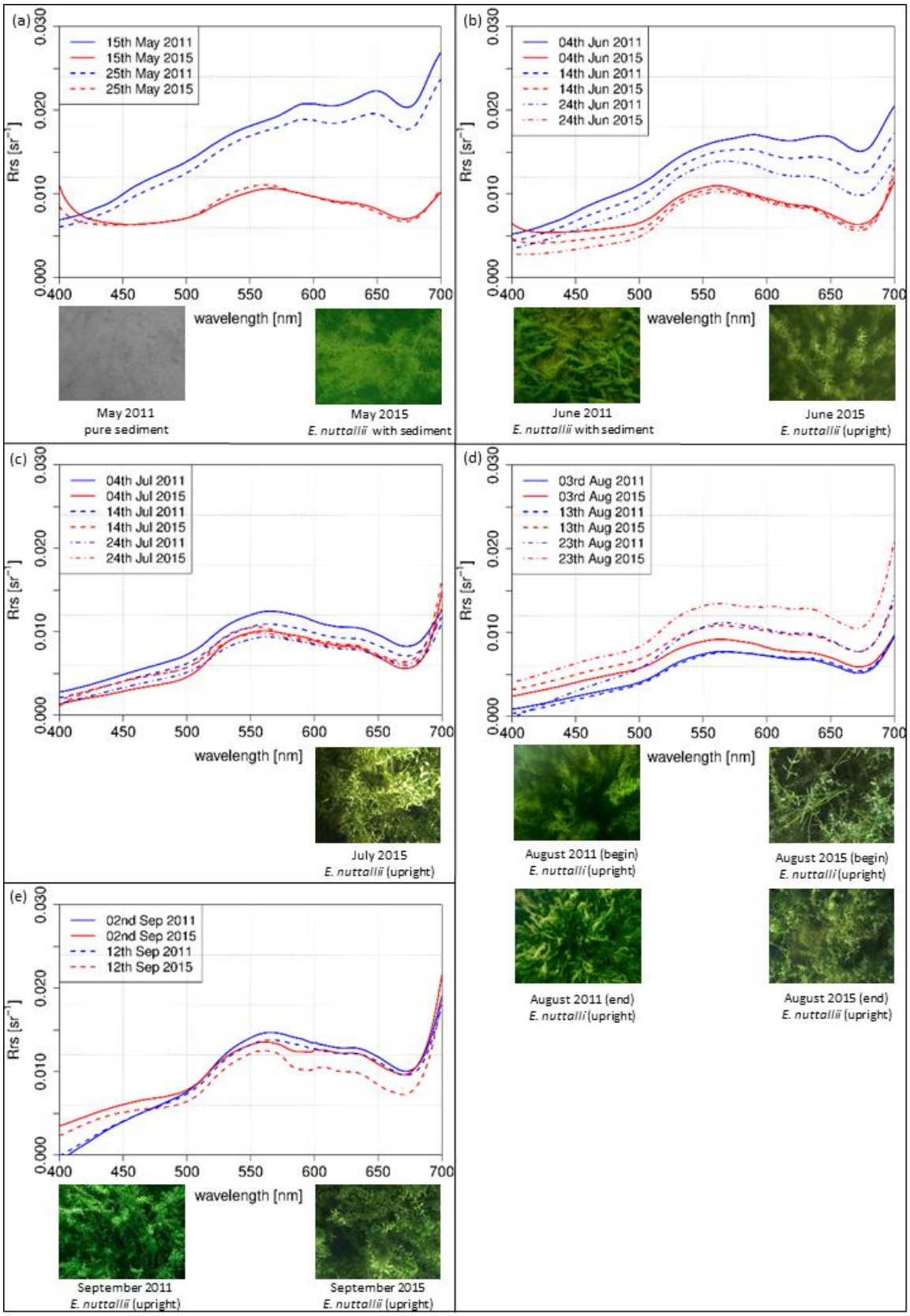

Figure 3.8. Simulated R_{rs} intensities of *E. nuttallii* modelled with a linear interpolation method of 2011 (blue) and 2015 (red). Top view photos of the investigated test sites of the sampling days: (**a**) May; (**b**) June; (**c**) July; (**d**) August; and (**e**) September.

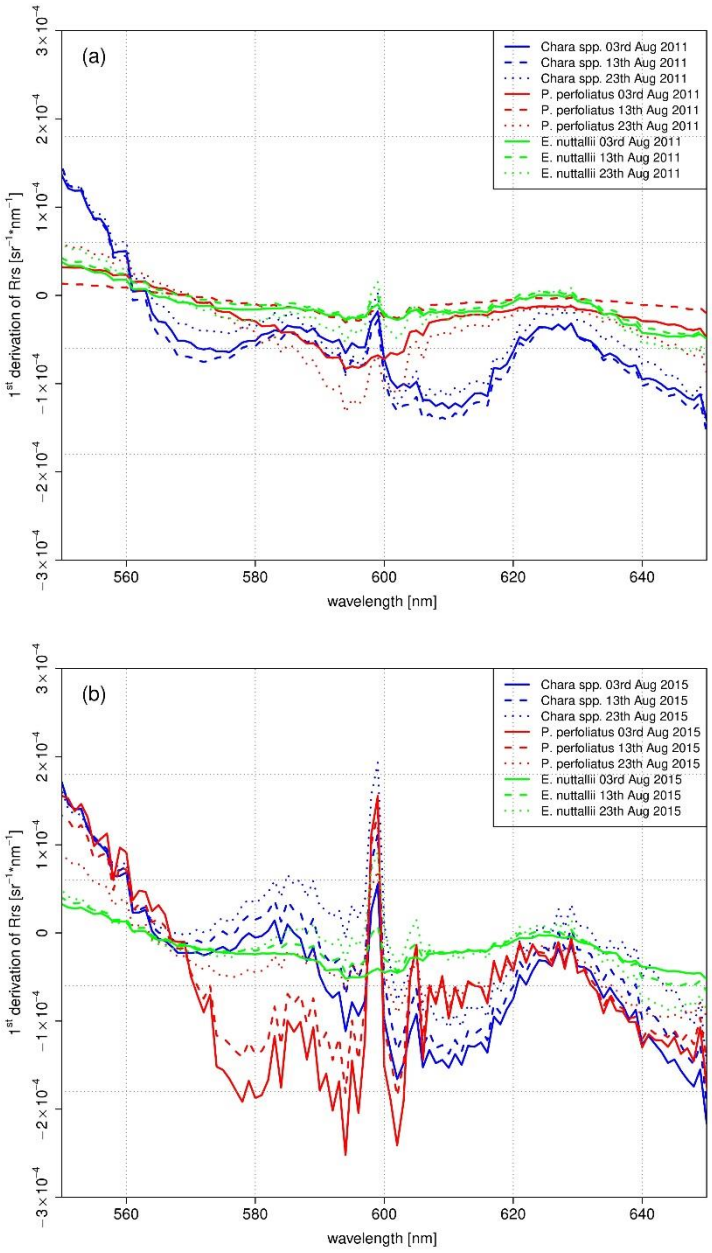

Figure 3.9. 1st Derivation of *in situ* R_{rs} spectra of: August 2011 (**a**); and August 2015 (**b**), in a wavelength range between 550 nm and 650 nm.

Table 3.1. Results of the stepwise classification after Wolf (2014) for *Chara* spp., *E. nuttallii* and *P. perfoliatus*.

Date	Test site	Test site	Test site	Test site	Test site	Test site
	***Chara* 2011**	***Chara* 2015**	***P. perfoliatus* 2011**	***P. perfoliatus* 2015**	***E. nuttallii* 2011**	***E. nuttallii* 2015**
15 May		100% plant/sediment	-	-		99.99% plant
	100% sediment	100% *Chara* spp. 1.1	-	-	100% sediment	100% *E. nuttallii*
						100% *E. nuttallii* 2.1
25 May						100% plant
		100% plant/sediment	30 May	30 May		100% *E. nuttallii*
	100% sediment	100% *Chara* spp. 1.2	100% sediment	100% sediment	100% sediment	
						100% *E. nuttallii* 2.1
4 June		100% plant/sediment	100% plant/water		100% plant/sediment	100% plant/water
	100% sediment	100% *Chara* spp. 1.2	100% *P. perfoliatus* 1	100% sediment	100% *Chara* spp. 1.2	100% *P. perfoliatus* 1
14 June	100% plant/sediment	100% plant/sediment	100% plant/water	100% plant/water	100% plant/sediment	100% plant/sediment
	100% *Chara* spp. 1.2	100% *Chara* spp. 1.2	100% *P. perfoliatus* 1	100% *P. perfoliatus* 1	no stage classifiable	no stage classifiable
24 June		100% plant	100% plant/water	100% plant/water	100% plant/sediment	100% plant
	100% plant/sediment	100% *Chara* spp.	100% *P. perfoliatus* 1	100% *P. perfoliatus* 1	no stage classifiable	100% *E. nuttallii*
	100% *Chara* spp. 1.2	100% *Chara* spp. 2				100% *E. nuttallii* 2.2
4 July		100% plant	100% plant/water	100% plant/water	100% plant/sediment	100% plant
	100% plant/sediment	100% *Chara* spp.	100% *P. perfoliatus* 1	100% *P. perfoliatus* 1	no stage classifiable	100% *E. nuttallii*
	100% *Chara* spp. 1.2	100% *Chara* spp. 2				100% *E. nuttallii* 2.2

14 July	100% plant/sediment 100% *Chara* spp. 1.1	100% plant 100% *Chara* spp. 100% *Chara* spp. 2	100% plant 100% *P. perfoliatus* 100% *P. perfoliatus* 2	100% plant/water 100% *P. perfoliatus* 1	100% plant/sediment no stage classifiable	100% plant 100% *E. nuttallii* 100% *E. nuttallii* 2.2
24 July	100% plant/sediment 100% *Chara* spp. 1.1	100% plant 100% *Chara* spp. 100% *Chara* spp. 2	100% plant 100% *P. perfoliatus* 100% *P. perfoliatus* 2	100% plant/water 100% *P. perfoliatus* 1	99.99% plant/sediment no stage classifiable	100% plant 100% *E. nuttallii* 100% *E. nuttallii* 3
3 August	99.91% plant/sediment 100% *Chara* spp. 1.1	100% plant 100% *Chara* spp. 100% *Chara* spp. 2	100% plant 99.48% *E. nuttallii* 100% *E. nuttallii* 2.3	100% plant 100% *P. perfoliatus* 100% *P. perfoliatus* 2	99.82% plant/sediment no stage classifiable	100% plant 100% *E. nuttallii* 100% *E. nuttallii* 2.3
13 August	89.58% plant/sediment no stage classifiable	99.99% plant 100% *Chara* spp. 100% *Chara* spp. 2	99.99% plant 100% *E. nuttallii* 100% *E. nuttallii* 2.3	100% plant 100% *P. perfoliatus* 100% *P. perfoliatus* 2	99.99% plant/sediment no stage classifiable	99.99% plant 100% *E. nuttallii* 100% *E. nuttallii* 2.3
23 August	99.90% plant/sediment no stage classifiable	100% plant 100% *Chara* spp. 100% *Chara* spp. 3.1	99.99% plant 99.98% *P. perfoliatus* 100% *P. perfoliatus* 3.1	100% plant 100% *P. perfoliatus* 100% *P. perfoliatus* 3.1	100% plant/sediment no stage classifiable	99.99% plant 100% *E. nuttallii* 100% *E. nuttallii* 2.3
2 September	100% plant/sediment no stage classifiable	99.99% plant 100% *Chara* 100% *Chara* 3.1	100% plant 100% *P. perfoliatus* 100% *P. perfoliatus* 3.1	100% plant 100% *P. perfoliatus* 100% *P. perfoliatus* 3.1	100% plant/sediment no stage classifiable	100% plant 100% *E. nuttallii* 100% *E. nuttallii* 2.3
12 September	100% plant/sediment no stage classifiable	100% plant/sediment no stage classifiable	100% plant 100% *P. perfoliatus* 100% *P. perfoliatus* 3.1	100% 100% plant/water no stage classifiable	100% plant/sediment no stage classifiable	100% plant 100% *E. nuttallii* 100% *E. nuttallii* 2.3

3.5 Discussion

The main research question, whether *in situ* measured spectral variations within the growing season can be linked to phenologic stages of macrophyte populations, was confirmed by our results. An interrelation between macrophyte growth and water temperature was also demonstrated for the indigenous species *Chara* spp. and *P. perfoliatus*, but not for the invasive species *E. nuttallii*. The reflectance models developed based on the spectral signatures taken within the growing season and over the course of the day, proved to be able to mitigate gaps in *in situ* data collection (e.g., due to cloud coverage). The models deliver simulated spectra for each day and all sun positions of possible optical satellite data takes (approximate ±2 h around noon). The inversion of the models for *Chara* spp. and *P. perfoliatus* with the aim of macrophyte classification on species level is successful. Restricting the search period based on external information about the weather history of that season and giving an estimate of the phenologic development stage additionally improve the classification success. Especially in that direction, we expect further advances by linking the modelling runs for species identification with external information on extreme events such as drought or rainy periods.

3.5.1 Phenologic development in R_{rs} spectra and water temperature

The general phenologic development scheme we observed is similar for the investigated species in both investigated years. Phenologic development stages control the changes in spectral response within the growing season (Rooney and Kalff 2000, Wolf et al. 2013). Differing bottom coverage and species-specific structure elements like biomass, chlorophyll content, canopy height and alignment explain the variations of the shape of the spectra within the growing season. The species-specific phenologic development depends on the environmental conditions such as water temperature, water clarity, morphology and nutrient load (Blindow 1992, Rooney and Kalff 2000, Shuchman et al. 2013). To characterize the response of different macrophyte species to different

environmental conditions, the species-specific spectral signatures within two growing seasons within two growing seasons is most informative. Water temperature was the only relevant variable available for both years. It is well-known that freshwater lakes buffer air temperature changes very well, which is explained by their thermal properties. The effects are smoothed and result in delayed water temperature effects. Nevertheless, these temperature fluctuations affect the biologic activities in the lake, affecting growth processes of submersed macrophytes as well.

In our discussion, we concentrate on August because the maximum of vegetation development is expected and greatest temperature effects (both acutely and accumulated) are expected at this time point. The most significant changes were observed in the green to red wavelength region, on which we concentrate in our analysis.

For the test sites *Chara* (**Figure 3.6**d; **Figure 3.6**e) and *P. perfoliatus* (**Figure 3.7**d; **Figure 3.7**e) the flattened shape of the spectral signature in the yellow and orange wavelength region is interpreted as a variation in leaf pigment ratio (Sims and Gamon 2002, Wolf et al. 2013). The intraspecific variations are illustrated by the derivation of the spectra for August (**Figure 3.9**). Especially, a lower Chl-a content in ageing leaves induces such a shift in yellow and orange wavelengths (Gitelson and Merzlyak 1994, Sims and Gamon 2002). Higher water temperatures during the main growing season in July and August 2015 (**Figure 3.2**) may have resulted in a shortened growing season with earlier senescence (Barko and Smart 1981, Rooney and Kalff 2000). The earlier senescence is demonstrated by a flattened shape (550 nm and 650 nm) with a slight gradient (**Figure 3.9**). The change in bottom coverage ratio (**Figure 3.6**e) and macrophyte structure (**Figure 3.7**d) confirms the assumption that water temperature influences the length of growing season. The pictures clearly show the decrease of plant covered area as well as collapsed and degraded macrophytes, with both phenomena being connected to macrophyte degradation.

In contrast to the indigenous species, the species-specific development of the invasive species *E. nuttallii* reveals spectral differences at the beginning of the growing season (**Figure 3.8**a and **Figure 3.8**b). Higher water temperatures in the first quarter of 2015 (**Figure 3.2**) might explain induction of an earlier vegetation begin. During the main

vegetation time in July and August, neither the spectral shape nor the bottom coverage are affected by higher water temperatures (**Figure 3.9**). This might be attributed to the better adaption to higher water temperatures of *E. nuttallii* (McKee et al. 2002).

The interpretation of the measurements of the indigenous species *Chara* spp. and *P. perfoliatus* indicate a shortened growing season at warmer temperatures in 2015. For the test site *Chara*, the shape of the spectra on 13 August 2015 (**Figure 3.6**d) and 2 September 2011 (**Figure 3.6**e) are almost the same. Consequently, the growing season and phenologic stage in 2015 was about 20 days shorter for *Chara* spp. than in 2011. This result coincides with higher water temperature during the main growing season in July and August 2015. The observations for *P. perfoliatus* in 2015 are similar. The spectral signature reflects the beginning of macrophyte degradation already at the end of August, visible by a flattened signature curve especially in the yellow to red region of the spectra. Such a phenologic shift at the end of the growing season was not found in *E. nuttallii*. A shortened growing season for indigenous species might be linked to higher water temperatures. *E. nuttallii* is probably not affected due to a higher temperature tolerance compared to the investigated indigenous species (McKee et al. 2002).

3.5.2 Reflectance model

The developed reflectance models (**Figure 3.5**) provide species-specific spectral signatures throughout the complete growing season for every required sun position during a defined day. These protracted and detailed spectral pieces of information can strongly improve the knowledge of the seasonal variation of macrophyte species. The output spectra of these models provide a useful and necessary basis for bio-optical models such as BOMBER (Giardino et al. 2012) or WASI (Gege 2004, Gege 2014a).

The prediction limits are directly related to two variable groups: the daily and seasonal distribution of *in situ* measurements and the specific environmental frame conditions of the respective year. In case of the distribution of *in situ* measurements within the vegetation season there is a clear rule: the shorter the time-gaps between the *in situ* measurements, the more detailed are the reflectance models. With high probability, the

date of the vegetation maximum (e.g., maximum vegetation height and extension; highest biomass content) (Rooney and Kalff 2000) is between two sampling days and cannot be expected to be represented by the model. In addition, for the applied linear interpolation method, an extrapolation for situations before and after the beginning and end of the measurements series is not possible.

Environmental parameters such as water clarity, water temperature and nutrient load affect macrophyte expansion and phenologic development (Blindow 1992, Shuchman et al. 2013). Environmental parameters vary from year to year, affecting the prediction accuracy of the model outputs. The examined variable in this study, the water temperature, seems to trigger a variation in reflectance intensity and shape between the two investigated years (**Figure 3.5**a, **Figure 3.5**c, **Figure 3.5**e in contrast to **Figure 3.5**b, **Figure 3.5**d, **Figure 3.5**f). Further studies on the influence of light availability on the spectral variation might improve the accuracy of these reflectance models and the output spectra. In contrast, short-term events like draughts, floods or turbidity after an intense rainfall cannot directly be represented by the models. Such short-term and partial effects are highly different in different years. Due to the inertness and buffer action of freshwater lakes, these short-term events are attenuated and influence the models indirectly. We expect that this type of effects might be buffered and constrained by integration of external information into the inversion processes.

3.5.3 Model inversion for species level classification

The inversion of the reflection models with the aim of classifying macrophyte species and their phenologic stage for predefined daytimes and dates is successful. The inversion procedure delivers reliable spectra which we used for the comparison of phenologic development stages in 2011 and 2015. The analysis of the investigated macrophytes on species level (classification Step 2) based on phenologic development stages (**Table 1**) reveals an overall logic succession for the test sites *Chara* and *P. perfoliatus* for both investigated years.

The phenologic succession of *Chara* spp. was not accurately predicted for three dates in July and August 2011. The phenologic stage *Chara* spp. 1.1 induces a sediment proportion of 0.5 (Wolf 2014). One explanation is a temporary sediment deposition masking the plant canopy. Sediment cover inevitably will result in an apparently higher sediment fraction and accordingly higher signal intensity (Wolter et al. 2005).

In August 2011, a misclassification due to an interruption of the logic succession, on species level occurred for the test site *P. perfoliatus*. The *in situ* measurement and classification of single growing plants without a closed plant canopy is more difficult and error-prone than for dense populations (Sawaya et al. 2003). With the applied measurement setup, meadowy canopies such as *Chara* spp. allow a more stable spectral data collection resulting in a good to excellent classification success.

For the test site *E. nuttallii*, misclassification on species level occurred for 4 June in both years. A classification based on phenologic stages was not successful at all with the dataset for 2011. In 2015, the logic succession was interrupted. Slight water depth, shipping traffic, shading and a plant canopy up to the water surface hindered the *in situ* data collection which might explain the misclassifications at this test site.

The accuracy of the classification results depends on the number of spectra of the spectral database. To obtain more detailed information about species composition and canopy structure, several *in situ* measurements at different phenologic stages are required (Hestir et al. 2008). Spectral databases are able to provide day and daytime specific reference spectra of the lake bottom substrates. The knowledge of phenologic development related spectral response seems necessary when trying to improve the simulation and analysis of optical properties and light field parameters of deep and shallow waters in satellite datasets. This detailed information for the diverse phenologic stages of macrophytes are expected to improve the inversion success of bio-optical models such as BOMBER (Giardino et al. 2012) and WASI (Gege 2004, Gege 2014b). Such models presently are the most sophisticated methods for deriving optical properties and light field parameters of deep and shallow waters from satellite data. Such information is required for the monitoring of freshwater lakes and large water bodies in general as e.g., included in the

WFD. A further improvement of the prognosis accuracy of this evaluation chain is expected by steering the selection of the appropriated spectral signatures by e.g., detailed information about weather history of the respective growing season or the expected phenologic stage during data take.

3.6 Conclusions

Remote sensing methods offer a great potential to build up a monitoring system of submersed aquatic plants. A key requirement is the automatic discrimination of submersed macrophyte species. A spectral library with phenologic features as base for coupled growth and reflectance models seems essential for monitoring lake bottom substrates, especially for macrophytes. In the present study, the seasonal phenologic and spectral variability of aquatic plants at a test site at Lake Starnberg was investigated for 2011 and 2015. Water temperature was identified as one of the environmental driver explaining the phenologic shift by spectral signature analysis.

Investigations into the influence of the effects of small-scaled extreme weather conditions (e.g., light availability and turbidity) are highly recommended topics of future work. To improve the accuracy of the classification results, a large database is needed. Test sites are recommended in several lakes of diverse trophic states and on other macrophyte species, especially on potentially invasive species, to identify site-specific and species-specific variations of remote sensing reflectance. Further influences of the reflectance signal are related to periphyton coverage on macrophyte leaves.

4 Mapping development of submerged aquatic vegetation by using a Sentinel-2A time series at Lake Starnberg (Germany)

A similar version of this chapter was submitted: Fritz C., Dörnhöfer K., Schneider T., Geist J., Oppelt N. Mapping development of submerged aquatic vegetation by using a Sentinel-2A time series at Lake Starnberg (Germany).

4.1 Abstract

Submerged aquatic vegetation (SAV) plays an important role in freshwater lake ecosystems. Due to its sensitivity to environmental changes, several SAV species serve as bioindicators for the trophic state of freshwater lakes. Variations in water temperature, light availability and nutrient concentration affect SAV growth and species composition. To monitor the trophic state as regulated by the European Water Framework Directive (WFD), SAV needs to be monitored regularly. This study analyses and compares the results of littoral bottom coverage assessment using two different remote sensing based approaches, i.e. a semi-empirical method using depth-invariant indices and a physically based, bio-optical method using WASI-2D. For this, we analysed four Sentinel-2A scenes of Lake Starnberg acquired within the main growing season in August and September 2015. For a precise Sentinel-2 imaging by date and hour, satellite measurements were supported by lake bottom spectra delivered by *in situ* data based reflectance models. Both methods identified vegetated and non-vegetated patches in shallow water areas. Furthermore, tall- and meadow-growing SAV species can be differentiated. Both methods revealed similar results when focusing on the identification of sediment and SAV patches (R^2 from 0.5603 to 0.8137), but not for a differentiation on species level.

4.2 Introduction

Submerged aquatic vegetation (SAV) provides detailed information about the ecology of freshwater lakes (Melzer 1999). For instance, SAV is a highly suitable and often used bioindicator for trophic state assessments since it mirrors varying nutrient concentrations, water temperature, water level and water transparency (Skubinna et al. 1995, Melzer 1999, Penning et al. 2008, Søndergaard et al. 2010, Poikane et al. 2015). Changes in the trophic state induce variations in plant species composition, spatial distribution and extent, onset of SAV growth and senescence (Short and Neckles 1999, Rooney and Kalff 2000, Silva et al. 2008). According to the European Water Framework Directive (WFD) SAV should be mapped every three years (European Commission 2000). In consideration of the observed strong dynamics in SAV distribution and species composition, Palmer et al. (2015) even recommended more frequent observations. In contrast to conventional SAV monitoring by scientific divers, remote sensing offers a time- and cost-effective alternative to observe seasonal and annual changes in SAV coverage as an indicator of water quality (e.g. George 1997, Malthus and George 1997, Dekker et al. 2002, Pinnel et al. 2004, Giardino et al. 2007, Yuan and Zhang 2008, Wolf et al. 2013, Roessler et al. 2013a).

Using remote sensing data, the spectral signature is the primary information source for analysis of lake bottom surface types. The contributions of SAV and bare sediment for each pixel control the intensity of the spectral response. Organic overlay, such as detritus and epiphytes, additionally influences the spectral signature of sediment and SAV (Armstrong 1993, Fyfe 2003, Williams et al. 2003, Silva et al. 2008, Wolf et al. 2013). Furthermore, the spectral signature of SAV varies within the growing season. Variations in leaf size and orientation as well as pigment content and ratio lead to changes in shape and intensity of the spectral signature (Fyfe 2003, Silva et al. 2008, Wolf et al. 2013). Pigment degradation, especially of Chlorophyll-a, indicate leaf senescence (Gausman 1984, Gitelson et al. 2002, Wolf et al. 2013, Fritz et al. 2017b). Especially in case of tall-growing species, pigment decomposition processes are accompanied by structural changes such as the collapse of the canopy. These physiological plant characteristics, however, differ among SAV species. Therefore, Pinnel et al. (2004), Wolf et al. (2013), Fritz

et al. (2017b) and others suggested that a method capable of the different phenologic development stages of SAV may provide a valuable key for a refined taxonomic differentiation.

For identifying specific phenology-related characteristics in shallow water areas with remote sensing systems, high spatial, spectral and radiometric resolution data registered at high temporal frequency are mandatory. Analysing remote sensing data in a field-monitoring context additionally requires comparable data sets over time. Therefore, control and correction of external factors influencing the spectral signature of lake bottom types is necessary, i.e. changes in the atmosphere, within the water body and at the atmosphere/water interface. Different strategies exist to consider the attenuation by the water column. The most common approaches belong either to the semi-empirical (Lyzenga, 1978; 1981) or to the bio-optical model categories (e.g. Heege and Fischer 2004, Giardino et al. 2012, Gege 2014b).

Semi-empirical methods rely on *in situ* data for littoral bottom type discrimination. Lyzenga (1978; 1981) developed a semi-empirical method based on depth-invariant indices for detecting and distinguishing littoral bottom coverage. Armstrong (1993) used Landsat Thematic Mapper imagery to map seagrass and to estimate its biomass in the shallow water areas at the Bahamas. Brooks et al. (2015) and Shuchman et al. (2013) also used Landsat Thematic Mapper in combination with Multispectral Scanner Imagery time series to investigate SAV patterns at the Laurentian Great Lakes. Manessa et al. (2014) studied the distribution of seagrass and corals of shallow water coral reefs in Indonesia using WorldView2 imagery. Ciraolo et al. (2006) investigated the distribution of seagrass in a coastal lagoon in Italy using the hyperspectral sensor MIVIS (Multispectral Infrared Visible Imaging Sensor). A time series of RapidEye imagery was used to detect seasonal changes of SAV in two freshwater lakes of different trophic state (Lake Starnberg (Roessler et al. 2013a) and Lake Kummerow (Fritz et al. 2017a) in Germany.

Bio-optical model inversion requires information on the scattering and the absorption characteristics of water constituents. The bottom type and coverage determination relies on sample spectra from existing spectral libraries. Several studies have explored different

remote sensing data types by using bio-optical models. The changes of SAV patterns at Lake Garda, Italy, was investigated by Giardino et al. (2007) using the hyperspectral sensor MIVIS. Heblinski et al. (2011) used a bio-optical model to investigate the effects of water level changes on SAV structure at Lake Sevan, Armenia, using multi-spectral QuickBird imagery. To monitor invasive SAV, Roessler et al. (2013b) applied the bio-optical model BOMBER (Giardino et al. 2012) on hyperspectral Airborne Prism Experiment (APEX) imagery at Lake Starnberg, Germany. Giardino et al. (2015) used the same model to detect the interaction of suspended particulate matter, SAV and water depth using MIVIS sensor at Lake Trasimeno, Italy.

SAV expansion varies in successive years due to shifts in growing seasons, different water constituents, nutrient load and lake substrate remobilization processes, which all influence the detectability of SAV (Dekker et al. 2011). To detect expansion changes in the area vegetated by SAV, however, a short revisiting time and a high spatial and spectral resolution are key requirements for sensors to be applied for lake monitoring. Nowadays, hyperspectral, airborne sensor systems with their high spectral resolution (e.g. APEX, MIVIS) are still unsuitable for a continuous monitoring due to their high costs.

Due to the absence of operational hyperspectral satellites, a continuous and operational monitoring within close time intervals along the growing season with hyperspectral systems also seems unfeasible at present (Hunter et al. 2010). Several authors therefore suggested multi-seasonal images of high spatial resolution multispectral satellite data to compensate the reduced spectral information (e.g. Dekker et al. 2011, Roessler et al. 2013a, Palmer et al. 2015, Fritz et al. 2017a). Especially remote sensing systems with high revisiting frequencies in combination with a large area coverage seem to ideally complement laborious *in situ* observations of WFD by diver mappings. The expected synergies are the analysis of the expansion and shift in SAV species composition within the growing season in addition with information on the spatio-temporal SAV growth dynamics (Palmer et al. 2015, Fritz et al. 2017a, Dörnhöfer et al. 2018). Especially the multi-spectral Sentinel-2A, available since mid of 2015, provides good preconditions for mapping freshwater lakes and littoral bottom coverage types.

The key aim of this study was to test whether the multi-seasonal observation capability of Sentinel-2A provides sufficient information to support currently employed *in situ* mappings according to the WFD. Therefore, four Sentinel-2A data sets from August and September 2015 were analysed with the following objectives:

- To compare the performance of two methods for mapping littoral bottom coverage in shallow water areas of freshwater lakes, i.e. using a depth-invariant index and bio-optical modelling with WASI-2D.
- To investigate whether the spectral variations in the phenologic development of SAV species allows a differentiation of SAV on species level and whether the two used methods deliver comparable results.

4.3 Methods

4.3.1 Study site

Lake Starnberg (49.9°N, 11.3°E) is an oligotrophic lake, located in the alpine foreland about 25 km south of Munich. With an area of 56.4 km² and a maximum depth of 127.8 m, Lake Starnberg is the fifth largest lake in Germany (Wöbbecke et al. 2003). Low, groundwater-dominated inflows (3.6 $m^3 \cdot s^{-1}$) of small tributaries as well as low outflow rates (4.5 $m^3 \cdot s^{-1}$) (Melzer et al. 2003) result in a long residence time of water (21 years) (Wöbbecke et al. 2003).

In the shallow water regions, a variety of SAV species colonize the littoral bottom (**Figure 4.1**), making this an ideal study case for comparing alternative mapping approaches. Divers conducted a detailed mapping of SAV on species level on 30 and 31 July 2014 for the western part of Lake Starnberg (WWA Weilheim 2015) using the five-step scale of frequency after Kohler (1978). The composition of SAV varied in different water depths. At each transect, *Characeae*, such as *Chara contraria* and *Chara aspera* mainly in water depths down to 2 m. In the deeper zones, from 4 m downwards, several species of

Characeae (*Chara contraria, Chara virgata, Nitellopsis obtusa* and *Nitella opaca*) predominated. Several pondweed species such as *Potamogeton perfoliatus*, *Potamogeton filiformis* and *Potamogeton pusillus*) were present in all water depths. In our study, *Chara* spp., *Nitellopsis obtusa* and *Nitella opaca* were combined as meadow-growing species, *Potamogeton* spp. as tall-growing species.

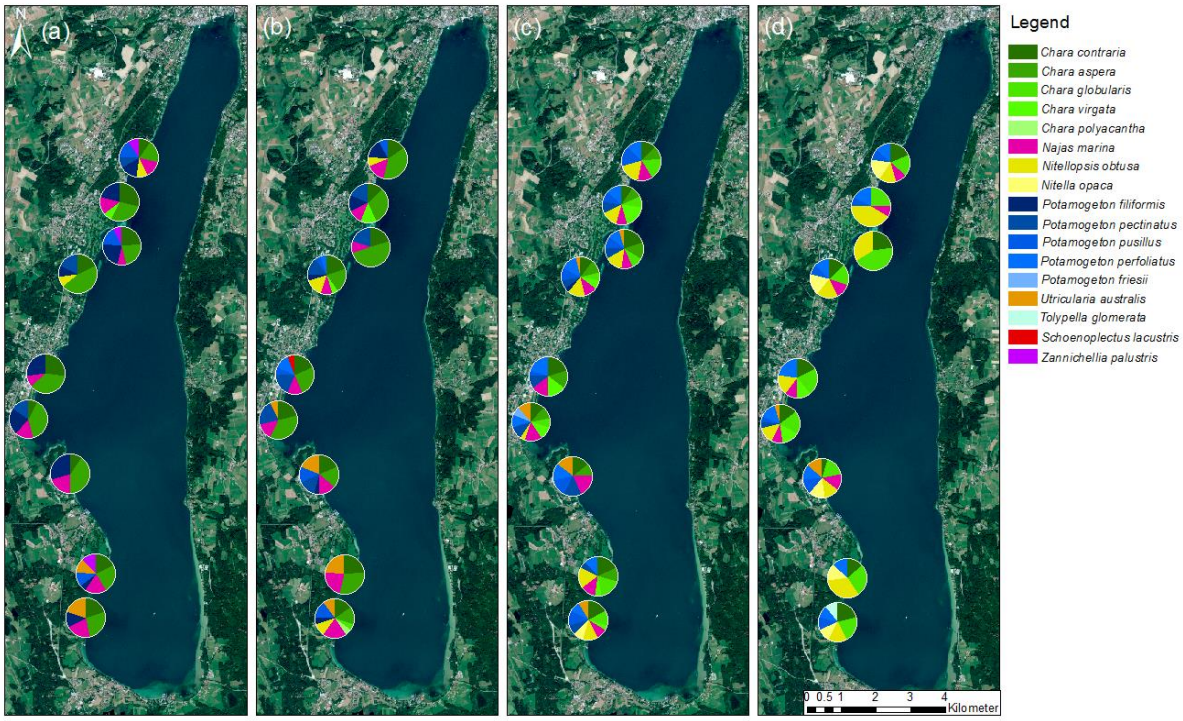

Figure 4.1: Distribution of SAV species in different water depths ((a) 0-1m; (b) 1-2m; (c) 2-4m; (d) > 4m) as result of the WFD mapping at the western shoreline of Lake Starnberg in 2014; frequency distribution of the species in a five-step scale after Kohler (1978) (background: Sentinel-2A true-colour composite R-G-B: 655 nm - 560 nm - 490 nm, acquisition date: 3 August 2015).

4.3.2 Data collection and processing

4.3.2.1 Spectral signature of SAV and sediment

Both applied approaches, i.e. unmixing bottom coverage based on a depth-invariant index and bio-optical modelling, require the spectral signature of bottom types as an input information, i.e. different SAV species and sediment. Spectro-radiometric *in situ* measurements with submersible instruments served as basis for the reflectance models of SAV as developed by Fritz et al. (2017b). A detailed description of the measurement setup, data processing and technical specifications is available in Wolf et al. (2013) and Fritz et al.

(2017a). Fritz et al. (2017a) already highlighted spectral variations between different SAV species and demonstrated a species-specific seasonal phenologic development. Using these reflectance models, the spectral signatures for this study were calculated for the date and time of Sentinel-2 imagery. The sediment spectrum originated from a reference measurement before the growing season started. Afterwards, the simulated reflectance spectra have been resampled to Sentinel-2A response curves as described in Dörnhöfer et al. (2016a). **Figure 4.2** schematically illustrates the pathway of data processing.

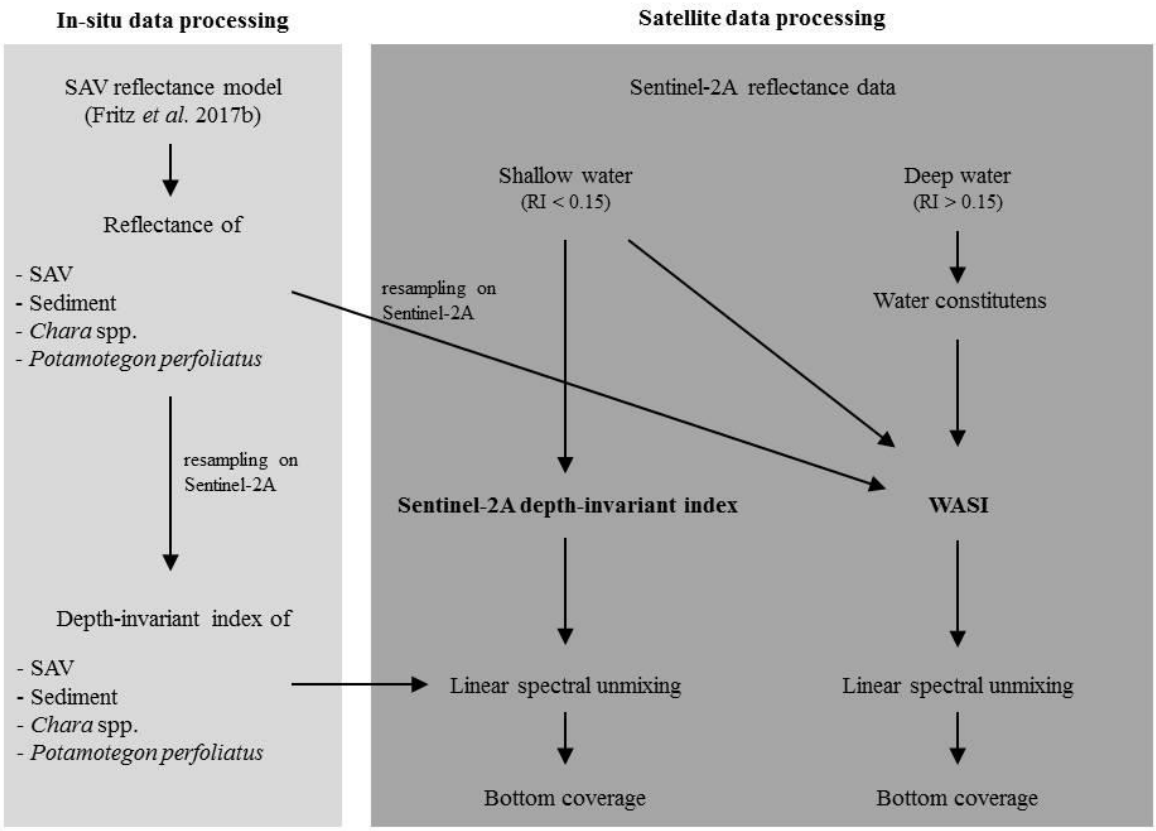

Figure 4.2: The pathway of *in situ* and satellite data processing.

4.3.2.2 Data processing of *in situ* data

For the Sentinel-2A data set, depth-invariant indices $Y_{i,j}$ of the different bottom types were calculated from spectral bands i and j. These indices, depending on the wavelength range (λ) covered by the employed bands, offer the potential to reduce the influence of water constituents and to investigate the lake bottom types. Ten index combinations

($Y_{1,2}$; $Y_{1,3}$; $Y_{1,4}$; $Y_{1,5}$; $Y_{2,3}$; $Y_{2,4}$; $Y_{2,5}$; $Y_{3,4}$; $Y_{3,5}$; $Y_{4,5}$) of Sentinel-2A bands 1 to 5 (band 1 = 443 nm; band 2 = 490 nm; band 3 = 560nm; band 4 = 665 nm; band 5 = 705 nm) were used. The method of Lyzenga (1978, 1981) was applied on *in situ* data assuming that the attenuation coefficients $K_d(\lambda_i)$ and $K_d(\lambda_j)$ (Maritorena 1996) account for the influence of present water constituent conditions and the water column itself (7).

$$Y_{i,j} = \frac{K_d(\lambda_j) * \ln(r_{shallow}(\lambda_i)) - K_d(\lambda_i) * \ln\left(r_{shallow}(\lambda_j)\right)}{\sqrt{K_d(\lambda_i)^2 + K_d(\lambda_j)^2}} \quad (7)$$

$i; j$ band i; band j, where $i < j$

$K_d(\lambda_i); K_d(\lambda_j)$ diffuse attenuation coefficients of $E_d(\lambda)$ at band i and j

$r_{shallow}(\lambda_i); r_{shallow}(\lambda_j)$ shallow water reflectance at band i and j

The remote sensing reflectance of shallow water areas ($r_{shallow}$) varied for different water depths (z), the remote sensing reflectance of the different bottom types (r_{bottom}) and the remote sensing reflectance of the water column ($r_{deepwater}$) (8).

$$r_{shallow}(\lambda_{i,j}) = r_{bottom}(\lambda_{i,j}) exp^{-2K_d(\lambda_{i,j})z} + r_{deepwater}(\lambda_{i,j})(1 - exp^{-2K_d(\lambda_{i,j})z}) \quad (8)$$

z water depth

$r_{bottom}(\lambda_{i,j})$ littoral bottom reflectance at band i, j

$r_{deepwater}(\lambda_{i,j})$ reflectance over optical deep water at band i, j

4.3.2.3 Data processing of satellite data

Sentinel-2A satellite data (processing baseline: 2.04, Tile: UPU) acquired on 3 August 2015, 13 August 2015, 23 August 2015 and 12 September 2015 were atmospherically corrected to remote sensing reflectance ($R_{rs}^{0+} = \frac{L_u(0^+)}{E_d(0^+)}$) by EoMAP GmbH & Co. KG using MIP (Modular Inversion and Processing System (Heege and Fischer 2004, Heege et al. 2014). MIP is a physically based, coupled atmospheric-water algorithm correcting the effects of atmosphere and water surfaces (sky glint). Recently, it turned out to perform well with

Sentinel-2A data at Lake Starnberg (Dörnhöfer et al. 2016a). To distinguish between deep water and shallow water areas the deep water Red Index (RI) (Spitzer and Dirks 1987) was applied on $R_{rs}^{0+}(\lambda)$ data (9). Water areas with RI higher than 0.15 sr^{-1} were classified as shallow water and were further investigated. To reduce computation time, the areas with more than 8 m water depths (official bathymetric chart (Bavarian Environmental Agency 2000)) were excluded from further processing.

$$RI = \frac{R_{rs}^{0+}(\lambda) - R_{rs}^{0+}(\lambda, \infty)}{R_{rs}^{0+}(\lambda)} \quad (9)$$

$R_{rs}^{0+}(\lambda)$ remote sensing reflectance value of each pixel in the red

$R_{rs}^{0+}(\lambda, \infty)$ mean red remote sensing reflectance over optically deep water

4.3.2.4 Spectral unmixing using depth-invariant indices

To transfer Sentinel-2A R_{rs}^{0+} data to the same level as *in situ* measured data, we applied the equation of Lee et al. (1998) (10).

$$R_{rs}^{0+}(\lambda) = \frac{(1-\sigma)(1-\sigma_L^-)}{n_W^2} * \frac{R_{rs}^{0-}(\lambda)}{1-\sigma^- * Q * R_{rs}^{0-}(\lambda)} \quad (10)$$

The equation of Lee et al. (1999) can be used to approximate the reflectance from above to beyond the water surface ($\frac{(1-\sigma)(1-\sigma_L^-)}{n_W^2} = 0.518;\ \sigma^- * Q = 1.562$; (11)).

$$R_{rs}^{0-}(\lambda) = \frac{R_{rs}^{0+}(\lambda)}{0.518 + 1.562 * R_{rs}^{0+}(\lambda)} \quad (11)$$

The ten different depth-invariant indices $Y_{i,j}$ ($Y_{1,2}$; $Y_{1,3}$; $Y_{1,4}$; $Y_{1,5}$; $Y_{2,3}$; $Y_{2,4}$; $Y_{2,5}$; $Y_{3,4}$; $Y_{3,5}$; $Y_{4,5}$) were calculated for the subsurface reflectance (R_{rs}^{0-}) of shallow water regions in the satellite data sets (12). Here, the subsurface reflectances of neighbouring bands were related to the diffuse vertical attenuation of the downwelling irradiance (K_d). K_d in combination with the deep water reflectance ($R_{rs}^{0-}(\lambda_{i,\infty})$) of the respective Seninel-2A data set account for the influence of

water column attenuation; $R_{rs}^{0-}(\lambda_{i,\infty})$ originated from a homogenous deep water area and was extracted for each acquisition date separately.

$$Y_{i,j} = \frac{K_d(\lambda_j) * \ln\left(R_{rs}^{0-}(\lambda_i) - R_{rs}^{0-}(\lambda_{i,\infty})\right) - K_d(\lambda_i) * \ln\left(R_{rs}^{0-}(\lambda_j) - R_{rs}^{0-}(\lambda_{j,\infty})\right)}{\sqrt{K_d(\lambda_i)^2 + K_d(\lambda_j)^2}} \quad (12)$$

$i; j$	band i; band j, where $i < j$
$K_d(\lambda_i); K_d(\lambda_j)$	Diffuse attenuation coefficients of $E_d(\lambda)$ at band i and j
$R_{rs}^{0-}(\lambda_i);\ R_{rs}^{0-}(\lambda_j)$	remote sensing reflectance at band i and j of each pixel
$R_{rs}^{0-}(\lambda_{i,\infty}); R_{rs}^{0-}(\lambda_{j,\infty})$	mean deep-water remote sensing reflectance at band i and j

The calculated $Y_{i,j}$ data set was the input for a linear spectral unmixing process performed with Sentinel Application Platform SNAP (version 4.0). The $Y_{i,j}$ index values of the different littoral bottom types represented the spectral endmembers. Linear spectral unmixing varies the share of the considered spectral endmembers at a pixel's signature assuming a linear contribution. Here, we assume that the unmixed share of an endmember (f_{i_Y}) represents the relative abundance (bottom coverage) of a littoral bottom type. To distinguish between areas of sediment and SAV, we used two bottom types (sediment and SAV). To differentiate the vegetated areas into tall- and meadow-growing species, we used three bottom types (sediment, tall-growing species and meadow-growing species). The input spectra with different sun elevations were simulated with the reflectance model (Fritz et al. 2017b) according to the respective overpass time of the satellite.

4.3.2.5 Spectral unmixing using WASI-2D

WASI-2D is a freely available software tool, which enables the retrieval of water constituents, bottom characteristics and water depths by inversely modelling atmospherically corrected multispectral or hyperspectral imagery (Gege 2014b). WASI-2D models the R_{rs}^{+} using physically based equations, measured or modeled constants and parameters. Some parameters, i.e. fit parameters, can be varied during modelling. In

shallow water, WASI-2D considers the spectral influence of the water depth, fractional contribution from bottom reflectance (e.g. different shares of pure reflectance from sediment and SAV) and light absorbing (Chlorophyll-a (CHL), coloured dissolved organic matter (CDOM) and backscattering (TSM) water constituents (technical details and specific equations in Gege (2014b). For this study, fit criterions were the water depth, bottom types and fractions of bottom coverage.

To avoid overfitting of the model, concentrations of CHL, TSM and CDOM were set constant. To obtain reasonable values for the model parameters we first retrieved water constituent concentrations (CHL, CDOM, TSM and the CDOM slope factor S_{CDOM}) in deep water of each acquisition date with a setting as described in Dörnhöfer et al. (2016a) (**Table 4.1**).

Table 4.1: Water constituent concentrations over optically deep water for Sentinel-2A acquisition dates, retrieved with a setting as described in Dörnhöfer et al. (2016a).

Parameter	3 Aug 2015	13 Aug 2015	23 Aug 2015	12 Sep 2015
CHL [mg·m^{-3}]	0.97	3.45	2.86	0.5
TSM [g·m^{-3}]	1.25	3.56	2.38	2.18
CDOM [m^{-1}]	0.183	0.182	0.227	0.398
S_{CDOM} [nm^{-1}]	0.0163	0.0163	0.0093	0.0065

We used the arithmetic mean of deep water results as constant parameter values for shallow water inversion. Water depth was considered as a fit parameter, which could vary between 0.1 and 8.0 m. WASI-2D calculates the reflectance from the bottom ($R_b(\lambda)$) as the sum of linearly mixing reflectance from different bottom types (13).

$$R_{rs}^{b}(\lambda) = \sum_{i=1}^{n} f_i \cdot B_i \cdot R_i^{b}(\lambda) \quad (13)$$

n number of bottom types

f_i fractional share of the bottom type within the pixel

B_i proportion of bottom reflectance towards the sensor

$R_i^b(\lambda)$ irradiance reflectance of the bottom type, originated from SAV reflectance model (Fritz et al. 2017b)

After resampling the spectral database of WASI-2D to the Sentinel-2A spectral response curves as described in Dörnhöfer et al. (2016a), WASI-2D inversely models the R_{rs}^{0+} and compares modeled and Sentinel-2A R_{rs}^{0+} spectra for each pixel. The model then varies the fit parameters in a predefined range until modelled and satellite R_{rs}^{0+} match a similarity criterion or, when no perfect match is feasible, a predefined maximum number of iterations is achieved.

To unmix the spectra to bottom constituents, the proportion of bottom reflectance towards the sensor was assumed to be angle-independent, i.e. Lambertian surfaces (B_i = 0.318 sr^{-1}). For each acquisition date, we fitted f_i to linearly unmix bottom types while considering variable water depths and a constant contribution of water constituents to the reflectance. Similar to the unmixing approach based on the depth-invariant index, we conducted model runs with two (n = 2: sediment and SAV) and three (n = 3: sediment, tall-growing species, meadow-growing species) bottom types. To reduce the influence of sun glint (not corrected by MIP) we additionally varied the share of directly reflected radiance (see Dörnhöfer et al. (2016a)).

4.3.2.6 Comparison between depth-invariant index and WASI-2D unmixing results

To compare the littoral bottom coverages retrieved with both methods, the results of depth-invariant indices (f_{i_Y}) and WASI-2D (f_{i_WASI}) were normalized to a range between 0 and 1. We conducted a linear regression analyses between the obtained and normalised

endmember shares, f_{i_Y} and f_{i_WASI}, using the software R (Version 3.4.2, R Core Team). For each Sentinel-2A data set, both parameters were compared in scatterplots based on the complete shoreline. Calculated correlation parameters (coefficient of determination,R^2) supported assessing the similarities and differences between the resulting littoral bottom coverage of both approaches.

4.4 Results

4.4.1 Seasonal spectral variation within the growing season

The spectra of the three investigated littoral bottom types (sediment, meadow-growing species and tall-growing species) were consistently different, following bimonthly modelling with the SAV reflectance models (Fritz et al. 2017b) for the 1st and 15th of June, July, August and September (**Figure 4.3**). Resampled to Sentinel-2A bands, the spectral response of the surface types also differed clearly in spectral shape and intensity at each of the observed dates within the growing season. Overall, while the intensity of the remote sensing reflectance remained low in the visible wavelength regions (400 nm to 700 nm), the intensity increased strongly towards the near infrared region (> 700 nm, **Figure 4.3**). In the visible wavelength region, the reflectance of sediment was the highest. Reflectance of meadow- and tall-growing species was similar in spectral shape, but differed in intensity. The reflectance intensity of meadow-growing species was slightly higher than the intensity of tall-growing species.

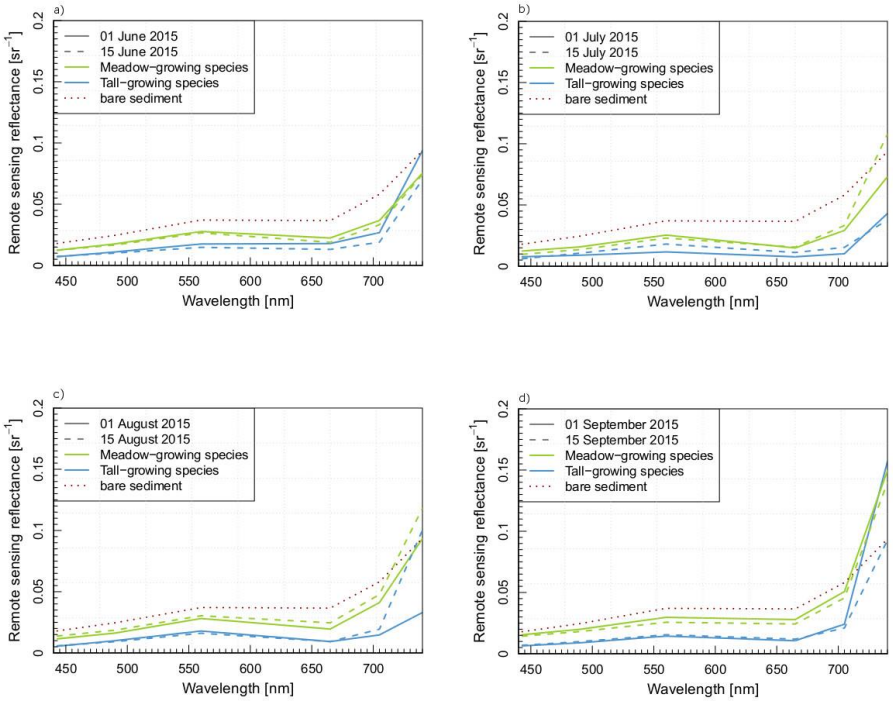

Figure 4.3: Remote sensing reflectance of meadow- and tall-growing species, simulated with the reflectance model and resampled on Sentinel-2A bands, for the 1st and 15th of a) June, b) July, c) August, d) September. The sediment spectrum was constant for each day.

4.4.2 Spectral unmixing of shallow water areas using depth-invariant indices

Depth-invariant index analysis of the littoral bottom types of the three test sites at Lake Starnberg (test sites 'Roseninsel', 'Karpfenwinkel' and 'Seeshaupt') based on the pre-processed Sentinel-2A data sets revealed a different spatial extension of SAV (green) and sediment (red) patches (**Figure 4.4**) and a different SAV species composition (sediment (red), meadow-growing (green) and tall-growing (blue) SAV species, **Figure 4.5**) for the investigated dates. The spatial distribution of sediment and SAV species changed during the growing season. The spatial extension of shallow water areas depended on the *RI* index, which may differ for each Sentinel-2A data set.

At the test site 'Roseninsel', the first index run classified large sediment and mixed sediment dominated patches (**Figure 4.4**, **Table 4.2**). Mixed SAV dominated patches were identified at the western shoreline of Lake Starnberg and at the south-eastern part of the island 'Roseninsel'. For all Sentinel-2A acquisition dates, the sediment dominated patches

were similarly large (up to 100%) and clearly zoned from vegetated areas. For the test site 'Karpfenwinkel', large sediment dominated patches were classified in the centre at the beginning of August. This clear spatial distinction between sediment and SAV areas decreased during August, resulting in a large mixed area. On 12 September, only a small band at the shoreline was classified as SAV dominated (32.25%). At the test site 'Seeshaupt', the classified littoral bottom coverages changed solely in mid-September. The first index run further identified large sediment dominated areas in the south-western part of this test site (up to 45.59%), while SAV patches were tagged in the south-eastern part near the shoreline. On 12 September, the former sediment area at the eastern shoreline was classified as mixed area (75.70%).

The results of the second run revealed more details on the distribution of SAV types in the mixed and dense SAV patches (**Figure 4.5**, **Table 4.3**). On 3, 13 and 23 August, the majority of the shallow water area at the test site 'Roseninsel' was tagged as sediment, while small patches of tall- (up to 7.68%) and meadow-growing (up to 4.99%) species were located at the south-eastern part of the island and a narrow stripe along the shoreline was classified as meadow-growing species. On 12 September, the situation changed and nearly the entire shallow water area was classified as a mixture of sediment and tall-growing species (99.45%) . On 3, 13 and 23 August, a large sediment mixed area patch dominated the centre of the test 'Karpfenwinkel'. Meadow-growing species populated the shallow areas in the south (up to 14.57%), while tall-growing species predominated in deeper areas in the north (up to 37.10%). During August, the patches of tall-growing species increased (from 21.27% to 37.10%). On 12 September, only a narrow stripe along the shoreline was detected as shallow water, dominated by a mixture of sediment and tall-growing species. On 3, 13 and 23 August, meadow-growing species were situated in the south-eastern near the shore line part and sediment patches in the south-western part of test site 'Seeshaupt'. Tall-growing species were located in deeper zones, the eastern shoreline was classified as a mixture of sediment and meadow-growing species. On 12 September, the entire shallow water area was classified as a mixture of sediment, tall- and meadow-growing vegetation dominating the entire shallow water area.

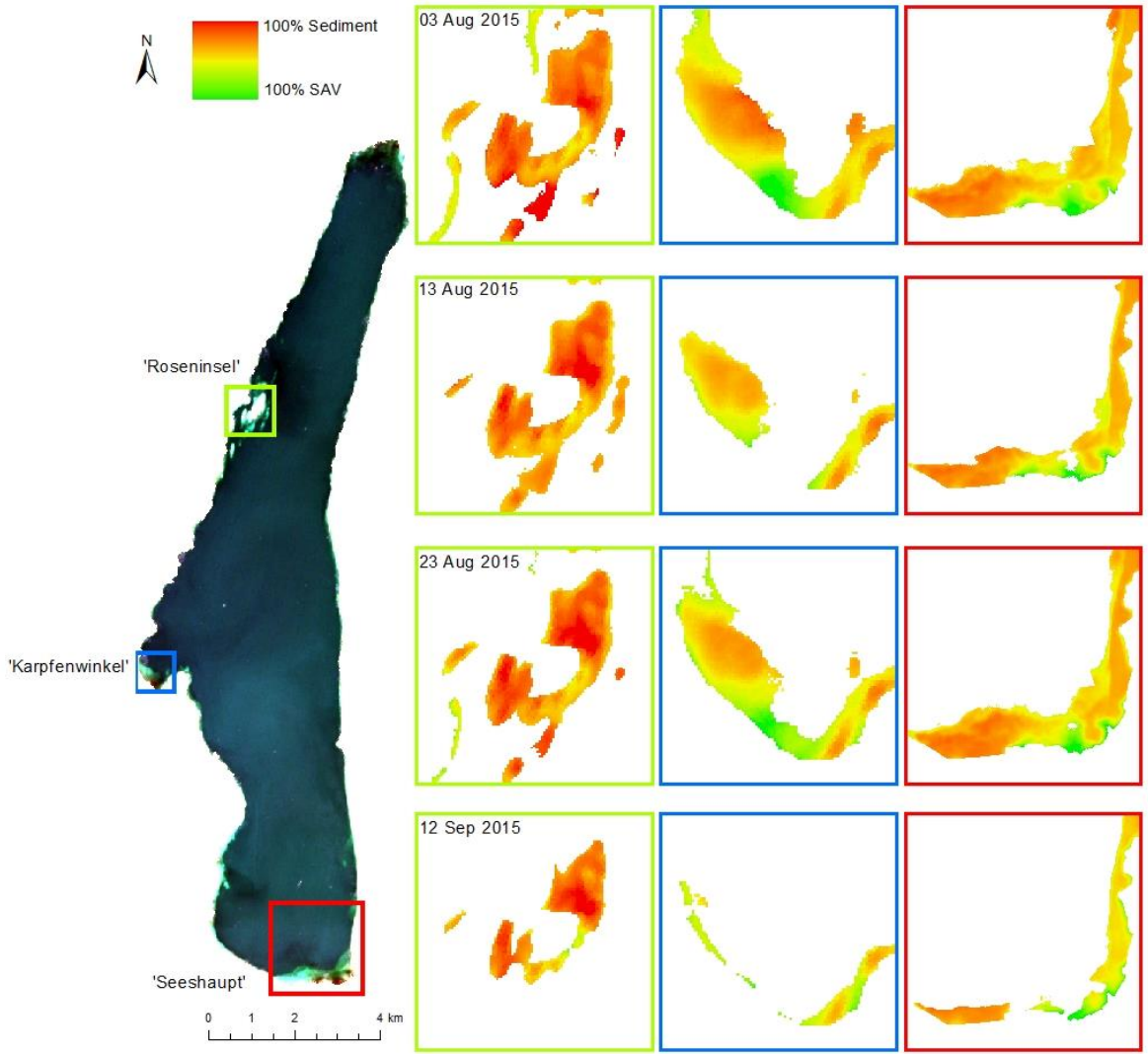

Figure 4.4: Littoral bottom coverage of the investigated shallow water areas at Lake Starnberg illustrated after the linear spectral unmixing using the depth-invariant indices on 3 August 2015, 13 August 2015, 23 August 2015 and 12 September 2015 (Sentinel-2A true-colour composite R-G-B: 665 nm-560 nm-490 nm, acquisition date: 3 August 2015; left). The boxes represent the investigated shallow water areas from left to right: 'Roseninsel' (green box), 'Karpfenwinkel' (blue box) and 'Seeshaupt' (red box). The linear spectral unmixing of 2 bottom types displays 100% bare sediment areas in red and 100% dense vegetated areas in green, mixed areas in yellow. Land and deep water areas are masked.

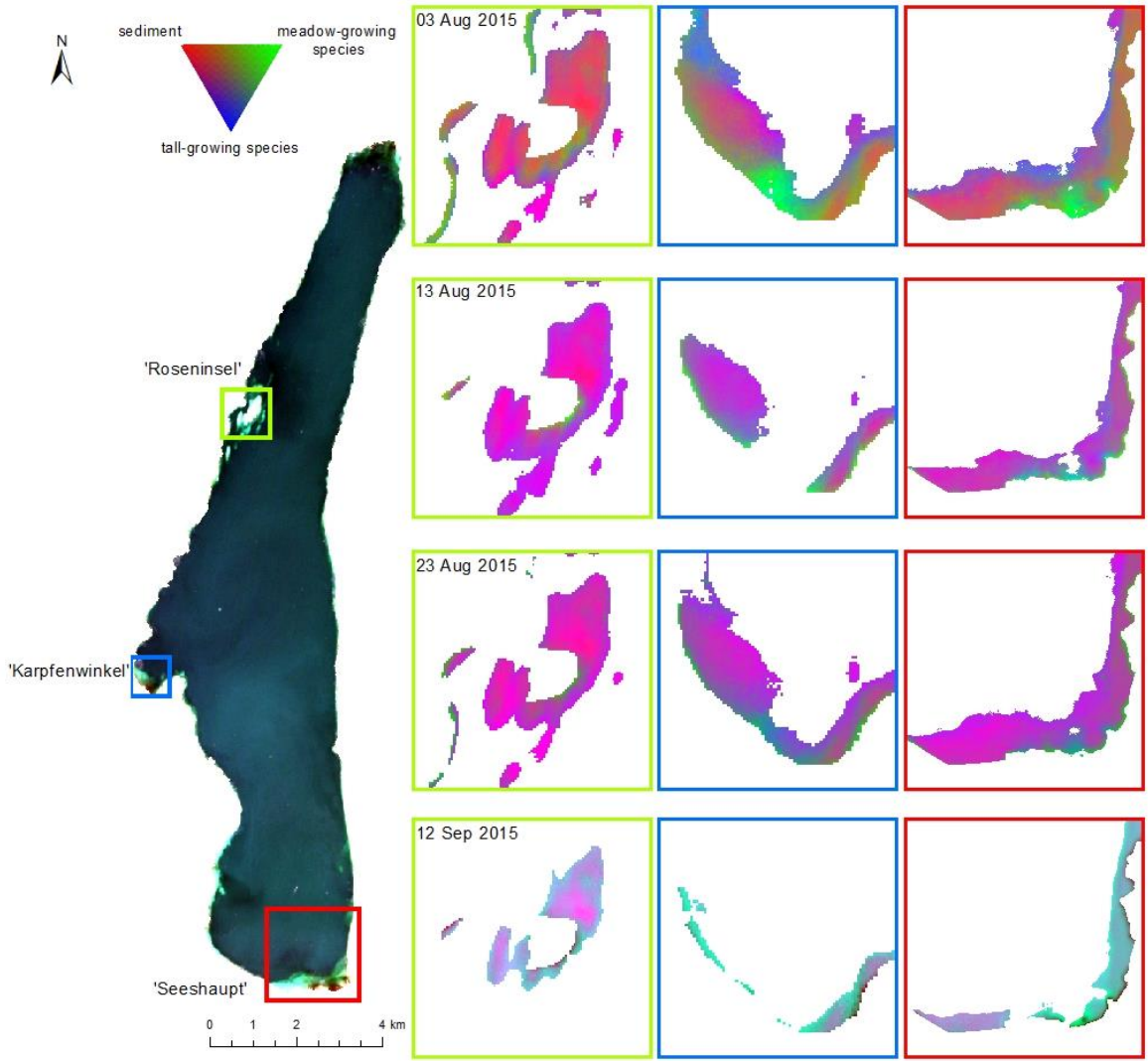

Figure 4.5: Littoral bottom coverage of the investigated shallow water areas at Lake Starnberg illustrated after the linear spectral unmixing using the depth-invariant indices on 3 August 2015, 13 August 2015, 23 August 2015 and 12 September 2015 (Sentinel-2A true-colour composite R-G-B: 665 nm-560 nm-490 nm, acquisition date: 3 August 2015; left). The boxes represent the investigated shallow water areas from left to right: 'Roseninsel' (green box), 'Karpfenwinkel' (blue box) and 'Seeshaupt' (red box). The result of 3 bottom types displays areas of bare sediment (red), meadow-growing plant species (green) and tall-growing plant species (blue). Land and deep water areas are masked.

Table 4.2: Areas classified for each littoral bottom type using depth-invariant index and the two-bottom-type approach (sediment < 0.3, mixed sediment dominated: 0.3-0.5; mixed SAV dominated: 0.5-0.7; dense SAV > 0.7).

Two-bottom-type approach		**Depth-invariant index data (%)**			
Test site	**Littoral bottom type**	**3 Aug 2015**	**13 Aug 2015**	**23 Aug 2015**	**12 Sep 2015**
'Roseninsel'	Sediment	0.73	64.07	76.43	77.46
	Mixed sediment dominated	56.69	35.93	23.06	21.20
	mixed SAV dominated	42.43	0	0.51	1.34
	dense SAV	0.15	0	0	0
'Karpfenwinkel'	Sediment	0	14.69	25.34	2.50
	Mixed sediment dominated	13.23	81.95	63.43	65.25
	mixed SAV dominated	74.16	3.36	10.95	32.00
	dense SAV	12.61	0	0.28	0.25
'Seeshaupt'	Sediment	0	32.34	45.59	20.55
	Mixed sediment dominated	14.95	60.36	48.99	61.68
	mixed SAV dominated	77.86	5.89	4.67	14.02
	dense SAV	7.19	1.42	0.76	3.75

Table 4.3: Areas classified for each littoral bottom type using depth-invariant index and the three-bottom-type approach.

Three-bottom-type approach		Depth-invariant index data (%)			
Test site	**Littoral bottom type**	**3 Aug 2015**	**13 Aug 2015**	**23 Aug 2015**	**12 Sep 2015**
'Roseninsel'	Sediment	56.79	4.36	10.67	0.95
	meadow-growing species	4.99	1.22	1.13	0.55
	tall-growing species	7.68	5.14	4.66	12.27
	mixed area	30.54	89.29	83.54	86.22
'Karpfenwinkel'	Sediment	22.14	3.77	2.18	0.50
	meadow-growing species	14.57	6.94	2.12	9.00
	tall-growing species	21.27	35.99	37.10	21.25
	mixed area	42.02	53.30	58.60	69.25
'Seeshaupt'	Sediment	37.91	9.34	7.30	0.05
	meadow-growing species	10.11	5.10	2.33	6.33
	tall-growing species	20.85	25.47	16.43	15.46
	mixed area	31.13	60.08	73.95	78.16

4.4.3 Spectral unmixing of shallow water areas using WASI-2D

WASI-2D based unmixing was also carried out for the test sites 'Roseninsel', 'Karpfenwinkel' and 'Seeshaupt'. Again, two unmixing runs were conducted, i.e. one to differ between sediment (red) and SAV (green) (**Figure 4.6**) and one to distinguish between sediment (red), meadow-growing (green) and tall-growing (blue) SAV species (**Figure 4.7**).

At the test site 'Roseninsel', the first run revealed large sediment patches around the island Roseninsel for all Sentinel-2A acquisition dates (**Figure 4.6**, **Table 4.4**). On 3 and 13 August, towards deeper water mixed areas dominate, followed by patches classified as dense SAV. On 23 August and 12 September, the area classified as sediment increased (80.28%) and SAV patches disappeared (2.82%). At the test site 'Karpfenwinkel', SAV dominated patches were dominating almost the complete shallow water area on 3, 13 and 23 August (up to 76.89%); sediment and patches of mixed bottom types were located in the north and in the south-east. The sediment dominated patches increased noticeably on 23 August (60.93%). On 12 September, only a narrow stripe at the shoreline was classified as shallow water, which was dominated by sediment and mixed areas. At the test site 'Seeshaupt', sediment patches and mixed areas appeared at the western part and at the eastern shoreline for all Sentinel-2A acquisition dates. On 3 August, the majority of the shallow water area in the south was classified as dense SAV (17.22%). This SAV patch decreased on 23 August (3.96%) and 12 September (0.90%), resulting in an increase of sediment dominated patches (90.75%). The pattern was similar on 12 September, although the shallow water area was considerably smaller.

The results of the second run (**Figure 4.7**, **Table 4.5**) revealed large sediment areas around the island (up to 69.42%), followed by patches of tall-growing species in deeper water at the test site 'Roseninsel' on 3, 13 and 23 August. Small isolated patches of meadow-growing species (up to 6.29%) occurred between tall-growing areas (up to 23.31%). On 23 August, however, the area classified as sediment increased strongly (69.42%), while tall- (8.33%) and meadow-growing (2.45%) patches decreased. At the beginning of August, large patches of tall-growing species were classified in the centre and meadow-growing

species and sediment patches in the south of the test site 'Karpfenwinkel'. On 13 August, a mixture of sediment and meadow-growing species with isolated patches of tall-growing species (7.43%) covers the shallow water area. These sediment patches (23.73%) increased on 23 August, framed by tall-growing species. Meadow-growing species were located in the south of the test site. In September, sediment dominated the narrow stripe along the shoreline classified as shallow water. At the test site 'Seeshaupt', large sediment areas were classified in the south-western part and at the eastern shoreline for all Sentinel-2A acquisition dates. At the beginning of August, large areas of tall-growing species (22.58%) with isolated small patches of meadow-growing species dominated the centre of this test site. On 13 and 23 August, the areas tall-growing species strongly decreased; sediment dominated the shoreline, meadow-growing species the deeper water. In September most of the shallow water area was tagged as sediment (68.83%).

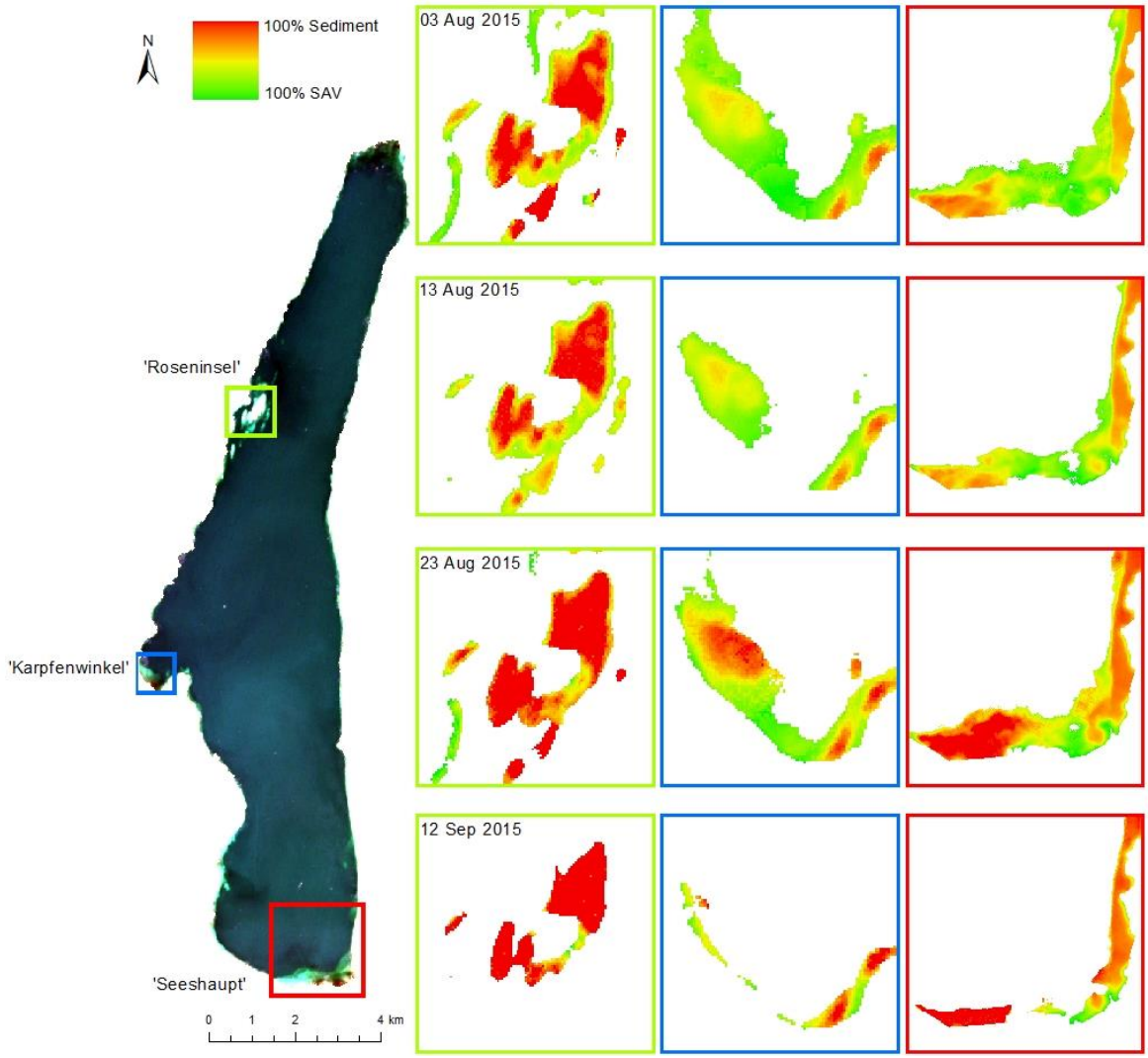

Figure 4.6: Littoral bottom coverage of the investigated shallow water areas at Lake Starnberg illustrated after linear spectral unmixing using the bio-optical model WASI-2D on 3 August 2015, 13 August 2015, 23 August 2015 and 12 September 2015 (Sentinel-2A true-colour composite R-G-B: 665 nm-560 nm-490 nm, acquisition date: 3 August 2015; left). The boxes represent the investigated shallow water areas from left to right: 'Roseninsel' (green box), 'Karpfenwinkel' (blue box) and 'Seeshaupt' (red box). The result of 2 bottom types displays 100% bare sediment areas in red and 100% dense vegetated areas in green, mixed areas in yellow. Land and deep water areas are masked.

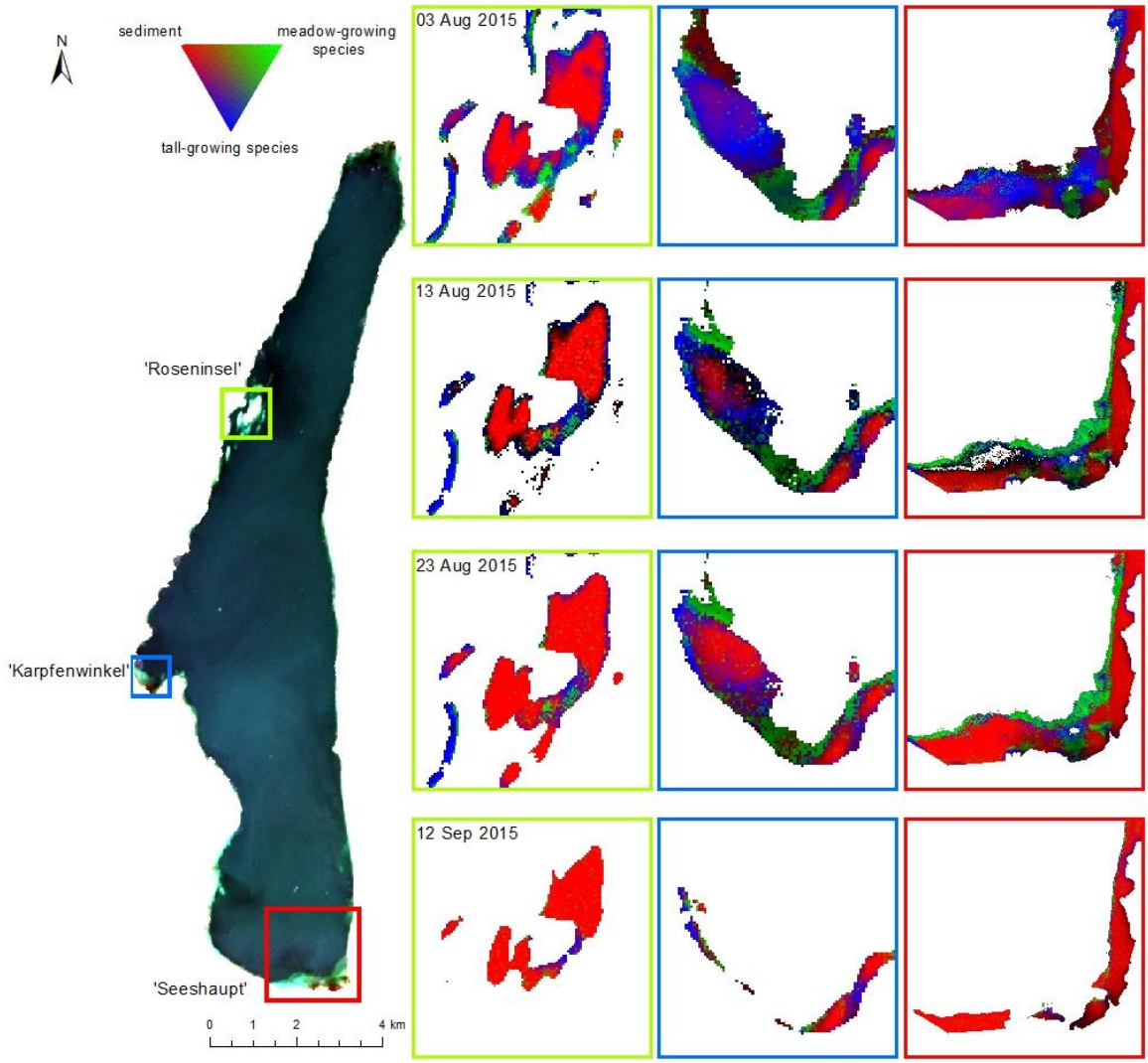

Figure 4.7: Littoral bottom coverage of the investigated shallow water areas at Lake Starnberg illustrated after linear spectral unmixing using the bio-optical model WASI-2D on 3 August 2015, 13 August 2015, 23 August 2015 and 12 September 2015 (Sentinel-2A true-colour composite R-G-B: 665 nm-560 nm-490 nm, acquisition date: 3 August 2015; left). The boxes represent the investigated shallow water areas from left to right: 'Roseninsel' (green box), 'Karpfenwinkel' (blue box) and 'Seeshaupt' (red box). The result of 3 bottom types displays areas of bare sediment (red), meadow-growing plant species (green) and tall-growing plant species (blue). Land and deep water areas are masked.

Table 4.4: Areas classified for each littoral bottom type using bio-optical modelling and the two-bottom-type approach (sediment < 0.3, mixed sediment dominated: 0.3-0.5; mixed SAV dominated: 0.5-0.7; dense SAV > 0.7).

Two-bottom-type approach		**Bio-optical modelling data (%)**			
Test site	**Littoral bottom type**	**3 Aug 2015**	**13 Aug 2015**	**23 Aug 2015**	**12 Sep 2015**
'Roseninsel'	Sediment	51.24	50.73	80.28	68.07
	Mixed sediment dominated	18.27	34.74	12.25	26.05
	mixed SAV dominated	23.95	14.53	4.65	5.04
	dense SAV	6.54	0.00	2.82	0.84
'Karpfenwinkel'	Sediment	3.79	7.09	30.66	45.31
	Mixed sediment dominated	19.32	48.57	30.27	37.32
	mixed SAV dominated	49.72	44.25	33.11	17.37
	dense SAV	27.18	0.08	5.96	0.00
'Seeshaupt'	Sediment	21.61	30.97	55.64	74.64
	Mixed sediment dominated	22.06	34.28	29.38	16.10
	mixed SAV dominated	39.11	31.30	11.02	8.35
	dense SAV	17.22	3.45	3.96	0.90

Table 4.5: Areas classified for each littoral bottom type using bio-optical modelling and the three-bottom-type approach.

Three-bottom-type approach		**Bio-optical modelling data (%)**			
Test site	**Littoral bottom type**	**3 Aug 2015**	**13 Aug 2015**	**23 Aug 2015**	**12 Sep 2015**
'Roseninsel'	Sediment	42.22	43.65	69.42	90.96
	meadow-growing species	6.29	2.52	2.45	0.15
	tall-growing species	23.31	8.73	8.33	2.38
	mixed area	28.18	45.10	19.80	6.51
'Karpfenwinkel'	Sediment	3.64	6.02	23.73	38.50
	meadow-growing species	3.02	4.90	4.90	3.29
	tall-growing species	32.17	7.43	7.47	15.02
	mixed area	61.17	81.65	63.90	43.19
'Seeshaupt'	Sediment	19.07	28.50	48.66	68.83
	meadow-growing species	0.87	12.30	11.83	1.04
	tall-growing species	22.58	2.00	1.90	0.35
	mixed area	57.48	57.20	37.61	29.78

4.4.4 Analysing the results of the spectral unmixing of both methods

To compare the results both methods, a scatterplot with linear regression lines was performed for both methods for each bottom type and acquisition date. **Figure 4.8** shows a comparison of the two-bottom-type approach (grey) and of the three-bottom-type approach (red). Both approaches showed a correlation, though the results of two-bottom-types approach were less scattered. The results of both approaches differentiating between two littoral bottom types (**Figure 4.4** and **Figure 4.6**) also emphasised visually a similar spatial distribution of sediment and dense SAV patches. For example, at the test site 'Roseninsel', both approaches showed predominating sediment (red) areas for all acquisition dates. When using the depth-invariant index (**Figure 4.4**), the remaining patches were mixed areas (yellow and orange), while at the same test site those patches were classified as mixed (yellow) and dense SAV areas (green) when using WASI-2D (**Figure 4.6**).

The results for meadow-growing species (green) and tall-growing species (blue) indicated widely scattered values (**Figure 4.9**), with low coefficients of determination (R^2, see **Table 4.6**). The highest coefficients of determination were achieved for two-bottom-type approach (R^2 up to 0.8137). The R^2 values of the results of the three-bottom-type approach were consistently lower (R^2 up to 0.4194). Meadow- and tall-growing species correlations obtained the lowest R^2 values (R^2 = 0.006996 and R^2 = 0.002654). The results of the three-bottom-type approach (**Figure 4.5** and **Figure 4.7**) demonstrated a similar spatial distribution of sediment and SAV patches, but showed no comparable spatial distribution for SAV on species level. For example, for the test site 'Karpfenwinkel', the results of both methods completely differed on 3 and 13 August: WASI-2D derived a large patch of tall-growing species whereas the depth-invariant index detected sediment and mixed areas of sediment and meadow-growing species.

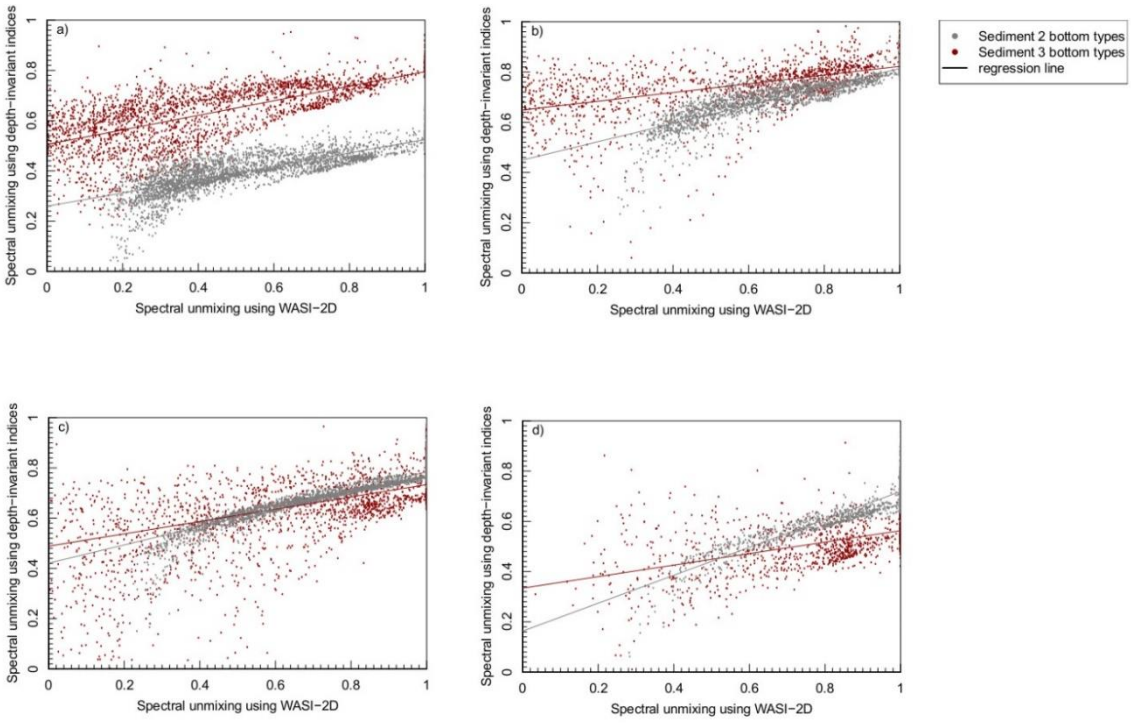

Figure 4.8: Scatterplot with regression line of sediment for the acquisition dates 03 August 2015 (a), 13 August 2015 (b), 23 August 2015 (c) and 12 September 2015 (d). Results of spectral unmixing of 2 bottom types for sediment (grey) and results of the spectral unmixing of 3 bottom types for sediment (red).

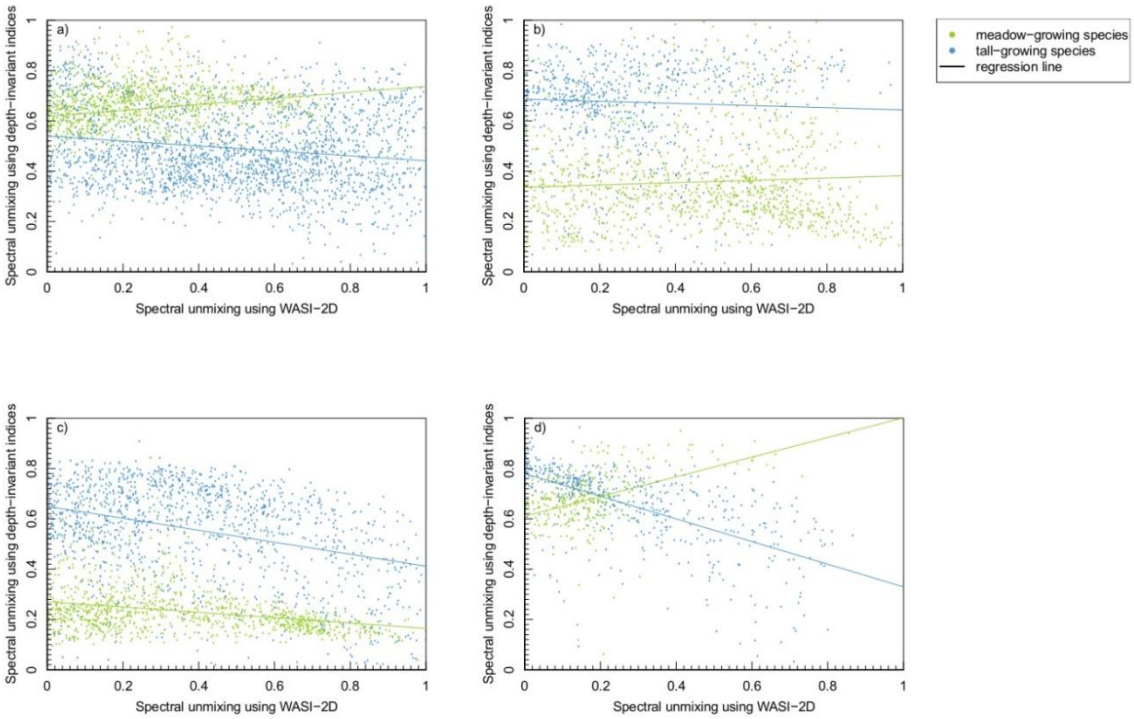

Figure 4.9: Scatterplot with regression line of the different bottom types for the acquisition dates 03 August 2015 (a), 13 August 2015 (b), 23 August 2015 (c) and 12 September 2015 (d). Results of the spectral unmixing of 3 bottom types for meadow-growing species (green) and tall-growing species (blue).

Table 4.6: R^2 values for the different littoral bottom types for each acquisition date.

Littoral bottom type	03 Aug 2015	13 Aug 2015	23 Aug 2015	12 Sep 2015
Sediment (2 bottom types)	0.5603	0.6621	0.8137	0.7948
Sediment (3 bottom types)	0.4194	0.2664	0.3073	0.2352
Meadow-growing species	0.06476	0.006996	0.05015	0.1091
Tall-growing species	0.03649	0.002654	0.1821	0.3858

4.5 Discussion

One aim of this study was to compare the performance of two methods for mapping littoral bottom coverage in shallow water areas by using Sentinel-2A data. Both methods, i.e. depth-invariant index and bio-optical modelling with WASI-2D, can be applied on the shallow water areas at Lake Starnberg. When differentiating between sediment and SAV, both methods identify a similar spatial distribution of the patches. The second aim of this study was to investigate whether spectral variations in the phenologic development of SAV species allow a differentiation on species level. The modelled spectra used for initializing the two approaches indicate that a differentiation should be possible, but the used methods revealed different results in SAV species patch distribution.

4.5.1 Seasonal spectral variation within the growing season

In our study, we focused on a period in late summer for the investigation of the phenologic SAV development. Within these time period, SAV is expected to change significantly with maximal plant height and patch extension in August (main vegetation time) to degrading and dying SAV patches in September. The modelled and resampled SAV reflectance spectra showed differences in the spectral shape at the investigated littoral bottom types within the growing season (**Figure 4.3**). Moreover, variation in these spectra were sufficiently high to track the species-specific development during the monitoring period; Sentinel-2A therefore seems to be suitable for the differentiation between SAV species, especially in the range of bands 4 and 5, which are sensitive to Chlorophyll-a variations.

At the end of the growing season in September, the spectral shape of meadow-growing species is flattened in the yellow and orange wavelength region (560 nm – 630 nm); moreover the Chlorophyll-a absorption maximum is less spectral distinct. This is due to variations in leaf pigment ratio (Sims and Gamon 2002, Wolf et al. 2013), when lower Chlorophyll-a contents in ageing leaves cause such a spectral shift (Gitelson and Merzlyak 1994, Sims and Gamon 2002).

We expect that access to spectral information of sensors such as Sentinel-2A within the complete growing season may significantly improve the accuracy of SAV mappings, even on species level. Knowledge of species-specific variations within a growing season, however, is essential for identifying and monitoring SAV on species level by using remote sensing approaches. To avoid classification errors we therefore recommend a phenologic adaption of the implemented spectra.

4.5.2 Analysing the results of the spectral unmixing of shallow water areas using depth-invariant indices and WASI-2D

Both approaches were able to retrieve bottom substrate maps, which indicate the potential suitability of Sentinel-2A for monitoring littoral bottom coverage. Both methods provided noticeable differences in SAV extent and distribution (**Figure 4.4** and **Figure 4.6**, **Table 4.2** and **Table 4.3**). Sediment dominates shallow water zones exposed to wind and waves (e.g. the test site 'Roseninsel') and shipping traffic (e.g. the western part of test site 'Seeshaupt') due to a high level of disturbances (Koch 2001). Calm and protected areas with a broad reed belt (e.g. the test site 'Karpfenwinkel' and the south-eastern part of test site 'Seeshaupt') allow the development of a dense SAV patch. Areas with mixed coverage are characteristical for detritus overlay on sediment, plant residuals, epiphytes or sparsely growing SAV with sediment influence (Armstrong 1993, Fyfe 2003, Williams et al. 2003, Silva et al. 2008, Wolf et al. 2013).

The results of the linear spectral unmixing of three littoral bottom types display a spatial distinct differentiation between sediment areas and areas of tall- and meadow-growing SAV species (**Figure 4.5** and **Figure 4.7**, **Table 4.4** and **Table 4.5**). The shallow water area near the harbour 'Seeshaupt' is highly disturbed and therefore classified as sediment. Clam water regions and deeper water zones allow a dense SAV coverage (e.g. test site 'Karpfenwinkel' and south-eastern part of test site 'Seeshaupt'). The distribution of different SAV species seemed to depend on the water depth. While tall-growing species predominate in deeper water regions, meadow-growing species populate shallower areas close to the shoreline. Differing growth height and plant structure may explain this

distribution detected by remote sensing data. The characteristic spectral response of tall-growing species dominates the reflectance signal in the deeper zones. In the satellite data only the canopy of the tall-growing species is visible, because they cover the meadow-growing species and therefore superimpose their characteristic reflectance signal. This behaviour may explain existing differences in classification results of remote sensing data and diver mappings (**Figure 4.1**). In the shallow water regions, meadow-growing species dominate the remote sensing signal, because low water levels aggravate growth of tall-growing species, which therefore are unable to develop a dense canopy. This modifies the characteristic spectral signature and hinders a mapping based on remote sensing.

12 September has to be considered separately, because large parts of the shallow water area are masked wrongly as deep water. The performance of *RI* highly depends on a homogenous deep water reflectance in red wavelengths (630 nm - 700 nm). Differing water constituent concentrations at this acquisition date (see **Table 4.1**) therefore may have affected the *RI* calculation. Improving automatic shallow water delineation may avoid such misinterpretation of its spatial extent. Nevertheless, the linear spectral unmixing of three bottom types using depth-invariant indices also shows some irregularities for this acquisition date. The unmixing results are fundamentally different to those of pervious acquisition dates, which is probably also due to an insufficient consideration of the water constituent concentration in the depth-invariant index calculation.

Comparing the results of both investigated methods showed similarities as well as differences between the spectral unmixing of two or three littoral bottom types (**Figure 4.8** and **Figure 4.9**). In general, for both methods the results for sediment (**Figure 4.8**) scatter less than the results for SAV species (**Figure 4.9**); sediment further showed higher R^2 values (**Table 4.6**). This can be attributed to the spectral differences that are more distinct between sediment and SAV than between SAV species. For both methods, low coefficients of determination demonstrate that an unmixing at SAV species level seems infeasible so far. For this, further research on SAV species differentiation is required. We therefore recommend detailed *in situ* investigation to understand how the spectral signal of SAV

species changes with their phenologic development in freshwater lakes with different trophic states.

A major shortcoming of our study is the lack of validation data. For a meaningful validation, however, large-scale *in situ* measurements on SAV species level are mandatory. Our study showed, that the currently available information based on transect mappings is insufficient for a solid validation of remote sensing data. We expect that large-scale mappings would be more promising to record extend and coverage of SAV patches.

4.6 Conclusions

This study used four Sentinel-2A scenes of August and September 2015 to map the spatio-temporal development of SAV in shallow water areas of the oligotrophic Lake Starnberg (Southern Germany). To map sediment and SAV distribution as well as growth and distribution on species level, we applied the semi-empirical method of depth-invariant indices and the bio-optical model WASI-2D. To provide endmember spectra for the monitoring period, we applied spectral reflectance models of different SAV types for different phenologic stages. The results confirm other studies demonstrating that the spatial and spectral resolution of Sentinel-2A data is suitable for SAV monitoring. Both applied methods provide similar spatial distributions of sediment and SAV. None of the methods, however, was able to show a clear distinction between meadow- and tall-growing SAV species. To improve a proper validation of unmixing results, large-scale *in situ* mappings carried out simultaneously to the satellite overpasses are needed. We further recommend setting up a spectral database of SAV species at different phenologic stages, because an integration of SAV endmember spectra at the proper growth stage may enhance discrimination of SAV at species level. In view of global warming, a multi-year time-series may obtain information about trends in SAV coverage and species distribution. Satellite systems with high spatial resolution and a frequent revisit time such as Sentinel-2 offer the potential to support *in situ* SAV mappings as required by the WFD.

5 General discussion

The studies presented in this thesis provide a novel approach on the mapping of submerged aquatic macrophytes using remote sensing methods on freshwater lakes. The results show that currently practiced monitoring methods of SAV have gaps in spatial and temporal coverage. As presented here, the use of remote sensing methods and satellite data can close these deficits by providing detailed information on the littoral bottom texture of shallow water areas several times a year. The knowledge of detailed species-specific spectral information at different moments within the phenologic development is the basis of this approach. The embedding of the macrophyte phenology variations in the mapping process can increase the classification accuracy of satellite data. Based on these new findings, the previous monitoring methods are critically questioned and novel monitoring approaches are presented (Chapter 5.2), especially regarding to the impact of climate change induced effects (Chapter 5.3).

5.1 Water quality assessment by remote sensing methods

As submerged aquatic macrophytes are sensitive to changes of the environmental conditions such as nutrient conditions, water temperature, water level and transparency (Skubinna et al. 1995, Penning et al. 2008, Søndergaard et al. 2010, Poikane et al. 2015), they serve as biological indicator for the assessment of the ecological status and the water quality of freshwater lakes (Melzer 1999). So far, the water quality assessment is based on the results of *in situ* investigations conducted by a team of divers along the shoreline.

To improve the water quality assessment, remote sensing methods offer great possibilities. As defined by O'Neill et al. (2011), the requirements for detecting submerged aquatic macrophytes using remote sensing methods are the following:

- The spectral characteristics of macrophytes can be separated from the influence of the water column and the atmosphere.
- The spectral properties differ from the surrounding littoral bottom coverage.

- The spectral resolution of the sensor is adequate for resolving these unique spectral characteristics.
- The spatial resolution of the sensor is adequate for recording the spatial patterns of the SAV of interest.

As shown in **Figure 5.1**, several challenges below the water surface (6 – 10) concerning the radiation transfer in the water column and the interaction at the littoral bottom have been investigated, developed and improved in this thesis. The applicability of RapidEye satellite data to map SAV patches in shallow areas of eutrophic freshwater lakes (6 & 7) has been successful (Chapter 2). The spatial distribution and the spatio-temporal development of SAV could be illustrated. Reflectance models of several SAV species and sediment (Chapter 3) provide insight into the spectral variations (8 & 9) within the growing season. Those variations can be linked to the phenologic stages of SAV populations. The inversion of this reflectance models is an important step towards the SAV classification on species level. The simulated SAV spectra have been used to map SAV patches on species level (Chapter 4) by using a Sentinel-2A time series (10).

As suggested by O'Neill et al. (2011), the influence of the water column on the spectral response has to be investigated and separated from the spectral characteristics of the SAV. Therefore, an automated implementation of the concentration of optically active water constituents of shallow (6) and deep water areas (7) in the process of water quality assessment was investigated and tested. To avoid transmission errors, the detailed knowledge of water constituent concentrations should be independent to punctual *in situ* measurement (Chapter 2). The freely available software tool WASI-2D (Gege 2014b) retrieves the concentrations of the optically active water constituents (Chlorophyll-a, cDOM and TSM) over optically deep water areas by inverse modelling of atmospherically corrected Sentinel-2A imagery (Chapter 4). Dörnhöfer et al. (2016a) described the settings to assign the concentrations of water constituents from optically deep water to shallow water areas. For this transfer, a constant value is needed to avoid overfitting in shallow water modelling.

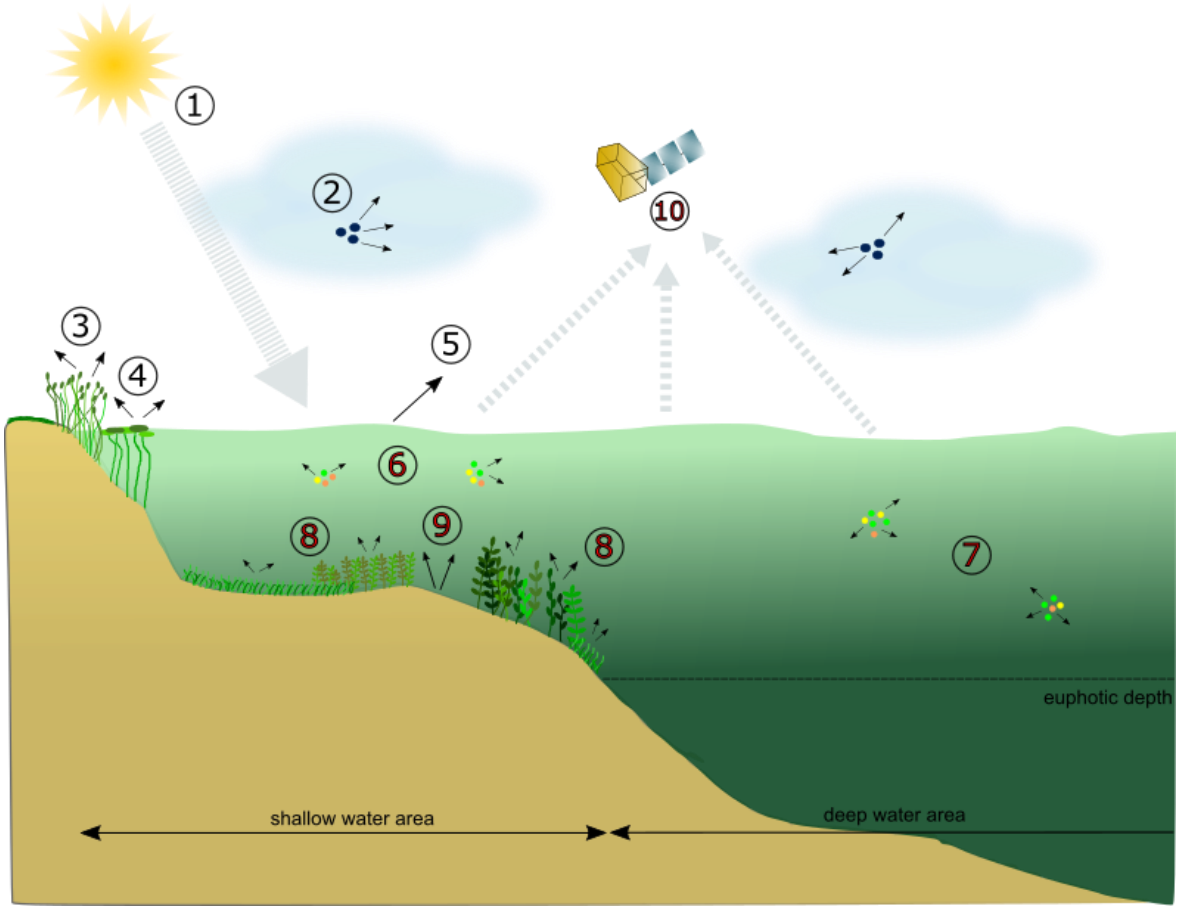

Figure 5.1: The pathway of solar radiation from top of atmosphere towards, in the water body and back to the sensor. The pathway of solar radiation from top of atmosphere towards, in the water body and back to the sensor. Along the path above the water body, the radiation (1) is influenced by particles in the atmosphere (2), by reflection at emergent (3) and floating (4) vegetation and the water surface (5). In the water body, water constituents in shallow (6) and deep (7) water zones and the characteristic reflectance of SAV species (8) and sediment (9) influence the radiation. The radiation arriving at the sensor (10) is the basis for an analysis of lake bottom substrate types by remote sensing satellite images.

The spectral distinction of SAV from the surrounding area is important (O'Neill et al. 2011). Here, the species-specific characterization of the spectral signature of SAV (8) as well as the spectral information of sediment (9) serves as basis of the phenologic fingerprint approach (Wolf et al. 2013). As reported in literature, the spatial and temporal changes in littoral bottom reflectance within one growing period are caused by the development of the coverage level from non-vegetated to fully grown patches (Wolf et al. 2013), by the changes in pigment composition (Peñuelas et al. 1993) and structural changes of the plants (Dierssen et al. 2003) and by the accumulation of periphyton (Drake

et al. 2003). Even bare sediment without visible macrophyte coverage is covered by algae (Stephens et al. 2003) and biotic microfilms (Decho et al. 2003).

The *in situ* collected spectral signatures are combined with the particular phenologic stage and environmental variables such as the temperature and the water constituent concentrations. They are stored in a spectral database (Wolf et al. 2013) and serve as basis for the reflectance models (Chapter 3). These models provide a day and daytime adjusted selection of reflectance spectra. Based on this information, specific images can be taken several times within the growing season. The results of this research (Chapter 3) show that the spectral database and the reflectance models need to be expanded to other SAV species and other lake types. For the expansion, the influence of environmental variables on the phenologic development such as the water temperature needs to be further investigated (Chapter 3). The influence of other environmental variables e.g. turbidity, bottom slope, bottom orientation and periphyton are still research gaps that need to be investigated in the future. A permanent expansion of the spectral library and the continuous development of the reflectance model are necessary to improve the classification of littoral bottom types of shallow water areas.

The spectral and spatial resolution of the applied sensor has to be sufficient to resolve and record the species-specific spectral characteristics and the spatial patterns of SAV. The investigation of freshwater lakes with novel satellite system types with high spatial and temporal resolution (e.g. RapidEye and Sentinel-2) (10) provides more profound information on the littoral bottom types (Chapter 2 and 4) several times within the growing season than common satellite constellations (e.g. Landsat 8). The higher the temporal, spectral and spatial resolution of the used satellite systems, the more precisely shallow water areas can be investigated and the more detailed information on the littoral bottom coverage can be obtained. A continuous adaptation and integration of prospective satellite systems, e.g. hyperspectral sensor types, remains a task in the future.

An accurate water quality assessment and the knowledge of a lakes trophic state is regulated by the WFD (European Commission 2000). The broad coverage of the earth surface by satellites and their high revisiting times constitute an excellent basis for a

monitoring system. In combination with *in situ* mappings by divers, remote sensing allows a close monitoring cycle and spatial-wide information. The knowledge of seasonal variations within the growing season of SAV ensures a precise insert of human resources for *in situ* mappings at places with abnormalities. Due to time series within the growing season, the temporal resolution is clearly improved. The simultaneously recording of a variety of lakes determines a clearly improvement in the monitoring of freshwater lakes as demanded by Palmer et al. (2015).

5.2 Prospective requirements of monitoring methods

According to the requirements of the WFD (European Commission 2000), the established monitoring of SAV is performed in a three-year monitoring cycle by punctual *in situ* investigations of divers. The regular monitoring of SAV provides an overview on the trophic state of freshwater lakes. In order to cover the temporal and spatial gaps and to be able to conduct a continuous and gapless SAV monitoring, further monitoring methods are additionally necessary. This is the only way to identify changes at an early stage, to investigate their cause and to solve feasible problems in time (Palmer et al. 2015).

Remote sensing offers the possibility of improvement of the previous monitoring method. With their high spatial resolution and temporal coverage, multispectral satellite systems (e.g. RapidEye, Sentinel-2A) are prerequisite for an investigation of shallow water areas. Conventional satellite systems (e.g. Landsat 8) have a revisit time of more than 2 weeks under optimal, cloud-free conditions. This means that often only a few data takes can be recorded within the growing season. A continuous data acquisition and analysis is not possible in this way. In contrast to punctual transect mappings, remote sensing approaches deliver spatial-wide information on SAV at short time intervals several times a year. In addition to the mentioned advantages, remote sensing approaches for water bodies also have their vulnerabilities. The greatest restriction of optimal remote sensing approaches is their weather-dependence. A free view from sensor to object and as few cloud coverage as possible are the best preconditions for successful satellite image. The absorption properties of water in the wavelength region above 700 nm complicate the

approach. In this region almost all incoming radiation is absorbed and spectral SAV characteristics cannot be integrated in a further monitoring process.

The presented approaches (Chapter 2 & 4) already deliver reliable results for mapping littoral bottom types and give a first overview of the littoral bottom coverage. As long as the mapping is limited to a differentiation between SAV and sediment, the monitoring approaches offer the possibility to detect variations of the littoral bottom coverage within one growing season. Both, the expansion of SAV patches while plant growing and the decrease of planted areas are displayed on the retrieved satellite data. Bare sediment areas that are exposed to wind and waves (Koch 2001) and that are highly frequented by humans can be clearly separated from vegetated patches. With the presented approaches, an identification of SAV on base of growth height or species level is currently not sufficiently feasible (Chapter 4). However, the studies show that there are noticeable spectral differences between the individual SAV species and between the phenologic stages within one species (Pinnel et al. 2004, Pinnel 2007, Wolf et al. 2013, Roessler et al. 2013a, Chapter 3). For an identification on species level, further systematic investigations of SAV and its phenologic development are highly recommended (Chapter 4). Nevertheless, together with the regular diving observations recommended by the WFD (European Commission 2000), the presented methods can be used for preliminary classification and may help to upscale punctual observations.

According to the presented results (Chapter 4), a SAV monitoring on species level as demanded by the WFD (European Commission 2000) cannot be performed yet with the presented methods, but they may support the *in situ* mappings carried out so far. As the mapping of SAV patches performs well with current methods and sensor techniques (Chapter 2 & 4), the improvement of a remote sensing based monitoring system needs further information on the level of SAV species. As presented in the results (Chapter 2), a differentiation of littoral bottom types in vegetated and non-vegetated areas can be applied all over the shallow water areas in freshwater lakes. The key element for a SAV monitoring on species level with remote sensing approaches is the detailed knowledge of the specific spectral phenologic development of SAV indicator species (Pinnel 2007, Wolf

et al. 2013). The spectral characteristics have to be included in the SAV mapping process to differentiate between the SAV indicator species (Chapter 3 & 4). These features are not only species-specific. Dependent on patch location, varying environmental parameters influence the SAV patches, their seasonal development and therefore their characteristic spectral signature (Barko and Smart 1986, Barko et al. 1991, Blindow 1992, Madsen and Brix 1997, Rooney and Kalff 2000, Squires and Lesack 2003, Zhu et al. 2008, Shuchman et al. 2013, Hoffmann et al. 2014, Singh and Singh 2015, Chapter 3). For embedding in the SAV monitoring process, detailed information on the water temperature, the lake's trophic state, nutrient load, periphyton growth on leaves, the lake morphology and the shading effects of the plant canopy is required.

A general weakness is the validation of SAV species detected by remote sensing. Especially, the validation of spatial-wide shallow water areas poses a problem. To improve the SAV monitoring process, a suitable validation is prerequisite. Pointed data takes with large-scales *in situ* mapping by divers where the SAV patches are precise documented in species and position are essential for spatial-wide validated data.

Anyway, a further development of the present monitoring methods is essential. An improvement of the monitoring methods allows a broad coverage of the investigation area (e.g. observation by remote sensing methods and satellite systems), a better use of human resources and a target-orientated and specified analysis of the investigation object (e.g. monitoring of the occurrence of target species on molecular level such as environmental DNA). The advantage of spatial-wide, continuous monitoring approaches is the early recognition of changes (e.g. SAV growth structure changes, changes of the lake's trophic state, desertification, changes in the shoreline). Spatial-wide monitoring methods with a possible loss of detailed information can be supported and improved by punctual measurements at particularly prominent points to save time, money and human resources. Without this transfer from punctual to spatially explicit monitoring a gapless data take of freshwater lakes will not be realizable.

5.3 The influence of climate change induced changes on the water quality

Aquatic ecosystems are expected to change noticeably in the future. Beside eutrophication and inorganic and organic contaminations, the effects of climate change (e.g. an increasing air and water temperature) are stressors for the ecological balance in freshwater lakes (Brönmark and Hansson 2002, Dudgeon et al. 2005, Hering et al. 2010, Moss 2012). Nevertheless, extreme events (e.g. heavy rainfall events, prolonged drought periods, mild winters and rainy summers) are expected to occur more frequently in the future. Both, the water quality as well as the ecology of freshwater lakes is influenced by those changes (Moss 2012). Consequences are for example variations in the length of growing season and a shift of vegetation growing within the year, a variation in the length of the growing season or changes in the shoreline (e.g. changing water level line and dry areas). Chapter 3 illustrates the influence of temperature on the spectral response of a SAV population and on the length of growing season. In the summer 2015, the air temperature was comparatively high. Differences between indigenous and invasive species have been observed. For example, the indigenous species *Chara* spp. shows changes in the phenologic development and the length of growing season. Their senescence phase started earlier and the degradation processes faster.

However, a changing of environmental conditions also may offer better habitat conditions for new, non-native species. Invasive species, originated from climate zones with higher temperatures, use the rising water temperatures to spread and to establish populations in new lakes. It is assumed that non-native, invasive species (e.g. *Elodea nuttalllii*) as well as indigenous, thermophile species (e.g. *Najas marina*) spread better and more extensively and thus push back or even replace indigenous species (e.g. *Chara* spp.) (McKee et al. 2002, Meerhoff et al. 2007, Hussner et al. 2010, Wolf et al. 2013). In warmer water bodies in northern and north-western Germany, 16 out of 21 aquatic neophyte species have established stable populations; in Southern Germany 11 neophyte species have been discovered so far (Hussner et al. 2010, Hussner 2012).

In order to be able to detect changes in the species composition and the distribution at an early stage, it seems advisable to take close monitoring recordings with simultaneously broad spatial coverage. This close monitoring grid enables a spatial-wide survey at close intervals. In this way, changes in littoral bottom coverage and species composition can be detected at an early stage. This seems to be the only way to counteract the displacement of indigenous SAV species and the loss of natural biodiversity in time.

5.4 Outlook

The continuously rising air temperature and the increasing likelihood of extreme events in the future underpin the importance of a targeted monitoring of changes in aquatic ecosystems. As shown in this thesis and in the cited literature, SAV plays an important role in the monitoring of freshwater lakes. The integration of more SAV species, targeted studies of climate change-related environmental impacts and a further development of monitoring procedures are recommended for prospective research.

In this thesis, the SAV species *Chara* spp., *P. perfoliatus* and *E. nuttallii* were investigated. The integration of other SAV species and other water quality types into the spectral database will improve the presented macrophyte models. Special attention should be given to indicator species (e.g. according to the WFD) and to invasive species. The investigation of one species at different lakes and lake types also improves the model.

Furthermore, targeted studies of climate change-related environmental impacts on SAV are recommended. For example, a continuously recording of air and water temperatures at several prominent points near the study areas allows an unambiguous link between the environmental parameters and the phenologic development of SAV. This additional information also flows into the spectral database and thus improves the SAV modelling.

A further development of monitoring procedures is to be expected in the future. The standardised monitoring needs to be adapted to novel options. In this way, remote sensing methods can already be used as support and help to detect changes of the littoral bottom coverage at an early stage. In order to further expand satellite-based monitoring,

the spectral resolution of the available sensors is of central importance. A further development in the direction of satellite-based hyperspectral sensors, which can also be used operationally, offers a significant improvement of the presented methods.

6 Author contributions

A similar version of chapter 2 was published: Fritz C., Dörnhöfer K., Schneider T., Geist J., Oppelt N. Mapping submerged aquatic vegetation using RapidEye satellite data: the example of Lake Kummerow (Germany). Water 2017, 9, 510.

Christine Fritz, Katja Dörnhöfer, Thomas Schneider, Juergen Geist and Natascha Oppelt conceived and designed the study. Christine Fritz wrote the majority of the paper and analysed image data. Katja Dörnhöfer conducted atmospheric correction and SAV evaluation. All authors contributed equally in reviewing and finalizing the manuscript.

A similar version of chapter 3 was published: Fritz C., Schneider T., Geist J. Seasonal variation in spectral response of submerged aquatic macrophytes: A case study at Lake Starnberg (Germany). Water 2017, 9, 527.

Christine Fritz and Thomas Schneider conceived and designed the experiments. Christine Fritz performed the experiments. Christine Fritz and Thomas Schneider analysed the data. Christine Fritz, Thomas Schneider and Juergen Geist conceived, structured and jointly wrote the paper.

A similar version of chapter 4 was submitted: Fritz C., Dörnhöfer K., Schneider T., Geist J., Oppelt N. Mapping development of submerged aquatic vegetation by using a Sentinel-2A time series at Lake Starnberg (Germany).

Christine Fritz, Katja Dörnhöfer, Thomas Schneider, Juergen Geist and Natascha Oppelt conceived and designed the study. Christine Fritz wrote the majority of the paper and analysed image data. Katja Dörnhöfer conducted atmospheric correction. All authors contributed equally in reviewing and finalizing the manuscript.

7 Publication list

The following papers were included in this thesis:

Fritz, C.; Dörnhöfer, K.; Schneider, T.; Geist, J.; Oppelt, N. Mapping Submerged Aquatic Vegetation Using RapidEye Satellite Data: The Example of Lake Kummerow (Germany). *Water* **2017**, *9*, 510.

Published online DOI: 10.3390/w9070510

Fritz, C.; Schneider, T.; Geist, J. Seasonal Variation in Spectral Response of Submerged Aquatic Macrophytes: A Case Study at Lake Starnberg (Germany). *Water* **2017**, *9*, 527.

Published online DOI: 10.3390/w9070527

Fritz C.; Dörnhoefer K.; Schneider T.; Geist J.; Oppelt N. Mapping development of submerged aquatic vegetation by using a Sentinel-2A time series at Lake Starnberg (Germany).

Co-authorships (not included in this thesis):

Dörnhöfer, K.; Liekefett, M.; **Fritz, C.**; Oppelt, N. Mapping benthos, bathymetry and water constituents of inland waters using Landsat 8 - a case study at Lake Kummerow near Rostock. Deutscher Luft- und Raumfahrtkongress 2015.

Oral contributions related to the thesis:

Fritz, C., Roessler, S., Wolf, P., Schneider, T. 2016. Spectral signature database of submersed aquatic plants in support of bio-optical model inversion based on satellite data. 3rd International Conference on Water Resources and Wetlands, September 8-10 2016, Tulcea, Romania.

Poster contributions related to the thesis:

Fritz, C., Dörnhöfer, K., Oppelt, N., Schneider, T. 2016. LAKESAT – Synergetische Nutzung von räumlich hoch- und mittelauflösenden Satellitendaten zur Analyse von Binnengewässern. Nutzung der Sentinels und nationalen Erdbeobachtungs-Missionen, DLR Raumfahrtmanagement, January 21 – 22 2015, Bonn, Germany.

Fritz, C., Schneider, T., Geist, J. 2015. Aquatic plants spectral signature database in support of bio-optical inversion based on satellite data, Mapping Water Bodies from Space, European Space Agency, March 18 – 19 2015, Frascati, Italy.

Fritz, C., Geist, J., Schneider, T. 2015. A spectral signature database of aquatic plants for a bio-optical model inversion based on satellite data, Fresh Blood for Fresh Water, Universität Innsbruck, April 15 – 17 2015, Mondsee, Austria.

Fritz, C., Roessler, S., Wolf, P., Schneider, T. 2016. Monitoring der Seebodenbedeckung mit multitemporalen RapidEye-Daten. RESA Workshop „Von der Zustands- zur Prozessanalyse – Nutzung von Zeitreihen des RESA“, DLR Raumfahrmanagement, March 15 – 16 2016, Bonn, Germany.

Fritz, C., Schneider, T. 2016. Comparing the annual shift of phenologic development of submersed macrophytes based on *in situ* remote sensing reflectance, ESA Living Planet Symposium, European Space Agency, May 09 – 13 2016, Prague, Czech Republic.

Fritz, C., Schneider, T., Dörnhöfer, K., Oppelt, N. 2018. Mapping Submerged Aquatic Vegetation by Using a Sentinel-2A Time Series at Lake Starnberg (Germany), Mapping Water Bodies from Space, European Space Agency, March 27 – 28 2018, Frascati, Italy.

8 Acknowledgements

I would like to thank the Federal Ministry for Economic Affiars and Energy (BMWi) for supporting the project LAKESAT (grant numbers 50EE1336 and 50EE1340) to make this study possible. Also thanks to the company Planet Labs, which provided us RapidEye satellite data within the RapidEye Research Archive project no. 194.

I would also like to thank many people without their support this work would not have been possible. These are primarily colleagues and friends at the Limnological Research Station Iffeldorf. Special thanks to my supervisor Prof. Dr. Jürgen Geist for his continuous support and his helpful comments and suggestions. Thanks to my mentor and project supervisor Dr. Thomas Schneider, who has created a unique working atmosphere through his unparalleled manner and his incredible creativity. I would like to thanks Prof. Dr. Natascha Oppelt from CAU Kiel for her support and helpful tips. In all friendship, I would like to thank my 'doctoral sister' Katja Dörnhöfer from CAU Kiel for our cooperation in the project LAKESAT, our measurement campaigns, our discussions and our mutual motivation. Many, many thanks Katja! I also thank the PhD students Stephanie Rüegg, Franziska Bauer, Andrea Hofmann, Simon Baier, Joachim Ruber, Sebastian Lenz, Pia Scherer, Nicolas Corti, Stefan Ossyssek and Wolfgang Küfner and Dr. Markus Hoffmann for the support and motivating cooperation. Also many thanks to Dr. Uta Raeder, Stefan Zimmermann, Brigitte Beier, Christina Dieminger, Maria Klatt und Hans Hatzl and all the other staff and students, I meet during my time in Iffeldorf. At this point, special thanks to Dr. Patrick Wolf. I wouldn't have had the idea of doing a PhD without you!

My deepest thanks are addressed to my parents, to my sister Gundi, to my friends and to Markus. Thank you very much for your support over all these years!

9 References

Akima, H., Gebhardt, A., Petzoldt, T.,Maechler, M. **2013**. akima: Interpolation of irregularly spaced data. R package version 0.5-11.

Albert, A.,Mobley, C. D. **2003**. An analytical model for subsurface irradiance and remote sensing reflectance in deep and shallow case-2 waters. *Optics Express 11*: 2873 -2890.

Arle, J., Blondzik, K., Claussen, U., Duffek, A., Grimm, S., Hilliges, F., Hoffmann, A., Leujak, W., Mohaupt, V., Naumann, S., Pirntke, U., Richter, S., Schilling, P., Schroeter-Kermani, C., Ullrich, A., Wellmitz, J., Werner, S.,Wolter, R. **2013**. Wasserwirtschaft in Deutschland. Teil 2. Gewässergüte. *Umweltbundesamt (UBA); Bonn, Germany, 2013.*

Armstrong, R. A. **1993**. Remote sensing of submerged vegetation canopies for biomass estimation. *International Journal of Remote Sensing 14*: 621-627.

Barko, J. W., Gunnison, D.,Carpenter, S. R. **1991**. Sediment interactions with submersed macrophyte growth and community dynamics. *Aquatic Botany 41*: 41-65.

Barko, J. W.,Smart, R. M. **1981**. Comparative Influences of Light and Temperature on the Growth and Metabolism of Selected Submersed Freshwater Macrophytes. *Ecological Monographs 51*: 219-235.

Barko, J. W.,Smart, R. M. **1986**. Sediment-related mechanisms of growth limitation in submersed macrophytes. *Ecology 67*: 1328-1340.

Bavarian Environmental Agency. **2000**. Digital Elevation Model of Lake Starnberg.

Bavarian Environmental Agency. **2016**. Bavarian Hyrological Service, www.gkd.bayern.de.

Bey, A., Sánchez-Paus Díaz, A., Maniatis, D., Marchi, G., Mollicone, D., Ricci, S., Bastin, J.-F., Moore, R., Federici, S.,Rezende, M. **2016**. Collect Earth: Land Use and Land Cover Assessment through Augmented Visual Interpretation. *Remote Sensing 8*: 807.

Blindow, I. **1992**. Long- and short-term dynamics of submerged macrophytes in two shallow eutrophk lakes. *Freshwater Biology 28*: 15-27.

Bolpagni, R., Bresciani, M., Laini, A., Pinardi, M., Matta, E., Ampe, E. M., Giardino, C., Viaroli, P.,Bartoli, M. **2014**. Remote sensing of phytoplankton-macrophyte coexistence in shallow hypereutrophic fluvial lakes. *Hydrobiologia 737*: 67-76.

Bostater, J. C. R., Ghir, T., Bassetti, L., Hall, C., Reyeier, E., Lowers, R., Holloway-Adkins, K.,Virnstein, R. In *Hyperspectral remote sensing protocol development for submerged aquatic vegetation in shallow waters*, 2004; pp 199-215.

Brando, V. E.,Dekker, A. G. **2003**. Satellite Hyperspectral Remote Sensing for Estimating Estuarine and Coastal Water Quality. *IEEE Transaction on Geoscience and Remote Sensing 41*: 1376-1387.

Bricaud, A., Babin, M., Morel, A.,Claustre, H. **1995**. Variability in the chlorophyll-specific absorption coefficients of natural phytoplankton: Analysis and parameterization. *Journal of geophysial research 100*: 13-13.

Brönmark, C.,Hansson, L.-A. **2002**. Environmental issues in lakes and ponds: current state and perspectives. *Environmental Conservation 29*: 290-307.

Brooks, C., Grimm, A., Shuchman, R., Sayers, M.,Jessee, N. **2015**. A satellite-based multi-temporal assessment of the extent of nuisance Cladophora and related submerged aquatic vegetation for the Laurentian Great Lakes. *Remote Sensing of Environment 157*: 58-71.

Carvalho, L., McDonald, C., de Hoyos, C., Mischke, U., Phillips, G., Borics, G., Poikane, S., Skjelbred, B., Solheim, A. L., Van Wichelen, J.,Cardoso, A. C. **2013**. Sustaining recreational quality of European lakes: minimizing the health risks from algal blooms through phosphorus control. *Journal of Applied Ecology 50*: 315-323.

Ciraolo, G., Cox, E., La Loggia, G.,Maltese, A. **2006**. The classification of submerged vegetation using hyperspectral MIVIS data.

Congalton, R. G. **1991**. A review of assessing the accuracy of classifications of remotely sensed data. *Remote Sensing of Environment 37*: 35-46.

Decho, A. W., Kawaguchi, T., Allison, M. A., Louchard, E. M., Reid, R. P., Stephens, F. C., Voss, K. J., Wheatcroft, R. A.,Taylor, B. B. **2003**. Sediment properties influencing upwelling spectral reflectance signatures: The "biofilm gel effect". *Limnology and Oceanography 48*: 431-443.

Dekker, A. G., Phinn, S. R., Anstee, J., Bissett, P., Brando, V. E., Casey, B., Fearns, P., Hedley, J., Klonowski, W.,Lee, Z. P. **2011**. Intercomparison of shallow water bathymetry, hydro-optics, and benthos mapping techniques in Australian and Caribbean coastal environments. *Limnol. Oceanogr. Methods 9*: 396-425.

Dekker, A. G., Vos, R. J.,Peters, S. W. M. **2002**. Analytical algorithms for lake water TSM estimation for retrospective analyses of TM and SPOT sensor data. *International Journal of Remote Sensing 23*: 15-35.

Diehl, S. **1993**. Effects of habitat structure on resource availability, dietand growth of benthivorous perch, Perca fluviatilis. *Oikos 67*: 403-414.

Dierssen, H. M., Zimmerman, R. C., Leathers, R. A., Downes, T. V.,Davis, C. O. **2003**. Ocean color remote sensing of seagrass and bathymetry in the Bahamas Banks by high-resolution airborne imagery. *Limnology and Oceanography 48*: 444-455.

Dogan, O. K., Akyurek, Z.,Beklioglu, M. **2009**. Identification and mapping of submerged plants in a shallow lake using quickbird satellite data. *Journal of Environmental Management 90*: 2138-2143.

Dörnhöfer, K., Göritz, A., Gege, P., Pflug, B.,Oppelt, N. **2016a**. Water Constituents and Water Depth Retrieval from Sentinel-2A—A First Evaluation in an Oligotrophic Lake. *Remote Sensing 8*: 941.

Dörnhöfer, K., Klinger, P., Heege, T.,Oppelt, N. **2018**. Multi-sensor satellite and in situ monitoring of phytoplankton development in a eutrophic-mesotrophic lake. *Science of The Total Environment 612*: 1200-1214.

Dörnhöfer, K.,Oppelt, N. **2016b**. Remote sensing for lake research and monitoring – Recent advances. *Ecological Indicators 64*: 105-122.

Drake, L. A., Dobbs, F. C.,Zimmerman, R. C. **2003**. Effects of epiphyte load on optical properties and photosynthetic potential of the seagrasses Thalassia testudinum Banks ex König and Zostera marina L. *Limnology and Oceanography 48*: 456-463.

Dudgeon, D., Arthington, A. H., Gessner, M. O., Kawabata, Z.-I., Knowler, D. J., Lévêque, C., Naiman, R. J., Prieur-Richard, A.-H., Soto, D., Stiassny, M. L. J.,Sullivan, C. A. **2005**. Freshwater biodiversity: importance, threats, status and conservation challenges. *Biological Reviews 81*: 163-182.

Elatawneh, A., Kalaitzidis, C., Petropoulos, G. P.,Schneider, T. **2014**. Evaluation of diverse classification approaches for land use/cover mapping in a Mediterranean region utilizing Hyperion data. *International Journal of Digital Earth 7*: 194-216.

European Commission. **2000**. The Water Framework Directive (Directive 2000/60/EC of the European Parliament and of the Council of 23 October 2000 Establishing A Framework for Community Action in the Field of Water Policy); Official Journal of the European Communities: Brussels, Belgium, 2000; pp. 1–72. *Offical Journal of the European Community 22*: 1-72.

Foody, G. M. **2002**. Status of land cover classification accuracy assessment. *Remote Sensing of Environment 80*: 185-201.

Fritz, C., Dörnhöfer, K., Schneider, T., Geist, J.,Oppelt, N. **2017a**. Mapping submerged aquatic vegetation using RapidEye satellite data: the example of Lake Kummerow (Germany). *Water 9*.

Fritz, C., Schneider, T.,Geist, J. **2017b**. Seasonal Variation in Spectral Response of Submerged Aquatic Macrophytes: A Case Study at Lake Starnberg (Germany). *Water 9*.

Fyfe, S. **2003**. Spatial and temporal variation in spectral reflectance: Are seagrass species spectrally distinct? *Limnology and Oceanography 48*: 464-479.

Gausman, H. W. **1984**. Evaluation of factors causing reflectance differences between Sun and Shade Leaves. *Remote Sensing of Environment 15*: 177-181.

Gege, P. **2004**. The water color simulator WASI: an integrating software tool for analysis and simulation of optical in situ spectra. *Computers & Geosciences 30*: 523-532.

Gege, P. **2014a**. A case study at Starnberger See for hyperspectral bathymetry mapping using inverse modeling. *Proceedings of WHISPERS*: 1-4.

Gege, P. **2014b**. WASI-2D: A software tool for regionally optimized analysis of imaging spectrometer data from deep and shallow waters. *Computers & Geosciences 62*: 208-215.

George, D. G. **1997**. The airborne remote sensing of phytoplankton chlorophyll in the lakes and tarns of the English Lake District. *International Journal of Remote Sensing 18*: 1961-1975.

Giardino, C., Bartoli, M., Candiani, G., Bresciani, M.,Pellegrini, L. **2007**. Recent changes in macrophyte colonisation patterns: an imaging spectrometry-based evaluation of southern Lake Garda (northern Italy). *Journal of Applied Remote Sensing 1*: 011509-011509-011517.

Giardino, C., Bresciani, M., Valentini, E., Gasperini, L., Bolpagni, R.,Brando, V. E. **2015**. Airborne hyperspectral data to assess suspended particulate matter and aquatic vegetation in a shallow and turbid lake. *Remote Sensing of Environment 157*: 48-57.

Giardino, C., Candiani, G., Bresciani, M., Lee, Z., Gagliano, S.,Pepe, M. **2012**. BOMBER: A tool for estimating water quality and bottom properties from remote sensing images. *Computers & Geosciences 45*: 313-318.

Gitelson, A.,Merzlyak, M. N. **1994**. Quantitative estimation of chlorophyll-a using reflectance spectra: Experiments with autumn chestnut and maple leaves. *Journal of Photochemistry and Photobiology B: Biology 22*: 247-252.

Gitelson, A. A., Zur, Y., Chivkunova, O. B.,Merzlyak, M. N. **2002**. Assessing Carotenoid Content in Plant Leaves with Reflectance Spectroscopy. *Photochemistry and Photobiology 75*: 272-281.

Heblinski, J., Schmieder, K., Heege, T., Agyemang, T. K., Sayadyan, H.,Vardanyan, L. **2011**. High-resolution satellite remote sensing of littoral vegetation of Lake Sevan (Armenia) as a basis for monitoring and assessment. *Hydrobiologia 661*: 97-111.

Heege, T., Bogner, A.,Pinnel, N. In *Mapping of submerged aquatic vegetation with a physically based processing chain*, SPIE-The International Society for Optical Engineering, Barcelona, Spain, 2003; E. Kramer, Ed. Barcelona, Spain, pp 43-50.

Heege, T.,Fischer, J. **2004**. Mapping of water constituents in Lake Constance using multispectral airborne scanner data and a physically based processing scheme. *Canadian Journal of Remote Sensing 30*: 77-86.

Heege, T., Kiselev, V., Wettle, M.,Hung, N. N. **2014**. Operational multi-sensor monitoring of turbidity for the entire Mekong Delta. *International Journal of Remote Sensing 35*: 2910-2926.

Hering, D., Borja, A., Carstensen, J., Carvalho, L., Elliott, M., Feld, C. K., Heiskanen, A.-S., Johnson, R. K., Moe, J., Pont, D., Solheim, A. L.,de Bund, W. v. **2010**. The European

Water Framework Directive at the age of 10: A critical review of the achievements with recommendations for the future. *Science of The Total Environment 408*: 4007-4019.

Herold, M., Metz, J.,Romsos, J. S. **2007**. Inferring littoral substrates, fish habitats, and fish dynamics of Lake Tahoe using IKONOS data. *Canadian Journal of Remote Sensing 33*: 445-456.

Hestir, E. L., Brando, V. E., Bresciani, M., Giardino, C., Matta, E., Villa, P.,Dekker, A. G. **2015**. Measuring freshwater aquatic ecosystems: The need for a hyperspectral global mapping satellite mission. *Remote Sensing of Environment 167*: 181-195.

Hestir, E. L., Khanna, S., Andrew, M. E., Santos, M. J., Viers, J. H., Greenberg, J. A., Rajapakse, S. S.,Ustin, S. L. **2008**. Identification of invasive vegetation using hyperspectral remote sensing in the California Delta ecosystem. *Remote Sensing of Environment 112*: 4034-4047.

Hoffmann, M.,Raeder, U. **2016**. Predicting the potential distribution of neophytes in Southern Germany using native Najas marina as invasion risk indicator. *Environmental Earth Sciences 75*: 1217.

Hoffmann, M., Sacher, M., Lehner, S., Raeder, U.,Melzer, A. **2013**. Influence of sediment on the growth of the invasive macrophyte Najas marina ssp intermedia in lakes. *Limnologica 43*: 265-271.

Hoffmann, M. A., Raeder, U.,Melzer, A. **2014**. Influence of environmental conditions on the regenerative capacity and the survivability of Elodea nuttallii fragments. *2014 74*.

Hunter, P. D., Gilvear, D. J., Tyler, A. N., Willby, N. J.,Kelly, A. **2010**. Mapping macrophytic vegetation in shallow lakes using the Compact Airborne Spectrographic Imager (CASI). *Aquatic Conservation: Marine and Freshwater Ecosystems 20*: 717-727.

Hussner, A. **2012**. Alien aquatic plant species in European countries. *Weed Research 52*: 297-306.

Hussner, A., Van De Weyer, K., Gross, E. M.,Hilt, S. **2010**. Comments on increasing number and abundance of non-indigenous aquatic macrophyte species in Germany. *Weed Research 50*: 519-526.

Kaufman, Y., Tanré, D., Gordon, H., Nakajima, T., Lenoble, J., Frouin, R., Grassl, H., Herman, B., King, M.,Teillet, P. **1997**. Passive remote sensing of tropospheric aerosol and atmospheric correction for the aerosol effect. *Journal of Geophysical Research: Atmospheres 102*: 16815-16830.

Kay, S., Hedley, J. D.,Lavender, S. **2009**. Sun glint correction of high and low spatial resolution images of aquatic scenes: A review of methods for visible and near-infrared wavelengths. *Remote Sensing 1*: 697-730.

Kirk, J. T. **1994**. *Light and photosynthesis in aquatic ecosystems*. Cambridge university press.

Kirk, J. T. O. **2011**. Light and photosynthesis in aquatic ecosystems.

Koch, E. W. **2001**. Beyond light: physical, geological, and geochemical parameters as possible submersed aquatic vegetation habitat requirements. *Estuaries 24*: 1-17.

Kohler, A. **1978**. Methoden der Kartierung von Flora und Vegetation von Süßwasserbiotopen. *Landschaft und Stadt; 10; 2; 73-85*.

Kutser, T., Miller, I.,Jupp, D. L. B. **2006**. Mapping coral reef benthic substrates using hyperspectral space-borne images and spectral libraries. *Estuarine, Coastal and Shelf Science 70*: 449-460.

Lee, Z., Carder, K. L., Mobley, C. D., Steward, R. G.,Patch, J. S. **1998**. Hyperspectral remote sensing for shallow waters. I. A semianalytical model. *Applied Optics 37*: 6329-6338.

Lee, Z., Carder, K. L., Mobley, C. D., Steward, R. G.,Patch, J. S. **1999**. Hyperspectral remote sensing for shallow waters: 2. Deriving bottom depths and water properties by optimization. *Applied Optics 38*: 3831-3843.

Levy, R., Hsu, C.,et al. **2015a**. MODIS Atmosphere L2 Aerosol Product (MYD04). NASA MODIS Adaptive Processing System, Goddard Space Flight Center, USA.

Levy, R., Hsu, C.,et al. **2015b**. MODIS Atmosphere L2 Aerosol Product (MOD04). NASA MODIS Adaptive Processing System, Goddard Space Flight Center, USA.

LU-MV. **2015**. Investigation of macrophytes in selected lakes Mecklenburg-Western Pomerania in the year 2013 (data set). Lake Kummerow (200010). Data set request at MLUV-MV. . *Ministerium für Landwirtschaft, Umwelt und Verbraucherschutz Mecklenburg-Vorpommern – Seenprogramm M-V (MLUV-MV)*.

Lyzenga, D. R. **1978**. Passive remote sensing techniques for mapping water depth and bottom features. *Applied Optics 17*: 379-383.

Lyzenga, D. R. **1981**. Remote sensing of bottom reflectance and water attenuation parameters in shallow water using aircraft and Landsat data. *International Journal of Remote Sensing 2*: 71-82.

Madsen, T. V.,Brix, H. **1997**. Growth, photosynthesis and acclimation by two submerged macrophytes in relation to temperature. *Oecologia 110*: 320-327.

Malthus, T. J.,George, D. G. **1997**. Airborne remote sensing of macrophytes in Cefni Reservoir, Anglesey, UK. *Aquatic Botany 58*: 317-332.

Malthus, T. J.,Karpouzli, E. **2003**. Integrating field and high spatial resolution satellite-based methods for monitoring shallow submersed aquatic habitats in the Sound of Eriskay, Scotland, UK. *International Journal of Remote Sensing 24*: 2585-2593.

Manakos, I., Karakizi, C., Gkinis, I.,Karantzalos, K. **2017**. Validation and Inter-Comparison of Spaceborne Derived Global and Continental Land Cover Products for the Mediterranean Region: The Case of Thessaly. *Land 6*: 34.

Manessa, M. D. M., Kanno, A., Sekine, M., Ampou, E. E., Widagti, N.,As-syakur, A. R. **2014**. Shallow-water benthic identification using multispectral satellite imagery:

investigation on the effects of improving noise correction method and spectral cover. *Remote Sensing 6*: 4454-4472.

Marion, L.,Paillisson, J. M. **2003**. A mass balance assessment of the contribution of floating-leaved macrophytes in nutrient stocks in an eutrophic macrophyte-dominated lake. *Aquatic Botany 75*: 249-260.

Maritorena, S. **1996**. Remote sensing of the water attenuation in coral reefs: a case study in French Polynesia. *International Journal of Remote Sensing 17*: 155-166.

McKee, D., Hatton, K., Eaton, J. W., Atkinson, D., Atherton, A., Harvey, I.,Moss, B. **2002**. Effects of simulated climate warming on macrophytes in freshwater microcosm communities. *Aquatic Botany 74*: 71-83.

Meerhoff, M., Clemente, J. M., De Mello, F. T., Iglesias, C., Pedersen, A. R.,Jeppesen, E. **2007**. Can warm climate-related structure of littoral predator assemblies weaken the clear water state in shallow lakes? *Global Change Biology 13*: 1888-1897.

Melzer, A. **1976**. Makrophytische Wasserpflanzen als Indikatoren des Gewässerzustandes oberbayerischer Seen. *Dissertationes Botanicae; 34; 1-195*: 195.

Melzer, A. **1999**. Aquatic macrophytes as tools for lake management. *Hydrobiologia 395*: 181-190.

Melzer, A.,Schneider, S. **2001**. Submerse Makrophyten als Indikatoren der Nährstoffbelastung von Seen *Handbuch Angewandte Limnologie*.

Melzer, A., Zimmermann, S.,Schorer, A. **2003**. Seelitorale in Bayern: Starnberger See, Makrophyten-Kartierungen 1979, 1989 und 2000.

Mertes, L. A. K., Smith, M. O.,Adams, J. B. **1993**. Estimating suspended sediment concentrations in surface waters of the amazon river wetlands from LANDSAT images. *Remote Sensing of Environment 43*: 281-301.

Mobley, C. D. **1999**. Estimation of the remote-sensing reflectance from above-surface measurements. *Applied Optics 38*: 7442-7455.

Mobley, C. D., Boss, E.,Roesler, C. Ocean Optics Web Book. Available online: http://www.oceanopticsbook.info/ (accessed on 10 July 2017)

Morel, A.,Belanger, S. **2006**. Improved detection of turbid waters from ocean color sensors information. *Remote Sensing of Environment 102*: 237-249.

Moss, B. **2012**. Cogs in the endless machine: Lakes, climate change and nutrient cycles: A review. *Science of The Total Environment 434*: 130-142.

Mumby, P. J., Clark, C. D., Green, E. P.,Edwards, A. J. **1998**. Benefits of water column correction and contextual editing for mapping coral reefs. *International Journal of Remote Sensing 19*: 203-210.

O'Neill, J. D., Costa, M.,Sharma, T. **2011**. Remote Sensing of Shallow Coastal Benthic Substrates: In situ Spectra and Mapping of Eelgrass (Zostera marina) in the Gulf Islands National Park Reserve of Canada. *Remote Sensing 3*: 975.

Palmer, S. C. J., Kutser, T.,Hunter, P. D. **2015**. Remote sensing of inland waters: Challenges, progress and future directions. *Remote Sensing of Environment 157*: 1-8.

Penning, W. E., Dudley, B., Mjelde, M., Hellsten, S., Hanganu, J., Kolada, A., van den Berg, M., Poikane, S., Phillips, G., Willby, N.,Ecke, F. **2008**. Using aquatic macrophyte community indices to define the ecological status of European lakes. *Aquatic Ecology 42*: 253-264.

Peñuelas, J., Gamon, J. A., Griffin, K. L.,Field, C. B. **1993**. Assessing community type, plant biomass, pigment composition, and photosynthetic efficiency of aquatic vegetation from spectral reflectance. *Remote Sensing of Environment 46*: 110-118.

Petr, T. **2000**. *Interactions between fish and aquatic macrophytes in inland waters: a review*. Food & Agriculture Org.

Pieterse, A. H., Murphy, K. J.,u.a. **1990**. *Aquatic Weeds - The Ecology and Management of Nuisance Aquatic Vegetation*. Oxford University Press.

Pinnel, N. **2007**. A method for mapping submerged macrophytes in lakes using hyperspectral remote sensing. *Limnologische Station, WZW, Department für Ökologie*

Pinnel, N., Heege, T.,Zimmermann, S. **2004**. Spectral discrimination of submerged macrophytes in lakes using hyperspectral remote sensing data. *SPIE Proceedings on Ocean Optics XVII 1*: 1-16.

Poikane, S., Birk, S., Böhmer, J., Carvalho, L., de Hoyos, C., Gassner, H., Hellsten, S., Kelly, M., Lyche Solheim, A., Olin, M., Pall, K., Phillips, G., Portielje, R., Ritterbusch, D., Sandin, L., Schartau, A.-K., Solimini, A. G., van den Berg, M., Wolfram, G.,van de Bund, W. **2015**. A hitchhiker's guide to European lake ecological assessment and intercalibration. *Ecological Indicators 52*: 533-544.

R Core Team. **2014**. R: A language and environment for statistical computing. *R Foundation for Statistical Computing, Vienna, Austria. URL http://www.R-project.org/*.

Richter, R. **1997**. Correction of atmospheric and topographic effects for high spatial resolution satellite imagery. *International Journal of Remote Sensing 18*: 1099-1111.

Richter, R.,Schläpfer, D. **2016**. Atmospheric / Topographic Correction for Satellite Imagery: ATCOR-2/3 User Guide, Version 9.1.0, DLR/ReSe, Wessling, DLR-IB 565-01/16, Oct. 2016. Available online: http://www.rese-apps.com/pdf/atcor3_manual.pdf (accessed on 30 November 2016)

Roessler, S., Wolf, P., Schneider, T.,Melzer, A. **2013a**. Multispectral Remote Sensing of Invasive Aquatic Plants Using RapidEye. *Earth Observation of Global Changes (EOGC)*: 109-123.

Roessler, S., Wolf, P., Schneider, T., Zimmermann, S.,Melzer, A. **2013b**. *Water constituent retrieval and littoral bottom mapping using hyperspectral APEX imagery and submersed artificial surfaces*. Vol. 12, p 44-57.

Rooney, N.,Kalff, J. **2000**. Inter-annual variation in submerged macrophyte community biomass and distribution: the influence of temperature and lake morphometry. *Aquatic Botany 68*: 321-335.

Santer, R.,Schmechtig, C. **2000**. Adjacency effects on water surfaces: primary scattering approximation and sensitivity study. *Applied Optics 39*: 361-375.

Savitzky, A.,Golay, M. J. E. **1964**. Smoothing and differentiation of data by simplified least squares procedures. *Analytical Chemistry 36*: 1627-1639.

Sawaya, K. E., Olmanson, L. G., Heinert, N. J., Brezonik, P. L.,Bauer, M. E. **2003**. Extending satellite remote sensing to local scales: land and water resource monitoring using high-resolution imagery. *Remote Sensing of Environment 88*: 144-156.

Schaeffer, B. A., Schaeffer, K. G., Keith, D., Lunetta, R. S., Conmy, R.,Gould, R. W. **2013**. Barriers to adopting satellite remote sensing for water quality management. *International Journal of Remote Sensing 34*: 7534-7544.

Schaumburg, J., Schranz, C.,Stelzer, D. **2011**. *Bewertung von Seen mit Makrophyten & Phytobenthos gemäß EG-WRRL – Anpassung des Verfahrens für natürliche und künstliche Gewässer sowie Unterstützung der Interkalibrierung*. Bayrisches Landesamt für Umwelt Augsburg/Wielenbach, Germany.

Schultz, R.,Dibble, E. **2012**. Effects of invasive macrophytes on freshwater fish and macroinvertebrate communities: the role of invasive plant traits. *Hydrobiologia 684*: 1-14.

Short, F. T.,Neckles, H. A. **1999**. The effects of global climate change on seagrasses. *Aquatic Botany 63*: 169-196.

Shuchman, R. A., Sayers, M. J.,Brooks, C. N. **2013**. Mapping and monitoring the extent of submerged aquatic vegetation in the Laurentian Great Lakes with multi-scale satellite remote sensing. *Journal of Great Lakes Research 39, Supplement 1*: 78-89.

Silva, T. S. F., Costa, M. P. F., Melack, J. M.,Novo, E. M. L. M. **2008**. Remote sensing of aquatic vegetation: theory and applications. *Environmental Monitoring and Assessment 140*: 131-145.

Sims, D. A.,Gamon, J. A. **2002**. Relationships between leaf pigment content and spectral reflectance across a wide range of species, leaf structures and developmental stages. *Remote Sensing of Environment 81*: 337-354.

Singh, S. P.,Singh, P. **2015**. Effect of temperature and light on the growth of algae species: A review. *Renewable and Sustainable Energy Reviews 50*: 431-444.

Skubinna, J. P., Coon, T. G.,Batterson, T. R. **1995**. Increased abundance and depth of submersed macrophytes in response to decreased turbidity in Saginaw Bay, Lake Huron. *Journal of Great Lakes Research 21*: 476-488.

Smith, G. M.,Milton, E. J. **1999**. The use of the empirical line method to calibrate remotely sensed data to reflectance. *International Journal of Remote Sensing 20*: 2653-2662.

Søndergaard, M., Johansson, L. S., Lauridsen, T. L., JØRGENSEN, T. B., Liboriussen, L.,Jeppesen, E. **2010**. Submerged macrophytes as indicators of the ecological quality of lakes. *Freshwater Biology 55*: 893-908.

Spitzer, D.,Dirks, R. W. J. **1987**. Bottom influence on the reflectance of the sea. *International Journal of Remote Sensing 8*: 279-308.

Squires, M. M.,Lesack, L. F. **2003**. Spatial and temporal patterns of light attenuation among lakes of the Mackenzie Delta. *Freshwater Biology 48*: 1-20.

Stendera, S., Adrian, R., Bonada, N., Cañedo-Argüelles, M., Hugueny, B., Januschke, K., Pletterbauer, F.,Hering, D. **2012**. Drivers and stressors of freshwater biodiversity patterns across different ecosystems and scales: a review. *Hydrobiologia 696*: 1-28.

Stephens, F. C., Louchard, E. M., Reid, R. P.,Maffione, R. A. **2003**. Effects of microalgal communities on reflectance spectra of carbonate sediments in subtidal optically shallow marine environments. *Limnology and Oceanography 48*: 535-546.

Sterckx, S., Knaeps, E.,Ruddick, K. **2011**. Detection and correction of adjacency effects in hyperspectral airborne data of coastal and inland waters: the use of the near infrared similarity spectrum. *International Journal of Remote Sensing 32*: 6479-6505.

Stoffels, J., Hill, J., Sachtleber, T., Mader, S., Buddenbaum, H., Stern, O., Langshausen, J., Dietz, J.,Ontrup, G. **2015**. Satellite-Based Derivation of High-Resolution Forest Information Layers for Operational Forest Management. *Forests 6*: 1982.

Trimble. **2016**. Datasheet. Trimble Juno SD Handheld GPS device. Available online: http://trl.trimble.com/docushare/dsweb/Get/Document-504948/022501-244B_Juno%20SD_DS_0712_MGIS_HR_nc.pdf (accessed on 30 November 2016).

TriOS. **2016**. RAMSES Radiometer. Available online: http://www.trios.de/en/products/sensors/ramses.html (accessed on 29 November 2016).

van Puijenbroek, P. J. T. M., Evers, C. H. M.,van Gaalen, F. W. **2015**. Evaluation of Water Framework Directive metrics to analyse trends in water quality in the Netherlands. *Sustainability of Water Quality and Ecology 6*: 40-47.

Villa, P., Bresciani, M., Bolpagni, R., Pinardi, M.,Giardino, C. **2015**. A rule-based approach for mapping macrophyte communities using multi-temporal aquatic vegetation indices. *Remote Sensing of Environment 171*: 218-233.

Vis, C., Hudon, C.,Carignan, R. **2003**. An evaluation of approaches used to determine the distribution and biomass of emergent and submerged aquatic macrophytes over large spatial scales. *Aquatic Botany 77*: 187-201.

Wang, P., Huang, C.,Brown de Colstoun, E. C. **2017**. Mapping 2000–2010 Impervious Surface Change in India Using Global Land Survey Landsat Data. *Remote Sensing 9*: 366.

Weaver, M. J., Magnuson, J. J.,Clayton, M. K. **1997**. Distribution of littoral fishes in structurally complex macrophytes. *Can.J.Fish.Aquat.Sci.; 45; 2277-2289*.

Wilcox, D. A.,Meeker, J. E. **1992**. Implications for faunal habitat related to altered macrophyte structure in regulated lakes in northern Minnesota. *Wetlands 12*: 192-203.

Williams, D. J., Rybicki, N. B., Lombana, A. V., O'Brien, T. M.,Gomez, R. B. **2003**. Preliminary investigation of submerged aquatic vegetation mapping using hyperspectral remote sensing. *Environmental Monitoring and Assessment 81*: 383-392.

Wöbbecke, K., Klett, G.,Rechenberg, B. **2003**. *Wasserbeschaffenheit der wichtigsten Seen in der Bundesrepublik Deutschland: Datensammlung 1981-2000*. Umweltbundesamt.

Wolf, P., Rößler, S., Schneider, T.,Melzer, A. **2013**. Collecting in situ remote sensing reflectances of submersed macrophytes to build up a spectral library for lake monitoring. *European Journal of Remote Sensing 46*: 401-416.

Wolf, P. K.-H. **2014**. *In situ*-Messungen als Basis für Wachstums-/Reflexionsmodelle submerser Makrophyten. *Limnologische Station, WZW, Department für Ökologie*.

Wolter, P. T., Johnston, C. A.,Niemi, G. J. **2005**. Mapping submergent aquatic vegetation in the US Great Lakes using Quickbird satellite data. *International Journal of Remote Sensing 26*: 5255-5274.

WWA Weilheim. **2015**. Makrophytenkartierung und WRRL-Gewässerzustandsmonitoring im Starnberger See. Data set request at WWA Weilheim.

Yuan, L.,Zhang, L.-Q. **2008**. Mapping large-scale distribution of submerged aquatic vegetation coverage using remote sensing. *Ecological Informatics 3*: 245-251.

Zambrano-Bigiarini, M. **2014**. hydroGOF: Goodness-of-fit functions for comparison of simulated and observed hydrological: R package version 0.3-8. Available online:https://cran.r-project.org/web/packages/hydroGOF/index.html (accessed on 10 July 2017).

Zhu, B., Mayer, C. M., Rudstam, L. G., Mills, E. L.,Ritchie, M. E. **2008**. A comparison of irradiance and phosphorus effects on the growth of three submerged macrophytes. *Aquatic Botany 88*: 358-362.